Aus dem
Leibniz-Forschungsinstitut für Molekulare Pharmakologie

DISSERTATION

# *Complementary methodologies and diverse model systems provide translational insight into the aggregation properties of neurodegenerative diseases*

-

# *Komplementäre Methoden und verschiedene Modellsysteme bieten translationale Einblicke in die Aggregationseigenschaften von neurodegenerativen Erkrankungen*

zur Erlangung des akademischen Grades
Doctor of Philosophy (PhD)

vorgelegt der Medizinischen Fakultät
Charité – Universitätsmedizin Berlin

von

Maria Lucia Pigazzini, M.Sc.

aus Lecco, Italia

Datum der Promotion: 26.06.2022

# 1. Table of Contents

## 2. List of Abbreviations

| | |
|---|---|
| AD | Alzheimer´s disease |
| ADP | Adenosine diphosphate |
| ALS | Amyotrophic lateral sclerosis |
| ASO | Antisense oligonucleotide |
| ATP | Adenosine triphosphate |
| ATPase | Adenosine triphosphatase |
| ATX | Ataxin (protein) |
| *C. elegans* | *Caenorhabditis elegans* |
| CFP | Cyan fluorescent protein |
| CRISPR | Clustered regularly interspaced short palindromic repeats |
| D2 | Dendra2 |
| FLIM | Fluorescence lifetime imaging |
| FP | Fluorescent protein |
| FRET | Förster resonance energy transfer |
| FTD | Frontotemporal dementia |
| Gln/Q | Glutamine |
| GST | Glutathione S-transferase |
| HD | Huntington´s disease |
| *HSP/Hsp* | Heat shock protein (gene) |
| HSP/Hsp | Heat shock protein (protein) |
| *HTT* | Huntingtin (gene) |
| HTT | Huntingtin (protein) |
| HTTEx1 | Huntingtin exon 1 |
| ND | Neurodegenerative disease |
| NEF | Nucleotide exchange factor |
| NPC | Neuronal progenitor cells |
| PAFP | Photoactivatable fluorescent protein |
| PD | Parkinson’s disease |
| PN | Proteostasis network |
| POI | Protein of interest |
| polyQ | Polyglutamine |

| | |
|---|---|
| RFP | Red fluorescent protein |
| RNA | Ribonucleic acid |
| RNAi | RNA interference |
| SCA | Spinocerebellar ataxia |
| siRNA | Small interfering RNA |
| Tau/$\tau$ | Lifetime |
| TCSPC | Time-correlated single photon counting |
| TEM | Transmission electron microscopy |
| YFP | Yellow fluorescent protein |

## 3. Abstract

Neurodegenerative diseases (NDs) are set to become a major burden to society. Understanding the mechanism behind their aetiology is paramount to find strategies for prevention and cure of these progressively debilitating disorders. A common feature of many NDs is the presence of aggregated proteinaceous material in the neurons. These aggregates, also known as amyloids, play a central role in neuronal degeneration. Intermediate structures, oligomers and protofibrils, that precede the formation of amyloids exhibit even greater cytotoxicity. Amyloid, protofibrils and oligomers are the downstream product of misfolded proteins. Proteins containing genetic mutations, such as those involved in ND pathology, or subject to stress, are prone to misfolding. To prevent misfolding and off-pathway formation of toxic species and maintain a general cellular homeostasis, the cell has evolved a set of systems collectively known as the proteostasis network (PN). The PN is responsible for the lifecycle of a protein: from ribosomal synthesis, to chaperone-assisted folding, to timely clearance and degradation. Impairment of any of these processes leads to imbalances of proteostasis and onset or exacerbation of disease. The aim of this dissertation is to present novel strategies designed to investigate aggregation-prone proteins involved in NDs and their relationship with the PN. First, we employ light microscopy and the model organism *C. elegans* to track the rate of degradation of the disease-causing protein huntingtin (HTT). By expressing HTT, fused with a fluorescent protein, in the neurons of the nematode, it is possible to monitor the location, synthesis, and clearance of HTT, *in vivo* and non-invasively, and gather information on the fate of both mutant or physiological HTT. Again leveraging the advantages of the nematode and employing fluorescent lifetime imaging (FLIM), we then characterise the presence of soluble, oligomeric and aggregated protein species in *C. elegans* models of NDs upon aging or stress. FLIM measures the lifetime of a fluorescently tagged aggregation-prone proteins and allows to distinguish, live and non-destructively, their conformational states and structural transitions. Lastly, employing a novel *in vitro* aggregation assay based on Förster resonance energy transfer (FRET), we uncovered a trimeric chaperone complex capable of both suppressing the innate aggregation of HTT, and actively driving disaggregation of preformed fibrils. Together these methodologies have a powerful transitional potential: to screen and identify biological factors or chemical compounds that can beneficially interfere with either the aggregation propensities of disease-causing proteins, or the PN components responsible

for their balance, ultimately establishing successful strategies for treatment or prevention of NDs.

# 4. Zusammenfassung

Neurodegenerative Erkrankungen (NE) werden zu einer großen Belastung für die Gesellschaft führen. Ein Verständnis der Mechanismen hinter ihrer Ätiologie ist von entscheidender Bedeutung, um Strategien zur Prävention und Therapie dieser Erkrankungen zu finden. Ein gemeinsames Merkmal vieler NE ist die Akkumulation von Proteinaggregaten in Neuronen. Diese Aggregate, die auch als Amyloide bezeichnet werden, spielen eine zentrale Rolle bei der neuronalen Degeneration. Intermediäre Strukturen wie Oligomere und Protofibrillen, die der Bildung von Amyloiden vorausgehen, weisen eine noch größere Zytotoxizität auf. Amyloide, Protofibrillen und Oligomere können aus fehlgefalteten Proteinen hervorgehen, die auf Mutationen beruhen können. Um eine Fehlfaltung und Bildung von toxischen Spezies zu verhindern und eine funktionale zelluläre Physiologie aufrechtzuerhalten, nutzt die Zelle das Proteostase-Netzwerk (PN). Das PN ist für den Lebenszyklus eines Proteins verantwortlich: von der ribosomalen Synthese über die Chaperon-unterstützte korrekte Faltung bis hin zum kontrollierten Abbau. Eine Beeinträchtigung eines dieser Prozesse kann zu einem Ungleichgewicht der Proteostase und dem Auftreten oder gar Verstärkung von Pathologien führen. Das Ziel dieser Dissertation ist es neue Strategien vorzustellen, um aggregationsanfällige Proteine, die an NE beteiligt sind und ihre Beziehung zum PN zu untersuchen. Mittels Lichtmikroskopie wurde im Modellorganismus *C. elegans* die Stabilität des krankheitsverursachenden Proteins Huntingtin (HTT) analysiert. Wildtyp und mutiertes HTT wurden hierfür mit einem Fluoreszenzprotein fusioniert und gezielt in Neuronen exprimiert, um Synthese und Abbau im lebenden Fadenwurm zu untersuchen. Die Fluorescence lifetime imaging (FLIM) Methode erlaubte eine Charakterisierung und Quantifizierung der löslichen, oligomeren und aggregierten HTT Proteinspezies in *C. elegans*. Mit FLIM konnte auch der Einfluss des Alterns und Stress auf das Aggregationsverhalten von HTT untersucht werden. FLIM misst die Lebensdauer von Fluoreszenzproteinen, die mit aggregationsanfälligen Proteinen wie HTT fusioniert sind. So wurde es möglich, Konformationszustände und -übergänge im lebenden Tier zu unterscheiden. Schließlich haben wir mit einem neuartigen in vitro Aggregationsassay auf der Basis von Förster-Resonanz-Energie-Transfer (FRET) einen trimeren Chaperonkomplex identifiziert, der sowohl die Aggregation von HTT unterdrücken als auch die Bildung von Fibrillen revertieren kann. Zusammen haben diese Methoden ein hohes Potential, biologische Faktoren oder chemische Verbindungen zu identifizieren,

die entweder die Aggregationsneigung von krankheitsverursachenden Proteinen oder die PN-Komponenten, die für deren Gleichgewicht verantwortlich sind, beeinflussen können, um letztendlich erfolgreiche Strategien zur Behandlung oder Prävention von NE zu etablieren.

# 5. Synopsis

***Complementary methodologies and diverse model systems provide translational insight into the aggregation properties of neurodegenerative diseases***

## *I. Introduction*

Neurodegenerative disorders (NDs) are set to become a critical and major socioeconomic burden to society. In high income countries, NDs are a leading cause of disability and death and the number of its fatalities will inevitably increase in the next decades [1]. The progressive and chronic nature of NDs and their selective and irreversible loss of neurons in specific brain areas are common and defining features of these debilitating illnesses. Aging is another common denominator underlining these diseases. Indeed, NDs mostly appear in later stages of life as the organism is already undergoing a slow decay [2]. Several lines of evidence have recently revealed that their aetiology may lie in complex interactions within the body. Loss of cardiovascular function, imbalances in trophic factors, dysregulation of the gut-brain axis and the microbiome, and the presence of senescent cells, are all processes that affect the stability and function of the nervous system, possibly endangering it years before the onset of specific ND pathologies [3]. The impact of a maladaptive immune system plagued by chronic inflammation is also emerging as a pathogenic driver, rather than a consequence, of degeneration [4]. Overall, the nervous system is undoubtedly the final site of progressive cellular and functional loss (Fig. 1A). As neurons are post-mitotic cells, they are born during embryonic development and, with some exceptions of neurogenesis and regeneration, retain their position and function until death. Their continuous high energy demand, rapid cell-to-cell molecular exchange and extensive transport of organelles over large distances, make them extremely fragile to external stressors and susceptible to even minor internal imbalances [5]. Neurons are particularly vulnerable to the presence of mutant disease-specific proteins, which have the ability to misfold and accumulate into large insoluble aggregated structures, known as amyloids - a hallmark of NDs [6]. Mutant misfolded proteins, their intermediate structures, their end-state accumulation into amyloid, and their ability to spread throughout the nervous system, are believed to be the underlying trigger of neurodegeneration (Fig. 1B) [7].

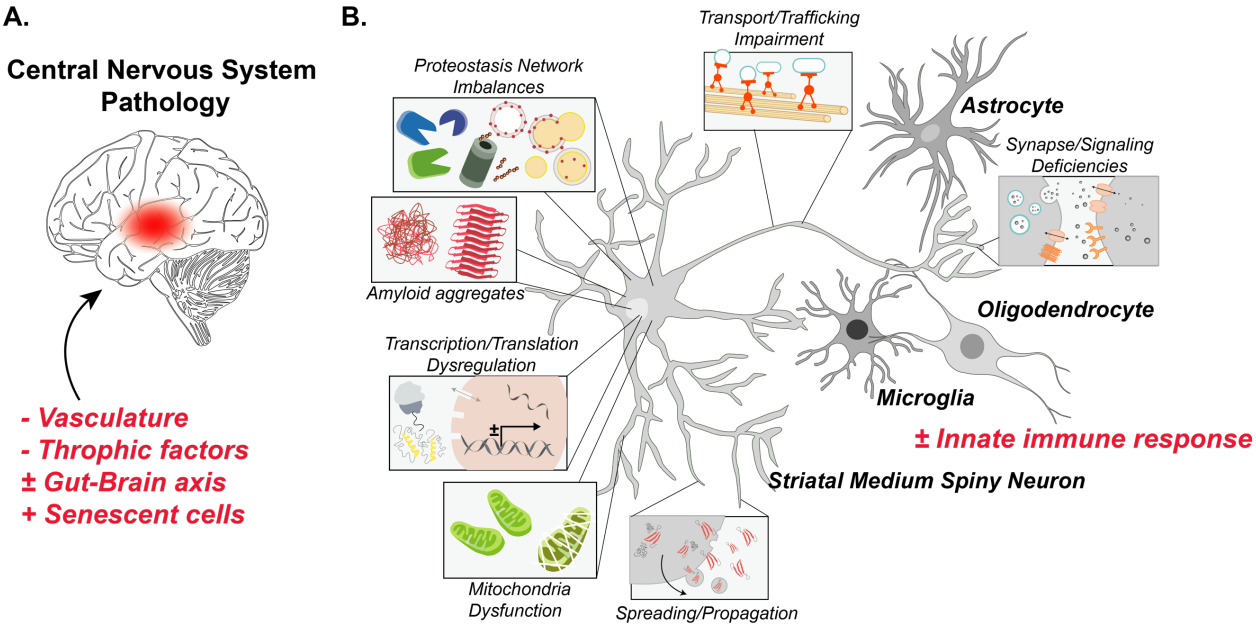


**Figure 1. Characteristics of neurodegenerative pathology**
**A.** Brain outline with highlighted basal ganglia region. The basal ganglia is the primary site of pathology for HD. Text in red describes the processes that contribute to degeneration of the central nervous system in HD and NDs in general. **B.** Schematic of the many cellular mechanism that are disrupted in HD: transcription and translation, mitochondria homeostasis, transport, trafficking, synaptic signalling, and proteostasis; and of the processes that characterize NDs: presence of amyloids, amorphous aggregates and their intermediates, and their ability to spread and propagate the disease.

The most common NDs include Alzheimer´s disease (AD), Parkinson´s disease (PD), frontotemporal dementias (FTDs), amyotrophic lateral sclerosis (ALS) and polyglutamine expansion disorders, including spinocerebellar ataxias (SCAs) and Huntington's disease (HD). These diseases present with distinct clinical manifestation, a wide range of symptoms, and affect different regions of the central and peripheral nervous system. Many of these are caused by well-established genetic mutations in precise genes, but most arise due to still unknown causes [8]. Yet, the mutant proteins, or combination thereof, responsible for these NDs are largely known: for example, the amyloid-β protein, in conjunction with the microtubule associated protein tau, are partially responsible for AD; PD is characterised by proteinaceous depositions, Lewy bodies, composed of the protein α-synuclein; fused in sarcoma and superoxide dismutase 1 are involved in ALS; and mutant huntingtin is the root cause of HD [8]. These individual proteins present no functional correlation, possess different amino acid composition and native folds but share a tendency to contain partially unfolded or intrinsically disordered regions [9]. Influenced by these sequences, disease-associated proteins can undergo

drastic structural transitions, largely driven by hydrophobic forces, towards lower energy states into amorphous aggregate and/or amyloids. Amyloids are postulated to be the absolute thermodynamically stable structure: an irreversible conformation that can be technically adopted by any protein, given the right conditions [10, 11]. Amyloids are threadlike fibrils of nanometres in diameter and microns in length: they possess distinctive tinctorial properties, are insoluble to detergents and were characterised via X-ray crystallography as possessing a very characteristic cross-β motif [12]. At an atomic level, the cross-β amyloid architecture is achieved by the repetitive alignment of β-strands perpendicularly to the fibril´s axis, with inter-strand networks stabilised by hydrogen bonding and adjacent β-sheets laterally held together by the tight interdigitation of their sidechains, in a structure known as a dry steric zipper [13] (Fig. 2A). Amyloid formation usually follows a nucleation-dependent mechanism [14]. First, in its nucleation stage, monomers slowly assemble into transient nuclei of intermediate oligomeric β-rich structures. As the rate of addition and dissociation of monomers into this critical unit is initially similar, the process is lengthy and very dependent on concentration, making it the rate limiting step of the cascade. Supplying preformed aggregates, or seeds, substantially shortens the elongation phase, creating a template structure onto which monomers can easily dock. Once sufficient nuclei have been formed during this initial lag phase, a rapid elongation phase begins: nuclei, or seeds, oligomers and monomers all interact to promote a cooperative transition into larger and more stable protofibrils. In this self-serving thermodynamically favourable phase, new intermediates facilitate and accelerate the growth and formation of further oligomers/protofibrils. Finally, in its saturation or stationary phase, a mature amyloid fold is achieved, and an equilibrium is reached where only few monomers or intermediates are available for further binding (Fig. 2B) [15].

Due to the intracellular or extracellular presence and accumulation of amyloids in most NDs, they were quickly deemed as the potential causative agents of neuronal death and general cytotoxicity, leading to the establishment of the ‘amyloid hypothesis’ of neurodegeneration [16]. However, research in post-mortem brains highlighted the presence of amyloids in patients without any ND symptoms or otherwise pathology. The absence of protein-specific aggregates in their disease-corresponding brain regions, or lack of correlation between amyloid load and severity of symptoms raised ulterior doubts on their pathogenicity. Furthermore, studies in animal models quickly revealed the inertia

and lack of toxicity of these amyloid deposits, compared to intermediate species [10]; finally, the emergence of β-motifs as biologically functional units further discredited the amyloid hypothesis [17]. Instead, an alternative ´oligomer hypothesis` was embraced, postulating that oligomeric species were the cause of toxicity and disease. Oligomers are necessary intermediates on-pathway of amyloid formation. They are by definition transient in nature, highly heterogenic in form and possess the propensity to interconvert rapidly to higher order structure (Fig. 2A) [18].

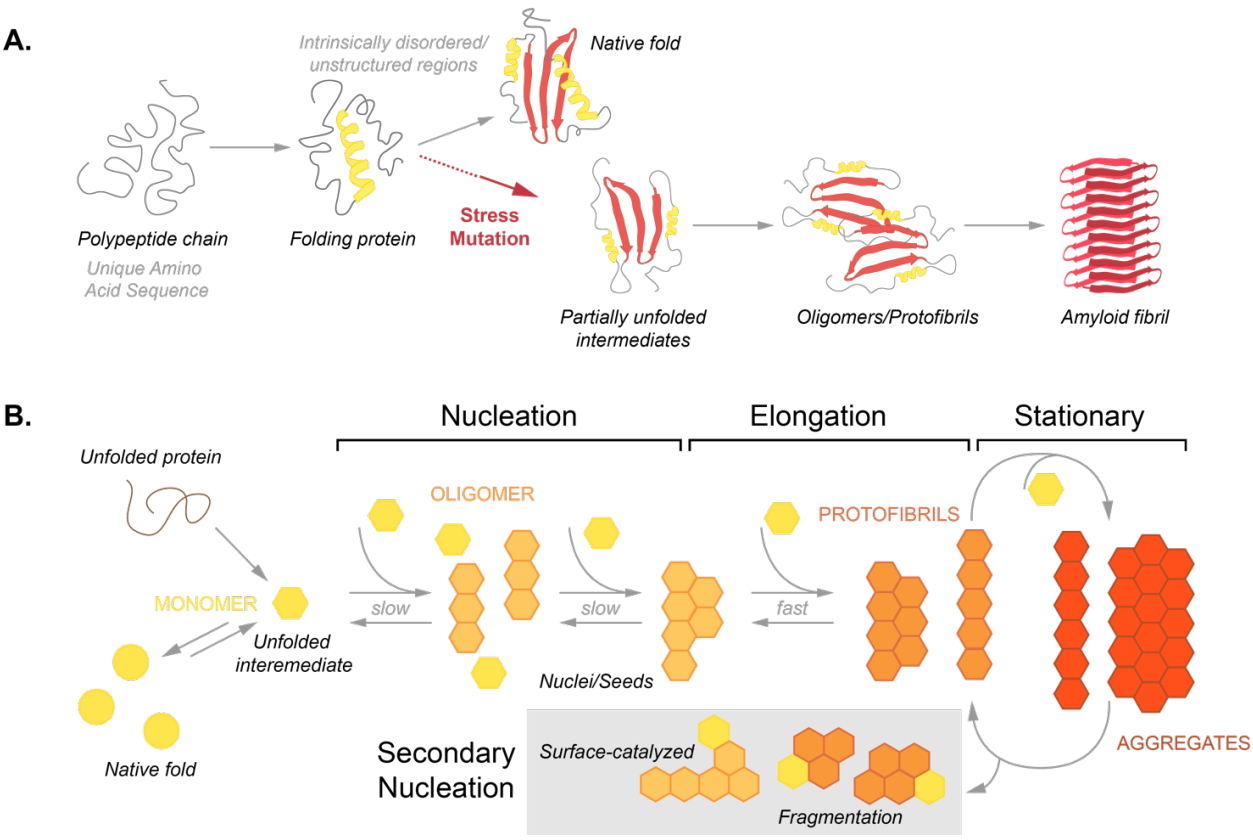


**Figure 2. Amyloid formation and the nucleation polymerization pathway**
**A.** Schematic illustrating the stages of protein folding/misfolding. A given protein folds into its native structure according to its unique amino acid conformation. In the presence of mutations or stress, a protein may fold into intermediates which progressively acquire higher order structures towards amyloid formation. **B.** Schematic representing the nucleation polymerization pathway of amyloid formation. Unfolded intermediates undergo a slow initial nucleation phase to form small oligomeric structures. These structures further polymerize into larger protofibrils in a fast elongation phase that creates more templates onto which monomers can attach, thus exponentially increasing the number of available protofibril/templates. Finally, a stationary phase is reached where large amyloids are present. In a parallel phase of secondary nucleation, amyloids can fragment to create new templates or act as a surface onto which monomers can branch.

Oligomer toxicity is principally determined by their surface exposure of hydrophobic patches, which allows for aberrant interactions. Their small size is a second driving factor of toxicity as high diffusion coefficients allow oligomers to freely and easily spread. From a structural perspective, their unstable and dynamic nature has made the oligomer shape hard to investigate and no unique oligomeric species has been found to be exclusively toxic in a disease specific manner [19, 20]. Instead, a wide variety of oligomer species have been reported to promote physiological, cytological and biochemical perturbations in neuronal and non-neuronal cells, via a multitude of deleterious interactions with lipid bilayers, receptors, metabolites, RNAs and other soluble proteins [10, 21]. As the 'oligomer hypothesis' gained traction, it resurfaced that amyloids themselves are far from innocuous and still play a significant role, albeit only as secondary contributors, in cellular pathology. Fibrils were found to interfere and disrupt the integrity of cellular membranes, disorganising the cellular environment, and moreover large fibrillar structures acted as a black hole for many molecules, actively depriving the cellular environment of necessary functional units [22]. Fibrils have also been shown to promote prion-like intercellular spreading, contributing to the advancement of pathology. Importantly, fibril fragmentation assists in secondary nucleation events by both generating toxic oligomers and increasing the number of templating fibres available (Fig. 2B), thus exacerbating cytotoxicity [23]. Finally, recent advances in cryo-electron microscopy techniques have allowed to visualise the ultrastructure of fibrillar deposits of tau and $\alpha$-synuclein purified from multiple AD and PD stricken brains [24, 25]. These studies revealed that fibrils composed of seemingly the same protein generated structures of very heterotypic intramolecular interactions, which conferred variating degrees of toxicity. The identification of amyloid polymorphism raises new questions on the relation between amyloid, their precursor oligomeric species, the nature of their toxicity, and their correlation with the heterogenous manifestation of NDs [26]; ultimately, in the search for the toxic culprit, both the amyloid and oligomer hypothesis may prove partially true.

Proteins are the building blocks of life: responsible for most cellular physiological functions but also guilty of many dysfunctions, as exemplified above. For proper biological functionality, proteins must reach a unique and thermodynamically stable three-dimensional structure, which is mostly dictated by its amino acid sequence [27]. However, on path to their native fold, most proteins populate transitional states of partially folded intermediates. In these intermediate states, proteins often expose hydrophobic patches

which increase their risk of misfolding and consequent aggregation, especially in the overcrowded cellular environment. Moreover, to fulfil their function, proteins often require large conformational flexibility or stabilizing binding partner interactions. This results in folded states that are only marginally stable or metastable, thus also heightening danger of misfolding [28]. It is therefore of critical importance for a cell to tightly regulate the processes that ensure correct folding, assembly, localisation and abundance of its proteins [29]. To guarantee the homeostasis and balance of the proteome, referred to as proteostasis, cells have evolved a complex and interconnected system known as the proteostasis network (PN) [30]. Simply described, the PN oversees three major steps of proteostasis: (i) accurate protein synthesis, coordinated by ribosomes and their associated factors; (ii) correct protein folding and maintenance of their conformational stability, sustained by molecular chaperones and their co-chaperones; and (iii) timely protein removal and degradation by either the ubiquitin-proteasome degradation or the autophagy-lysosomal pathways (Fig. 3A) [31]. Although these processes must be closely inter- and intra- regulated and controlled to guarantee cellular physiology, many are intrinsically error-prone and the integrity of the PN is constantly challenged by external environmental stressors or deleterious internal genetic variations. Importantly, the capacity of the PN decreases with the progression of aging, a decline that constitutes a critical factor in the emergence and exacerbation of NDs, which characteristically manifest in old age [32]. The capacity of the PN is also highly heterogenous according to cell type, partially underlining the vulnerability of neurons and their heightened sensitivity to proteotoxic stress, such as the presence of misfolded proteins [33].

To aid the proper folding and assembly, and prevent or reverse harmful misfolding, cells are equipped with a comprehensive network of molecular chaperones [34]. Historically, chaperones were classified as heat shock proteins (Hsps) - after the stress signal that was first described to induces them - and are subdivided into groups according to their molecular weight: a main class of ATP-dependent chaperones, including, Hsp70s, Hsp90 and Hsp110s, the chaperonins Hsp60s class, and a non-ATP dependent class of small Hsps; and a group of Hsp40s which act as collaborative co-chaperones to other Hsps and promotes selectivity and specificity in substrate recognition and targeting [35]. In a stereotypical folding process, chaperons act on the nascent polypeptide chain of a newly synthetized protein emerging from a ribosome. A complex of chaperones and cochaperones hold onto this substrate and, with subsequent ATP-dependent cycles of

binding and releasing, helps in shaping their client into its final functional structure (Fig. 3B) [36]. Chaperones can also target 'old' misfolded proteins and promote their refolding, thus actively intervening and suppressing off-pathway folding and preventing the

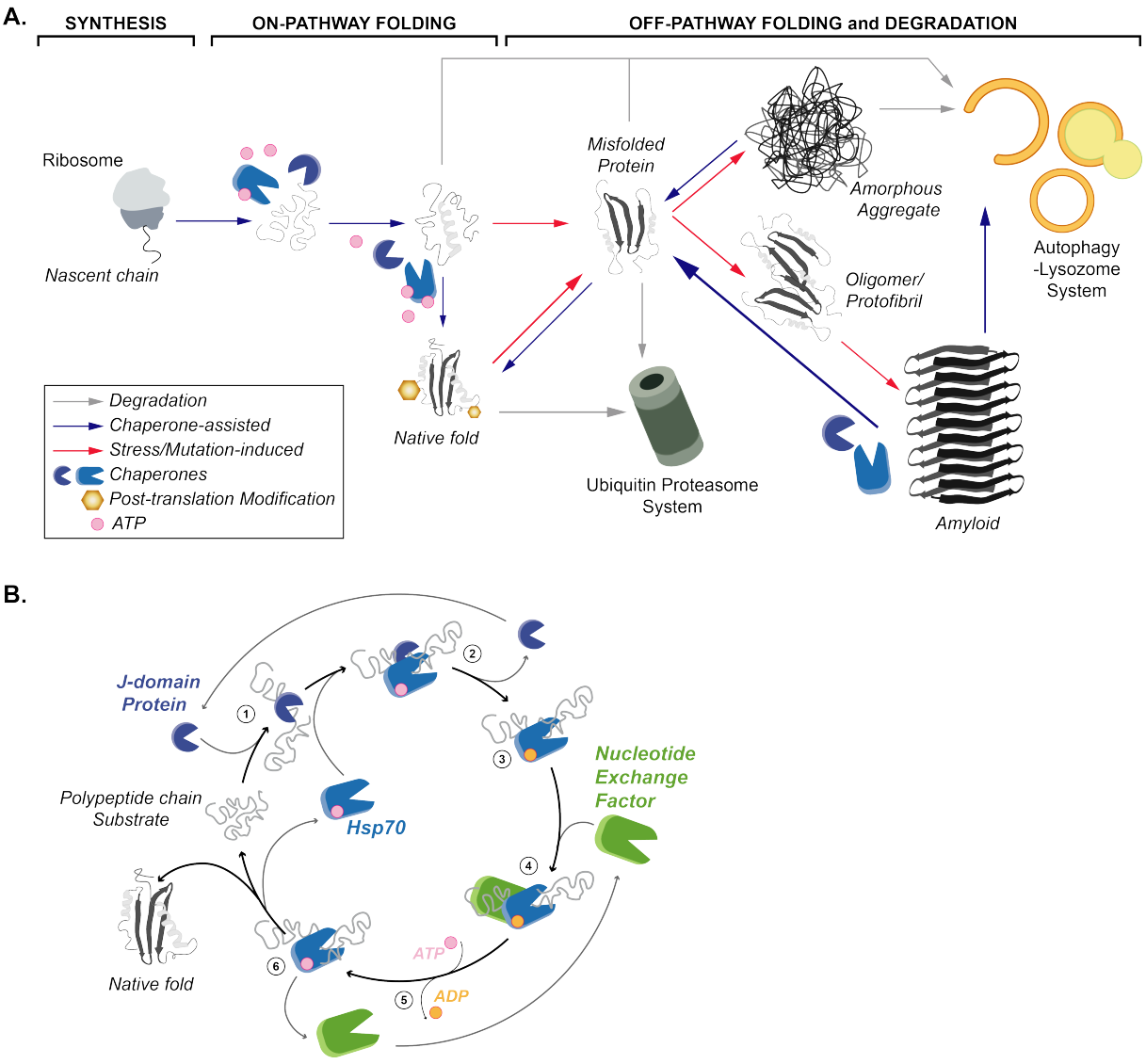


**Figure 3. Overview of the proteostasis network and protein folding pathways**
**A.** Schematic overview of the proteostasis network. Proteins are synthetized by the ribosome and immediately undergo an on-pathway folding process assisted by chaperones. When misfolded, proteins are reshaped into a native fold by the chaperones, targeted for degradation or initiate off-pathway events leading to aggregation. The PN consists of two main proteolytic systems: the ubiquitin proteasome system, which targets native, unfolded or misfolded proteins; and the autophagy lysozome system, which degrades almost any substrate, including amorphous and amyloid aggregates. **B.** Schematics of the HSP70 chaperone pathway. 1) A polypeptide chain is first recruited by a client-specific J-domain protein. 2) The J-domain protein stimulates the ATPase activity of HSP70, targets the substrate to the HSP70 and finally disengages from the complex. 3) HSP70 initiates an ATP dependent cascade to hold and fold the substrate. 4) A nucleotide exchange factor binds to the HSP70/substrate complex and 5) recharges HSP70 with a new ATP molecule. This cycle (3,4,5) is repeated until the substrate is fully folded. 6) once the substrate has reached its native state, both the NEF and HSP70 disjoin and are re-primed for folding a new substrate.

formation and toxicity of oligomeric species [37]. Importantly, they also target amyloid structures: they delay their formation, remodel their shape or even facilitate their disaggregation [38, 39]. However, within the cellular setting of aging or disease, and in the presence of large aggregates, many chaperome components and degradation machineries are sequestered within these inclusions. Sequestration completely abolishes their ability to neutralise toxic species and diminishes their capacity to deal with additional insults, contributing to the overload and collapse of the PN, and consequent cellular death [40]. The incredible versatility and ability of the chaperome to mediate and modulate many protein folding processes thus make it a very attractive target for therapeutic interventions in NDs [41].

Huntington´s disease (HD) is the main focus of this doctoral research work. HD is part of a class of NDs known as polyglutamine (polyQ) diseases. PolyQ diseases are triplet repeat disorders in which a stretch of CAG nucleotides, encoding for the amino acid glutamine (Gln, Q), is repeated over a defined physiological range. So far, nine polyQ diseases have been discovered. Except for their genetic aetiology, and the presence of an expanded CAG repeat, there is little similarity in their clinical manifestation and no further relationship between the function or amino acid sequence of the proteins responsible for each disorder [42]. The CAG expansion exhibits an inverse correlation with age of onset and symptom severity, with larger expansions typically leading to earlier onset and worse symptoms. HD was first described by George Huntington in a seminal paper in 1872 [43], but the locus harbouring the mutation was mapped to the small arm of chromosome 4 only a century later [44], and after another decade the disease cause was finally discovered. HD is a monogenic dominantly inherited ND caused by the expansion of the unstable polyQ stretch in the huntingtin (*HTT)* gene, which encodes for the eponymous protein huntingtin (HTT) [45]. Wild-type, physiological alleles encode between 11-35Qs, while alleles containing Q stretches over the threshold of 40Qs produce a fully penetrant disease. Intermediate allele of 36-39Qs might result asymptomatic or might give rise to disease later in life, and allele encoding between 25-36 repeats are at risk of expansion during meiotic replication. The average onset of disease is 45-50 years of age and progresses with a median span of 15-20 years till death [46]. However, the CAG length alone does not fully explain disease onset or penetrance and many genome-wide-associated studies in HD cohorts have identified genetic modifiers of pathogenesis. Among these, a prevalence of dysregulated DNA mismatch

and repair proteins emerged, which influence somatic instability, with obvious consequence on vulnerability and degeneration [47]. HD is relentless and unforgiving: it has a defined predictable pathogenic course, becomes fully debilitating and is, to this day, incurable. The beginning of HD passes usually undetected, with psychiatric changes starting to emerge first, followed by widespread depression and suicidal tendencies. The onset of movement deficiencies, and loss of independence, follows: the ability to control voluntary movements is lost and involuntary irregular and uncoordinated muscle contractions overtake the whole body. Finally, the linguistic and mental capacities and the sense of self start wavering: the onset of dementia signals the beginning of the end [48].

The molecular and cellular processes that bring about these changes in behaviour and physical impairments of HD are poorly understood. HTT is a very large protein expressed ubiquitously in all tissues, but with highest translational rates in the brain. The striatal medium spiny neurons of the caudate nucleus are the most vulnerable to the presence of mutant HTT, and their premature loss results in severe atrophy of the basal ganglia [49]. HTT´s native physiological function is still vastly uncharacterised but includes several basal cellular functions and its ability to interact with hundreds of other proteins implicates HTT in the modulation of many more [50]. HTT is necessary for embryogenesis and development, especially in relation to bone derived neurotrophic factor signalling [51, 52]. Throughout life, HTT is involved in transcriptional regulation, cytoskeletal signalling, ciliogenesis, endocytosis, mitochondria transport and biogenesis. It has important synaptic functions as a regulator of vesicular transport, endosomal trafficking, and glutamatergic signalling (Fig. 1B) [53]. HTT is also subject to several proteolytic cleavages and posttranslational modifications which can further modify its functionality, stability, binding partners, localisation and removal [54]. Impairment of these basal functions underscoring pathology, is likely promoted by the gain of toxic function perpetrated by the mutant form of HTT combined with the loss of physiological function provided by normal HTT, which is titrated away. In parallel with the decline caused by aging, the increasing lethal effects of mutant HTT overcome the wavering pro-survival ability of normal HTT, resulting in cytotoxicity and death [55].

Among many complex pathologic features, a key characteristic of the mutant form of HTT is its ability to misfold, prompted by the presence of the unstable polyQ stretch in

its first exon (HTTex1). Mutant HTTex1 is found freely and abundantly in the cell as the result of both sequential proteolytic cleavage of full-length HTT, and alternative RNA splicing [56]. Mutant HTT unfolding and misfolding prompts formation of fibrils following the typical nucleation mechanism. Fibrils adopt the characteristic **β**-structure architecture organised by glutamine side chains that twist into a polar zipper of greater compactness and stability as expansions increase [57]. Large inclusion bodies are found mainly cytosolically with some occurrence in the nucleus [58]; importantly they are mostly composed exon 1 fragments. As with other NDs described above, the role of inclusion bodies in toxicity and HD pathology is debated and incompletely characterised [58, 59]. HTT fibrils were visualised breaking through the membrane of the endoplasmic reticulum in mammalian cells and physically disrupting nuclear envelope pores, causing a loss of integrity [60]. Inclusion bodies were also found to sequester key components of the PN, such as Hsp40 and Hsp70 chaperones and members of the ribosomal quality control machinery. However, a large body of evidence also suggested that inclusion bodies may be protective and are a coping mechanism of a stressed cell, and act by sequestering mutant HTT forms, thus actively removing the toxic species from the cellular environment [61]. Mechanistically in fact, mutant HTT fails to perform or mimic the physiological functions of wild-type HTT. Soluble mutant HTT was recorded to gravely interfere with proteasomal activity, autophagy dynamics, and mitochondria homeostasis; in parallel, oligomeric species were found to target and interact with other low-complexity proteins, mainly involved in RNA binding, transcription, translation and transport. In this complex interplay between soluble and insoluble HTT forms, the PN strives to prevent the toxic capabilities of both [62]. Hsp40s, Hsp70s, the chaperonins and other PN machineries have all been demonstrated to interfere with fibril formation and toxicity with beneficial effects [63–65]. However, a PN which is critically dysregulated in HD, and further struggles with a functional decline during aging, ultimately fails in saving the cell. Additional mechanisms of toxicity are still being uncovered, including the contribution from RNA, other proteins, such as those generated from non-AUG translation, the cellular environment and genetic or epigenetic modifiers. A better understanding of the genome-wide imbalances in HD, alongside knowledge of structure and function of pathogenic HTT, and how it selectively targets and kills neurons, will uncover pathways and strategies that can prevent, delay or reverse the progressive nature of HD degeneration [66].

In this synopsis I summarise the research of three publication and the methodologies within that were partially established and developed in the Kirstein laboratory. The three publications are connected and support each other in their aim to investigate the properties of NDs and their relationship with the PN. Two papers outline, in a step-by-step protocol, the methodologies to 1) track simply and efficiently the degradation of disease-causing proteins *in vivo* [67], and 2) monitor and characterise the oligomeric and aggregates species formed by disease-causing proteins [68]. The goal of my first research project was to understand if and how the presence of a disease-causing protein impacted its rate of degradations, and what factors contribute to this, for example whether there are any differences between cell types or throughout organismal aging. Our second research goal was to establish if it was possible to distinguish the conformational protein species created *in vivo* by an aggregation-prone protein, and if these change overtime or during stress. Finally, in the publication described here last [69], we wondered which components of the PN where implicated in directly suppressing the aggregation propensities of the disease-causing protein huntingtin: what is their nature, by what mechanism do they achieve this, and could these components prove even more powerful by removing aggregates directly. To achieve these goals and answer these questions we employed a wide range of systems: from *in vitro* based approaches, to the use of *ex vivo* HD patient-derived reprogrammed induced pluripotent cells, to the extensive adoption of the *Caenorhabditis elegans (C. elegans)* model system. We subjected these models to a wide battery of biochemical assays, but our greatest innovation was the adoption of light microscopy to visualise the impact of aggregation-prone proteins *in vivo* during aging and disease progression.

## *II. Methodology and Results*

Much research into the mechanism and effects of aggregation is performed *in vitro* and in cell models. However, the behaviour of aggregation-causing proteins is likely affected and influenced by a multitude of factors at a system and organismal level and is significantly less understood. *C. elegans* has emerged as a very powerful model organism to study NDs, as it can faithfully recapitulate many of its characteristics and processes [70]. The nematode is extremely well characterised: its whole genome has been sequenced, with a reported 30% orthology to the human genome; its entire neuronal connectome, inclusive of neurotransmitter maps, has been carefully outlined, and most of its cellular lineages have been characterised [71]. This simple animal has all the properties of a complex organism, with the advantages that it is highly genetically malleable, easily tractable and economically scalable to obtain high *n* numbers. It also has a short lifespan of roughly 30 days, making it an extremely attractive model for studying aging and age-related decline and pathologies, such as NDs [72]. Furthermore, it has been comprehensively established that the PN of the *C. elegans* collapses during aging, and its capacity to maintain protein homeostasis is severely impaired before the end of reproductive capabilities, and further gradually drops over time [73]. Modifying the gene expression/translation to study downstream and phenotypic nematode behaviour is also relatively easy and failproof. RNA interference (RNAi) techniques were developed to knock down expression of selected genes by introducing the small interfering RNA (siRNA) construct in bacterial strains directly fed to the nematode [74]. Another distinguishing feature of the nematode is its optical transparency: its see-though cuticle allows for non-invasive and non-destructive visualisation of any protein of interest (POI) tagged with a fluorescent probe. The fate and localisation of any POI, from its biogenesis to its degradation, through all its transitional states, thus become available to be investigated via light microscopy techniques [75]. Light microscopy methodologies were also used here *in vivo* and *ex vivo* to monitor conformational transition from monomer to oligomer, aggregation kinetics and the impact of molecular chaperone overexpression and knockdown in mammalian cell cultures. Finally, the advantages of fluorescently labelled proteins are also exploited in the *in vitro* assays utilised in these works, which permit to follow aggregation, investigate its kinetics and reveal the impact of chaperone complexes on amyloid formation.

In the paper ***"In vivo quantification of protein turnover in aging C. elegans using photoconvertible Dendra2"*** by Pigazzini and Kirstein, we describe a microscopy-based technique to quantify the stability and turnover of the HTT protein in the nematode [67]. As mentioned above, the cell has evolved many systems to ensure its wellbeing. Proteins are constantly being synthetized, transported, and degraded to meet the physiological demands of the cell and its surroundings. Investigating these turnover processes has become simple and accurate thanks to the introduction of genetically encoded fluorescent proteins (FP). The advent of FPs in the early 1990s revolutionized many biological fields allowing for the non-invasive, non-destructive following of any POI [76]. The fate of a protein, its trafficking, location, compartmentalisation, along with many other protein-specific properties, or its interaction partners, can all be studied. FPs can be fused to a desired POI and autocatalytically fold without the need of any co-factor except oxygen [77]. Employed in this study is a new class of FP, known as photoconvertible, photo-switchable or photoactivatable FPs (FAFPs). Upon irradiation, FAFPs undergo a structural rearrangement reversibly or irreversibly changing their emission/excitation spectra [78]. Dendra2 is a second-generation FAFP which has been engineered to irreversible switch its spectrum, upon exposure of violet or blue light, from a green emitting protein to a red emitting one, with a 4000-fold increase in intensity. Importantly, because of the permanent nature of the conversion, it becomes possible to track the red moiety, over time but non-continuously, without collecting interfering signal from any newly synthetized green moiety [79, 80]. Dendra2 is a very stable monomeric and long-lived protein that matures quickly at physiological temperatures and pH, characteristics that make it a very desirable partner for in cell experiments and tagging of biologically relevant substrates. Dendra2 can be expressed in any model system attached to any desired POI [81]. Within the *C. elegans* system, conversion occurs by shining a laser light through the translucent body of the nematode. The photon beam of a laser scanning confocal microscope allows for the precise conversion of a clearly defined region of interest: it becomes therefore possible to convert and track the Dendra2 changes within a single neuron. The quantity of degraded POI tagged to Dendra2, or how much of it has been newly synthetized, within a defined time frame, can be calculated by comparing the difference between the emitted red, or green, signal intensities before and after its conversion [82]. The rate of degradation of a specific POI can thus uncover cell type differences, inform the inability to remove certain protein conformations, even over

prolonged time, or highlight the impact of aging or disease in clearance mechanisms, and generally confirm the gradual collapse of the PN [83].

In the research by Pigazzini and Kirstein, we investigated the rate of degradation of the HTT protein and the differences that arise in the presence of a pathological version of HTT compared to wild type [67]. We generated nematodes that overexpressed HTT under the control of a pan-neuronal promoter, from early development throughout life (Fig. 4A). The exon 1 of the HTT protein was fused to the Dendra2 FAFP and either contained a physiological stretch of 25Qs (hereafter HTTQ25-D2), or an expanded and pathological stretch of 97Qs (hereafter HTTQ97-D2) (Fig. 4B). Single neuron conversion occurred as expected in both nematode strains (Fig. 4A) and allowed us to obtain results relevant to the impact of the pathological HTT. First, we discovered that the neurons of the tail region of the nematode were more active in degrading HTTQ25-D2 over a two-hour timeframe, compared to those of the head. This cell-specific difference was lost in the presence of HTTQ97-D2, and head neurons were equally impaired in clearing HTTQ97-D2, which was also overall less degraded compared to HTTQ25-D2 (Fig. 4C). We then expanded the timeframe of degradation analysis to 24 hours and noticed that HTTQ25-D2 was extensively cleared both from the head and the tail regions of the nematode. However, tail neurons were again able to remove larger quantities of HTT from their cellular milieu compared to head neurons. Differences in the intrinsic epigenetic/proteomic make-up of the tail neuron compared to the head neurons may explain the different degradation rates. For HTTQ97-D2 however, no significant degradation occurred over prolonged time, and all neurons of the nematode were similarly unable to clear pathologic HTT (Fig. 4D). This result clearly indicated that pathological HTTQ97-D2 cannot be removed by any of the PN machineries in the nematode´s neurons. Importantly HTTQ97-D2 presents with foci or puncta that are recapitulations of the aggregation abilities of HTT, confirming that characteristics intrinsic to this protein, such as its amyloid forming ability and toxicity, are maintained in diverse organisms. Finally, we tested the effects of aging on the clearance of HTT. We compared the degradation rates in young versus old nematodes at day 4 and 10 of life. HTTQ25-D2 was removed almost equally during the nematode´s lifetime. As expected, HTTQ97-D2 was degraded less efficiently compared to wild type. To further highlight the deficiencies of neurons in aging, HTTQ97-D2 was even less cleared from the tail cells in old nematodes, pointing to the almost complete inability of a collapsing PN to deal with toxic

proteins (Fig. 4E). At this point, toxicity might be exacerbated as the lingering pathologic proteins inflict more and more damage to defenceless cells.

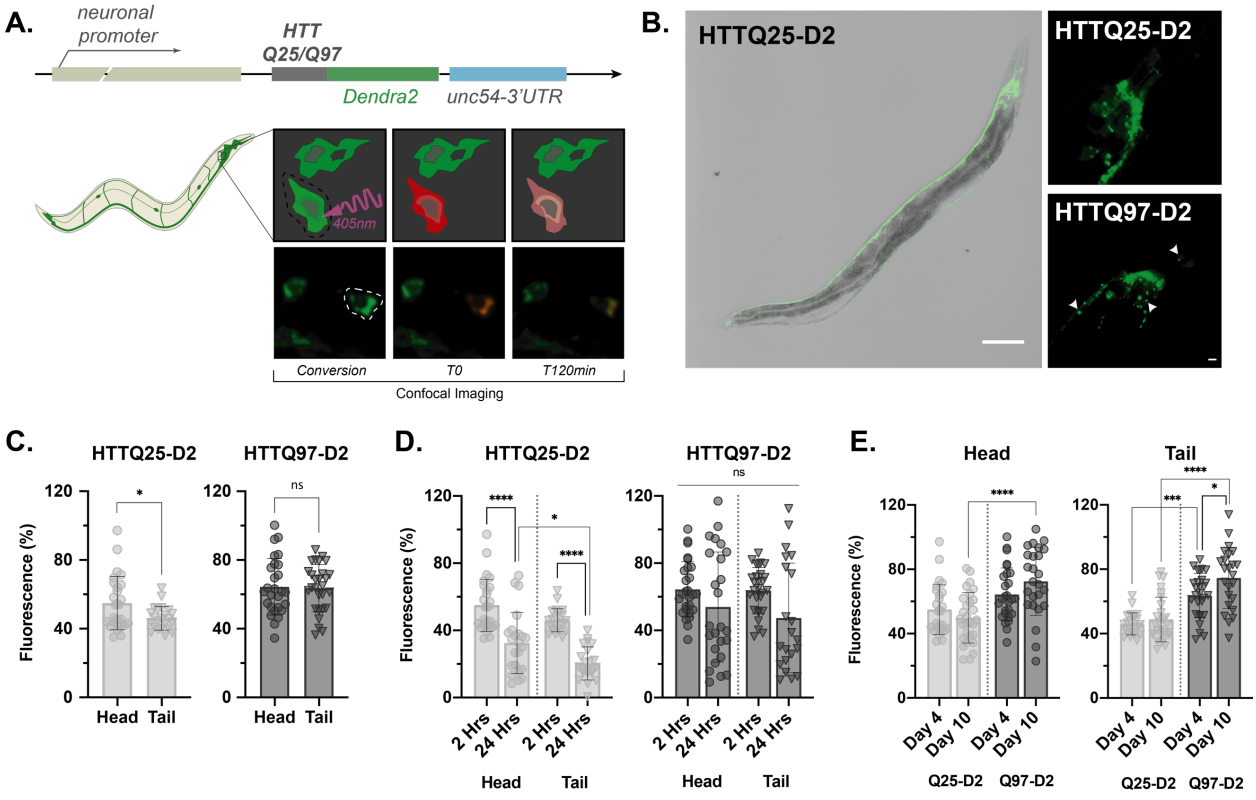


**Figure 4. Tracking degradation of huntingtin-Dendra2 in *C. elegans***
**A.** Schematic representation of the expression of HTT-D2 in *C. elegans* and illustration of the conversion mechanism. A single neuron is irradiated (conversion) and changes its emission spectra from green to red (T0). After a certain amount of time, the red signal is decreased as the protein is cleared (T120). **B.** Confocal imaging of the HTT-D2 strain. Large image represents a HTTQ25-D2 young nematode with green D2 expressed in the whole nervous system. Smaller images represent a magnification of the head region of both HTTQ25-D2 (top) and HTTQ97-D2 (bottom). Arrows point to foci/puncta of aggregated HTT in the head of the HTTQ97-D2 strain only. **C.** Bar graphs showing the quantification of HTT-D2 degradation in the head and tail region for both strains. HTTQ25-D2 nematodes only exhibited a significant decrease in degradation in the tail neurons compared to the head neurons after two hours. **D.** Bar graphs showing the quantification of the degradation rates between head and tail neurons, of both strains, after 24 hours. Even after this prolonged period of time, the pathological HTTQ97-D2 is not cleared from the neurons. Conversely, the soluble HTTQ25-D2 is removed already at 2 hours, and significantly more after 24 hours. **E.** Bar graph showing the quantification of HTT-D2 degradation in young vs old nematodes of both strains, for both head and tail neurons. Significantly less of the expanded HTT of HTTQ97-D2 is removed from the neurons, compared to the physiological HTTQ25 in old nematodes. Figures B, C, D and E have been adapted from the publication by Pigazzini and Kirstein [67].

Overall, with this methodology it was possible to establish the differences between the degradation rates of pathological versus wild-type HTT at an organismal level and over time during aging. This method can be the first step to unravel many more questions

on proteostasis, neurodegeneration and any of their modulators [84]. Importantly, it can be adapted to any biological system, from mammalian cell cultures to zebrafish. Any disease-causing protein can be investigated, as an overexpression or at an endogenous level, and almost all aspects of its life and fate can be investigated [85, 86]. The technique is not without limitations. PAFP constructs are of a chimeric nature and the added fluorescent protein potentially distorts the native fold or biochemical and physiological function of its conjugated POI. As with most microscopy methodology, *in vivo* biological samples are at risk of suffering phototoxicity [87]. Generally, however, the ease of the nematode system in combination with the spatiotemporal definition granted by PAFPs has made for an extremely powerful and incredibly versatile technique to investigate the life of any POI.

In the second work by Pigazzini *et al.,* titled "***Characterization of amyloid structures in aging C. elegans using fluorescence lifetime imaging"***, we describe a technique that allows to differentiate between aggregated versus soluble protein species in living and aging nematodes [68]. We took advantage of another powerful imaging tool: fluorescence lifetime imaging (FLIM). FLIM exploits the lifetime property of fluorescence, which are intrinsic to each fluorescent probe or protein [88]. When a fluorescent molecule is excited by a light source and absorbs its energy, its electrons jump from a ground state to a higher energy level; with certain probability these electrons will then return to the ground state via radiative or nonradiative energy loss. The lifetime of a fluorophore (tau, $\tau$) is thus defined as the average time (in ns) in which a fluorophore stays in its excited state or, equally, the average time it takes for a photon to decay back to its ground state (Fig. 5A) [89]. FLIM lifetime measurements are recorded in their time-domain with a method called time-correlated single photon counting FLIM (TCSPC-FLIM). A fluorophore is excited by short high-frequency pulses of light and its single exponential decay, or the time required for the photon to arrive at a detector, is recorded using fast electronics. In a stopwatch-like manner, TCSPC measures the time between the excitation and emission of the photon. The excitation pulses are repeated thousands of times over to promote detection of larger photon counts and improve accuracy of the measurement (Fig. 5B). Photons are distributed according to their time-of-arrival and fitted to a decay curve that ultimately unveils the lifetime of the excited sample (Fig. 5C) [90]. The lifetime of a selected fluorophore is uniquely defined by its precise physico-chemical properties.

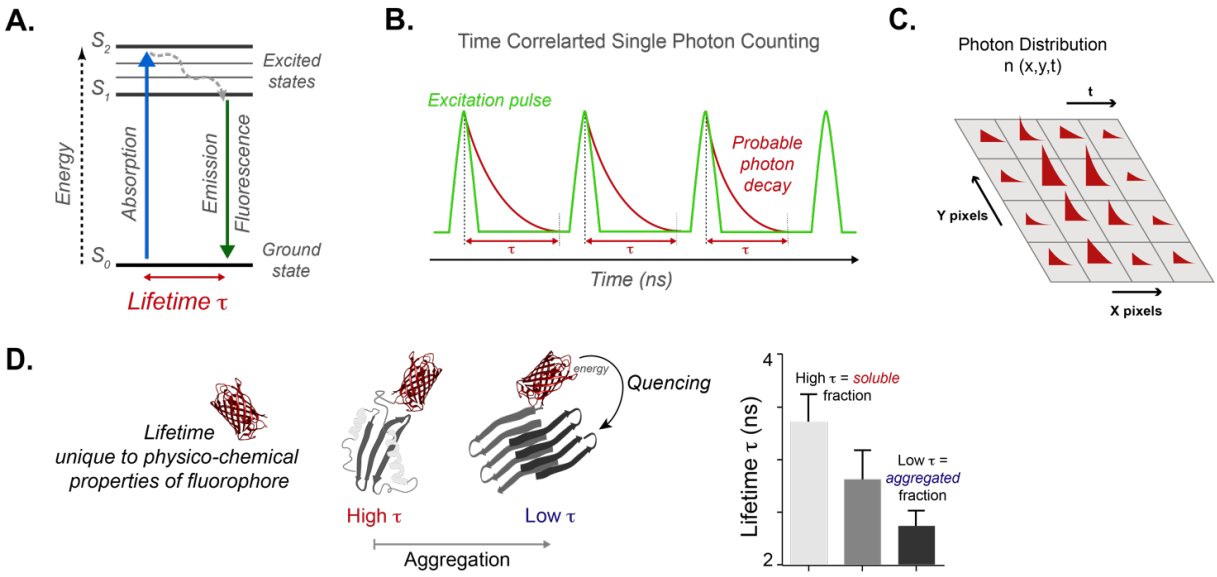


**Figure 5. A visual introduction to FLIM and its application in protein aggregation**
**A.** Jablonski diagram illustrating the electronic states of a molecule and its transitions through them. When a molecule absorbs a photon, it jumps to a higher energy level. As the photon is emitted and returns to its ground state, it releases energy in the form of fluorescence. A molecule´s lifetime is defined as the time it takes for a photon to return to its ground state after being excited. **B.** Schematic representation of the time domain technique TCSPC-FLIM. A pulsed light laser repeatedly excites a substrate and a single exponential decay curve is recorded over time. **C.** When scanning a sample, the distribution of the lifetimes of photons is collected with spatiotemporal coordinates. A map of lifetimes if generated from which it is possible to determine an average lifetime **D.** Lifetimes depend on the physico-chemical properties of the molecule, depicted here is a fluorescent protein. When then fluorophore is bound to a POI, its lifetime diminishes. Its lifetime further diminishes when the fluorophore is found in the constricted environment of a fibril, due to molecular quenching. Average lifetimes of a sample can inform on the conformational state of a protein: high lifetimes represent soluble moieties and low lifetimes represent aggregated species.

Changes in either the structural conformation of the fluorophore, its surrounding, its binding and interaction networks, result in changes in its lifetime. It therefore becomes possible to study the functional behaviour of a fluorescently tagged protein in its native biological environment, and any perturbations it suffers, by correlating these transitions to variations in its lifetime measurements [91]. Tagging a POI with a fluorescent protein will already provoke decreases in the absolute lifetime of the fluorophore, and further changes in the conformational states of the selected protein can be monitored by differences in its lifetime [92]. In a setting of misfolded and aggregation-prone proteins, soluble proteins retain a high/long lifetime, close to that of their conjugated fluorophore. However, when a POI is found in the constrained conformational fold of an amyloid structure, its lifetime decreases significantly. Trapped in the highly ordered β-sheet fold of a fibril, a photon is subject to a loss of energy via a non-radiative process known as molecular quenching, and quickly returns to its ground state, resulting in a decrease in

recorded lifetime. The photon decay of an excited fluorescent POI encapsulated within an aggregate is faster and translates into a shorter lifetime value [93]. Lifetime measurements provide information on the conformational species of any POI with high/long lifetime values representing soluble proteins, and lower/shorter lifetimes corresponding to aggregated populations (Fig. 5D) [94]. Importantly, intermediate lifetime values can also inform the presence of intermediate species of oligomers, thus illuminating a whole spectrum of folded and unfolded conformation and their transitional states, over time, within a biological sample.

In this work, we again leveraged the formidable and malleable genetics and optical advantages of *C. elegans*. To mimic and study NDs, several nematode strains have been created that harbour human disease-prone proteins. These strains authentically emulate the hallmark of their aggregation-prone protein behaviour: the formation of large inclusions, also termed foci or puncta [95]. We here employed three different nematode strains expressing homo-polyQ constructs of pathological lengths fused to different fluorophores. The polyQ constructs are expressed in three tissues of the nematode under the control of specific promoters: Q40 fused to cyan fluorescent protein (CFP) is expressed in the nervous system (hereafter nQ40-CFP); Q40 fused to red fluorescent protein (RFP) is expressed in the body wall muscles (hereafter mQ40-RFP); and either Q44 or Q85 are expressed in the intestine, fused to a yellow fluorescent protein (hereafter iQ44-YFP or iQ85-YFP) (Fig. 6A) [96]. In all tissues and regardless of their conjugated fluorophore, the polyQ proteins misfold and aggregate into insoluble inclusions in an age dependent manner [97]. By measuring the shifts in lifetimes of these polyQ proteins within their cellular environment, it becomes possible to distinguish the species of protein present and changing over time: from a soluble population into an aggregated form, and any intermediate oligomeric state [94]. In this study, the ability of FLIM to discriminate spectrally overlapping fluorophores is key to resolve the protein-specific and environment-specific characteristics of proteins tagged with the same fluorophore. Via lifetime measurements, we investigated the aggregation landscapes of aging on the polyQ tagged proteins in young and old nematodes at day 4 and 8. Furthermore, to investigate the involvement of the PN network on aggregation during stress, and especially the contribution of molecular chaperones, we observed the shift in aggregation patterns after partially depleting via RNAi the constitutively expressed heat shock protein 1 (*hsp-1*) (Fig. 6A). In our results, a shift in lifetimes, from higher to lower

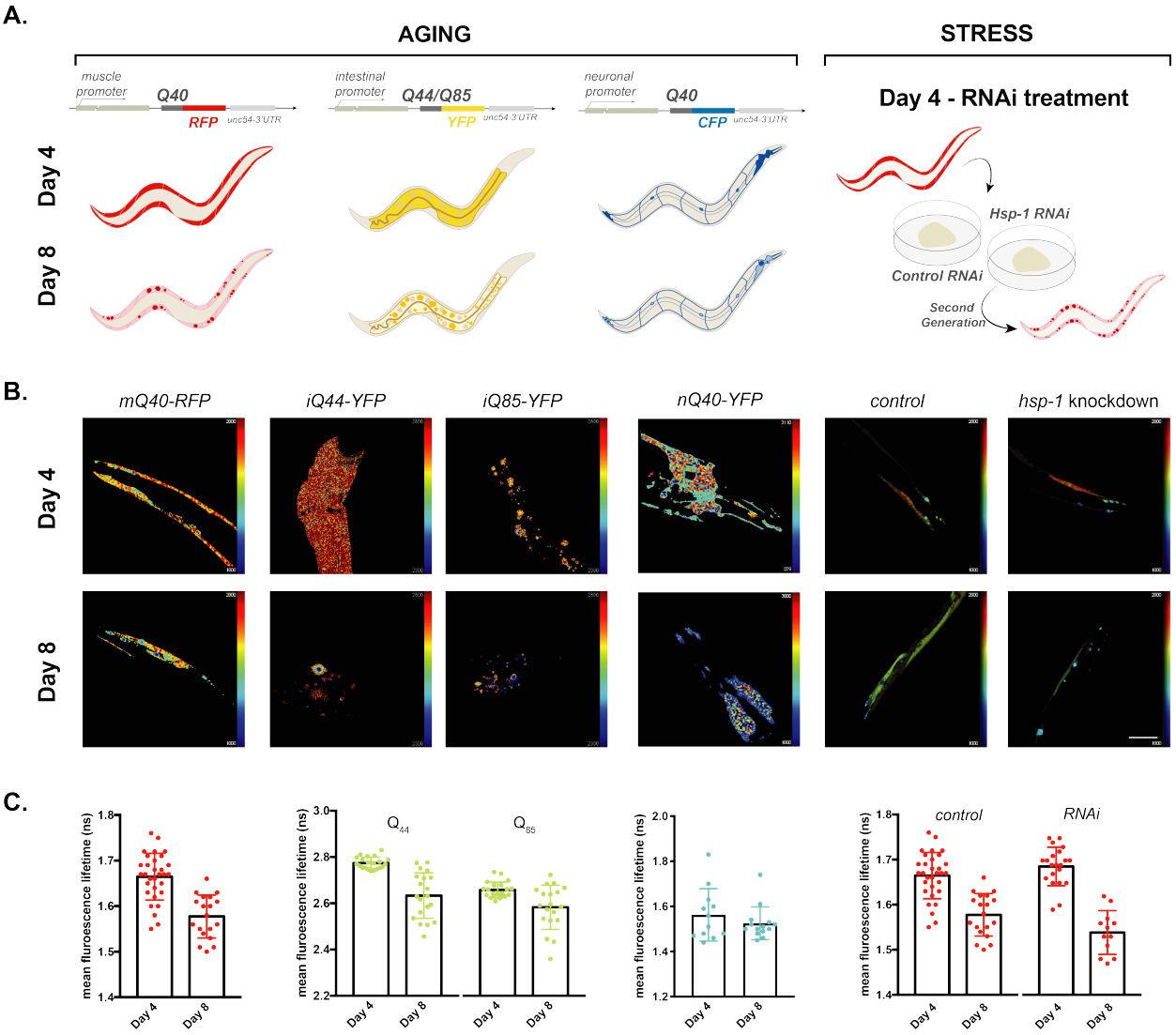


**Figure 6. FLIM characterizes soluble vs aggregated species in *C. elegans* models of NDs, during aging or stress**

**A.** Schematic representing the nematode stains utilized in this publication. Three different fluorophores are expressed fused to polyglutamine proteins in various tissues of *C. elegans*. At day 4 the polyQ constructs are still soluble but these present with large foci in old nematodesn at day 8. Similarly, large inclusions appear when animals are depleted of the chaperone hsp-1, via treatment with RNAi over two generations. **B.** Pixel-based pseudo colour maps of the lifetime of the polyQ constructs, for all strain examined. High lifetimes tend to the red colour and low lifetimes to the blue. **C.** Bar graph show the quantification of the average lifetime for each polyQ strain. Lifetime show a significant decrease in value from day 4 to day 8 of life, for mQ40-RFP and iQ44/iQ85-YFP but not nQ40-CFP. Similarly, subjecting the nematode to the stress of chaperone depletion resulted in a decrease in average lifetime of the treated vs untreated mQ40-RFP stains at day 8. Figures B and C have been adapted from the publication by Pigazzini *et al.* [68].

values, corresponding to a reduction in soluble fraction and an increase in aggregated population, was recorded in most samples, either due to aging, an excessive glutamine load, or stress. polyQ expressed in muscle and intestine cells registered a significant decrease in their lifetimes from day 4 to day 8, corresponding to the accumulation of

aggregated species, as clearly visible by the apparition of large foci in the affected tissues (Fig. 6B; example day 8 iQ44-YFP and day 4 iQ85-YFP). Importantly, the lifetime values of iQ85-YFP were significantly lower already at day 4 (Fig. 6C). This low lifetime in young nematodes is explained by the very extensive polyQ stretch, which is highly aggregation-prone due to its expansive hydrophobic misfolded stretch. A yet lower lifetime for iQ85-YFP was further recorded at day 8, highlighting the even more pronounced speed and condensed nature of aggregation of this specific protein structure. For polyQ constructs in the neurons, the lifetime did not significantly decrease possibly due to the PN´s capacity intrinsic to neuronal cells (Fig. 6C). However, during stress conditions upon knockdown of hsp-1 in neurons and muscles, the PN, already coping with toxic polyQs, becomes further challenged and impaired. Even in young nematodes, the depletion of a key chaperone significantly pushed the misfolded protein towards aggregation, as illustrated by the appearance of abundant small foci (Fig. 6C). In lifetime measurements, a broader set of values was recorded, signifying the presence of a more heterogenic population of protein species in between soluble and oligomeric conformation, and potentially in transition towards aggregation. FLIM can in fact assess the degree of aggregation, with a widespread distribution of lifetimes within a sample pointing to a complex composition of protein structures from monomeric to multimeric and all its intermediates. Importantly, because FLIM is not dependent on intensity values, it correctly identifies the aggregated nature of a protein based on the change of its conformational structure/surrounding when bound to other moieties into an amyloid structure [90]. It can therefore distinguish actual aggregates from material formed by high spatiotemporal protein concentration, which might appear as foci/puncta in intensity images.

Overall our results exemplify the versatility and strength of FLIM, which is largely independent of fluorophore choice, tissue expression patterns and especially protein translational levels. FLIM thus possess many advantages over steady-state intensity-based microscopy, which is utilised in most microscopy methodologies, as in the other works described here. Primarily, FLIM is independent of fluorophore concentrations, absolute detected intensity and variations in acquisition devices. As lifetimes are absolute self-referenced measurement, they are reproducible, comparable between instruments configurations and not subject to illumination discrepancies, producing little artefacts, and resulting in robust repeatable results [98]. However, this technique, although extremely powerful, also suffers from limitations. The physical and technical set up is financially

costly to obtain and maintain. From a sample perspective, because of the sensitivity of FLIM, changes in the general environment or in temperature, pH, ion concentrations, and oxygen saturation levels, as well as the presence of multiexponential lifetimes, can complicate interpretation of data [99]. Furthermore, TCSPC measurements require long acquisition times, which might prevent the visualisation of fast processes. Better acquisition hardware and promising new techniques are however pushing towards imaging of fast dynamic events, which will aid in better characterising protein conformational transition [100].

Finally, in the work of Scior *et al.,* "***Complete suppression of HTT fibrilization and disaggregation of HTT fibrils by a trimeric chaperone complex***" we demonstrated the ability of a specific trimeric chaperone complex to maintain HTTex1 in a soluble form, by suppressing its aggregation potential and even reversing its amyloid state, alleviating the cell of a potentially toxic burden [69]. To obtain mechanistic insight on the kinetics of self-assembly of HTT and discover the key chaperone complex that inhibits this process, an assay based on Förster resonance energy transfer (FRET) was established. FRET occurs between two light sensitive molecules: the first molecule, termed the donor, is exited at its defined wavelength and will transfer its energy to a second molecule, the acceptor, only when the couple are found sufficiently close in space; the now-excited acceptor will then emit light of its own wavelength. Here, HTTex1, containing a pathological stretch of 48Qs, was tagged with a donor cyan fluorescent protein CyPet and an acceptor yellow fluorescent protein YPet, together constituting a FRET pair [101]. As molecules of HTTEx1-CyPet come in very close proximity and merge into the tightly packed amyloid structure with the molecules of HTTEx1-Ypet, a transfer of energy from the CyPet-donor to the YPet-acceptor occurs and a FRET signal is recorded. The FRET efficiency thus acts as a readout for HTT aggregation. An absent FRET signal represents monomeric and soluble HTT moieties kept at great distance. Over time, as monomers of mutant HTT encounter each other and nucleation begins, HTT´s polymeric seeds incorporate further monomers and an increase in the FRET signal is recorded. In the subsequent elongation phase, oligomers, protofibrils and longer fibrillar structures are formed, exponentially increasing the FRET efficiency and signal. Once the FRET signal reaches a plateau, the amyloid is fully formed, and most monomers are now incorporated into large structures. To gain control over the precise starting point of

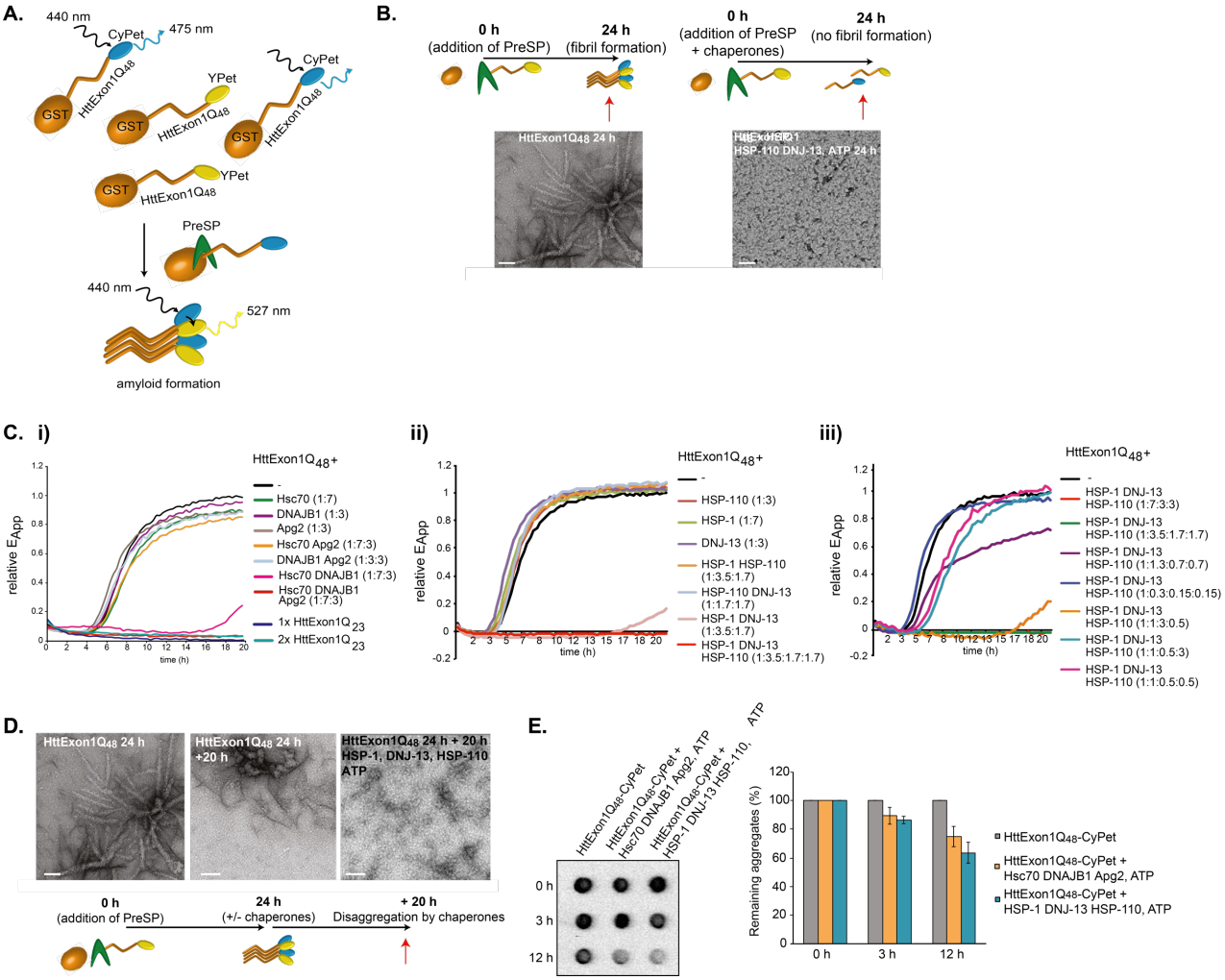


**Figure 7. A trimeric chaperone complex is able to suppress aggregation and promote disaggregation *in vitro***

**A.** Schematic representation of the FRET aggregation assay. Mutant HTTex1 is purified fused C-terminally to a fluorophore (CyPet or Ypet) and N-terminally to a GST-tag. Once the PreScission protease is added to the reaction, HTT starts its fibrilization, bringing the fluorophores together and producing a FRET signal. **B.** TEM images and accompanying schematics of the fibril formed by HTT, and the absence of these in the presence of chaperones after 24 hours. **C.** FRET analysis of HTT fibrillization: flat line represents suppression, sigmoidal curve represents full fibrilization, and curves in between point to partial suppression of aggregation. i) the DNAJB1/HSP70/APG2 trimeric complex exclusively suppresses fully HTT fibrilization; ii) nematode orthologs of the human trimeric complex also fully suppress HTT fibrilization; iii) a precise concentration of the co-chaperone DNAJB1 is necessary to achieve full suppression. **D.** TEM images and experimental schematic of the disaggregation process: after 20 hours, chaperones re-solubilize fully formed HTT fibrils. **E.** Filter retardation assay analysing the effective disaggregation activity of the chaperones over time, and correspondent quantification. Figures have been adapted from the publication by Scior *et al.* [69].

aggregation, HTTEx1-CyPet/YPet moieties were recombinantly purified attached to a GST-tag (Fig. 7A). The GST-tag aids in purification, maintains the HTT soluble and thus inhibits its spontaneous aggregation: initiation of fibril formation only occurs when the GST is cleaved by addition of a site-specific protease. This FRET assay thus allows high

temporal control and straightforward and robust interpretation of aggregation and becomes especially apt to study the impact of chaperones on amyloid formation (Fig. 7B). A complex of human chaperones comprising the chaperones Hsc70, the co-chaperone DNAJB1 and the nucleotide exchange factor APG2 (NEF), which was previously identified as disaggregating α-synuclein *in vitro* [102], was tested first in the FRET based HTT aggregation assay. In the presence of individual members of the trimeric complex, regardless of their concentration, HTT fibrillization occurred 'normally', as if no other factor was present in the reaction (Fig. 7C-i). Similarly, the presence of Hsc70 and DNAJB1 only resulted in partial suppression and a delay in aggregation. Finally, inclusion of Hsc70, DNAJB1 and APG2 resulted in the complete suppression of HTT fibrillization for a prolonged period of time. Importantly, the trimeric complex was always in excess of HTT and found to be optimally functional at a precise stoichiometry (Fig. 7C-i). To investigate if the ability of this complex was conserved throughout metazoans, the *C. elegans* orthologs of the human trimeric complex members were also tested in their ability to suppress HTT fibrillization [103]. Complete suppression was also observed in the presence of the complex composed of HSP-1, DNJ13 and HSP-110, albeit with slightly diverse chaperones to HTT concentrations (Fig. 7C-ii). Regardless of the origin of the chaperone protein, it emerged that the suppression process was absolutely dependent on the presence ATP, and the ATPase activity of HSP-70/HSP-1, and only optimally functional when inclusive of the bulky nucleotide exchange factor APG2/HSP-110 (Fig. 7C-ii). Moreover, many combinations of chaperones and co-chaperones were tested to establish the most potent suppressors. While several compositions of trimeric complex were less effective to various degrees, it became evident that the concentration and identity of the Hsp40 cochaperone is the limiting factor for fibril suppression, possibly due to its client selection and binding capacity (Fig. 7C-iii). Remarkably, and here described for the first time, the same chaperone members were found to be responsible for active re-solubilisation, or disaggregation, of preformed HTT fibrils (Fig. 7D). The combined presence of Hsc70/HSP-1, DNAJB1/DNJ13 and APG2/HSP-110 was able, via the conjunct ATP-dependent action of both HSC70/HSP-1 and APG2/HSP-110, to substantially remodel and take apart HTT moieties (Fig. 7E).

To validate the power of the trimeric complex, the *in vitro* results of HTT fibril suppression/disaggregation needed to be confirmed *in vivo* and *ex vivo*. Once again, the *C. elegans* model system, in combination with light microscopy and RNAi techniques,

was employed to study the effects of the trimeric complex chaperones of aggregation *in vivo*. siRNA-mediated knockdown of the chaperons was performed in nematode strains containing YFP-tagged fusion constructs of either HTT or ataxin (ATX) [104]. HTT and ATX are respectively responsible for HD and spinocerebellar ataxia and, when overexpressed in the nematode, mimic their aggregation patterns during aging. Upon individual knockdown of the nematode specific chaperones, HSP-1, DNJ-13 or HSP-110, the formation of large polyQ aggregates was increased compared to control, suggesting the involvement of these chaperones in maintaining solubility of HTT or ATX *in vivo* (Fig. 8A). To further substantiate these results in a clinically relevant model, the effects of the human trimeric complex were tested in neuronal progenitor cells (NPC) reprogrammed from HD patient [105]. siRNA induced knockdown in NPCs of DNAJB1 and, separately, APG2, resulted in a pronounced increase in HTT aggregation load (Fig. 8B).

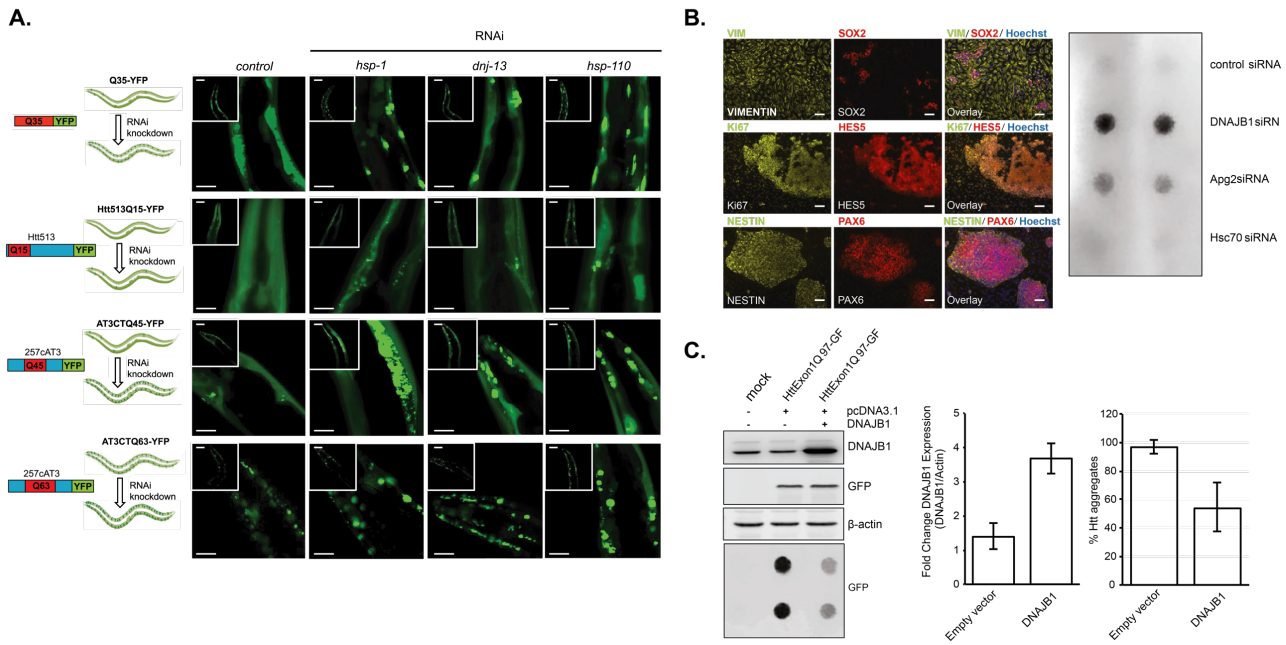


**Figure 8. *In vivo* validation of the impact of the chaperone on aggregation**
**A.** Schematic and confocal images of *C. elegans* strains subjected to depletion of chaperones via RNAi knockdown. Strains investigated include two ND models and a control. All stains showed significant increase in foci formation upon knockdown of the trimeric chaperone complex components. **B.** Characterization of neuronal progenitor cell derived from reprogrammed pluripotent stem cells from HD patients. NPC express the specific markers for their lineage**.** Filter retardation analysis of the effect of siRNA-mediated knockdown of the trimeric complex in NPCs shows that aggregation of endogenous HTT is exacerbated upon depletion of the DNAJB1. **C.** Western blot and filter trap analysis of the aggregation propensity upon upregulation of DNAJB1 in an overexpression cell model of HTTQ97-GFP. Upon overexpression of the co-chaperone DNAJB1 the aggregated fraction of HTT is significantly reduced. Quantification of these experiments is shown in the bar graphs on the right. All figures have been adapted from the publication by Scior *et al.*[69].

Conversely, overexpression of DNAJB1 alone in mammalian cultures overexpressing toxic variants of HTT exhibited a rescue effect, and by interacting with HTT, reduced it aggregation propensity. In agreement with its role played *in vitro*, DNAJB1 thus confirms itself as a key chaperone capable, in cooperation with Hsp70 and APG2, of preventing HTT aggregation, promoting suppression and possibly ameliorating aggregation-induced cytotoxicity (Fig. 8C). Suppression and disaggregation were also confirmed *in vitro* by complementary biochemical assays such as the filter retardation assay or sedimentation analysis, and by visualisation of both fibrils and monomers/oligomers via transmission electron microscopy (TEM), and immunogold labelling followed by TEM for colocalization of chaperones with HTT fibrils. For *in vivo* assays extensive immunohistochemistry coupled with light microscopy was performed. Although the trimeric complex function has been comprehensively characterised, its relevance at an organismal level, and its specific involvement in neurons is still missing. Nevertheless, the combination of all reported assays, from *in vitro*, to *ex vivo*, and *in vivo*, conclusively establishes the trimeric complex as a powerful player of the PN, capable of maintaining HTT solubility and functionality, and preventing it from forming off-pathway intermediates and harmful aggregates [106]. Information on the exact binding sites between chaperones and their oligomeric/protofibrillar structures, or with the monomers, if different, is however still unknown. Unmasking these domains would yield important information on which domain to target to boost the PN. The PN´s singular capability to disaggregate and reshape the aggregation landscape further make the trimeric complex a desirable target of therapeutic potential.

### *III. Clinical applications and future questions*

The strength of all techniques here described lays in their translational potential. To this date there is still no cure for any ND. Although NDs are heavily studied interdisciplinary, the lack of a full understanding of their mechanistic aetiology has restricted therapeutic intervention [10]. Highlighting the complexities of these disorders, is the failure of strategies that show great potential in animal models, only to be terminated as ineffective, or even counterproductive, in clinical trials. Many drugs have been developed, based on either biological agents (i.e. monoclonal antibodies) or chemical compounds, to stop the production of disease-relevant protein [107]. Recently a new class of drugs based on RNA interference has reported success for both HD and ALS. This approach utilises antisense oligonucleotides (ASOs) which bind and degrade messenger RNA resulting in dose-dependent reduction in protein levels. Great promise also lies in the application of genome-editing CRISPR-Cas9 technology, especially for monogenic disorders such as HD, where cutting out glutamines from the expanded allele would effectively abolish the disorder [108]. Finally, modulation of the PN to enhance its cellular quality control to maintain protein homeostasis is a fundamental therapeutic strategy. To reinforce the natural cellular defences, activators, enhancers, inhibitors and repressors of various components of the PN are all being continuously developed [109].

In this scenario, the methodologies and results described in this research summary may prove useful (Fig. 9). The *in vitro* FRET assays can be employed in large-scale small-molecule screens to identify novel synthetic or biological compounds that prevent or promote aggregation both in the presence or absence of the powerful trimeric chaperone complex. The mechanism of any ‘hit’ can then be assessed biochemically or via cellular models to establish whether they function, for example, by direct fibril binding or by boosting the singular or synergistic activity of chaperones. For further testing at an organismal level, or indeed rescan the libraries of available compounds, the *C. elegans* model can be once again utilised. Several strains of nematodes expressing disease-relevant proteins are already available that reproduce characteristic NDs features, as for example the newly generated HTT-expressing strains described here, which exhibit large aggregate formation alongside reduced proteostasis activity [110]. With the use of FLIM, and its ability to visualise the presence of soluble, oligomeric and insoluble material live and over time, the impact of any pharmacological intervention can be monitored live to

distinguish between aggregation-enhancing and aggregation-reducing tactics. Similarly, useful, is the employment of photo conversion to trace the turnover of any disease-relevant protein. Testing *in vivo* the power of selected compounds in enhancing or slowing clearance of toxic proteins becomes easily quantifiable and can be a guideline on which substances show most promising future results. Furthermore, *C. elegans* phenotypic readouts can provide information on the efficacy of combinatorial drug-treatments that together improve energy metabolism, immune response, and diminish aggregate load [111].

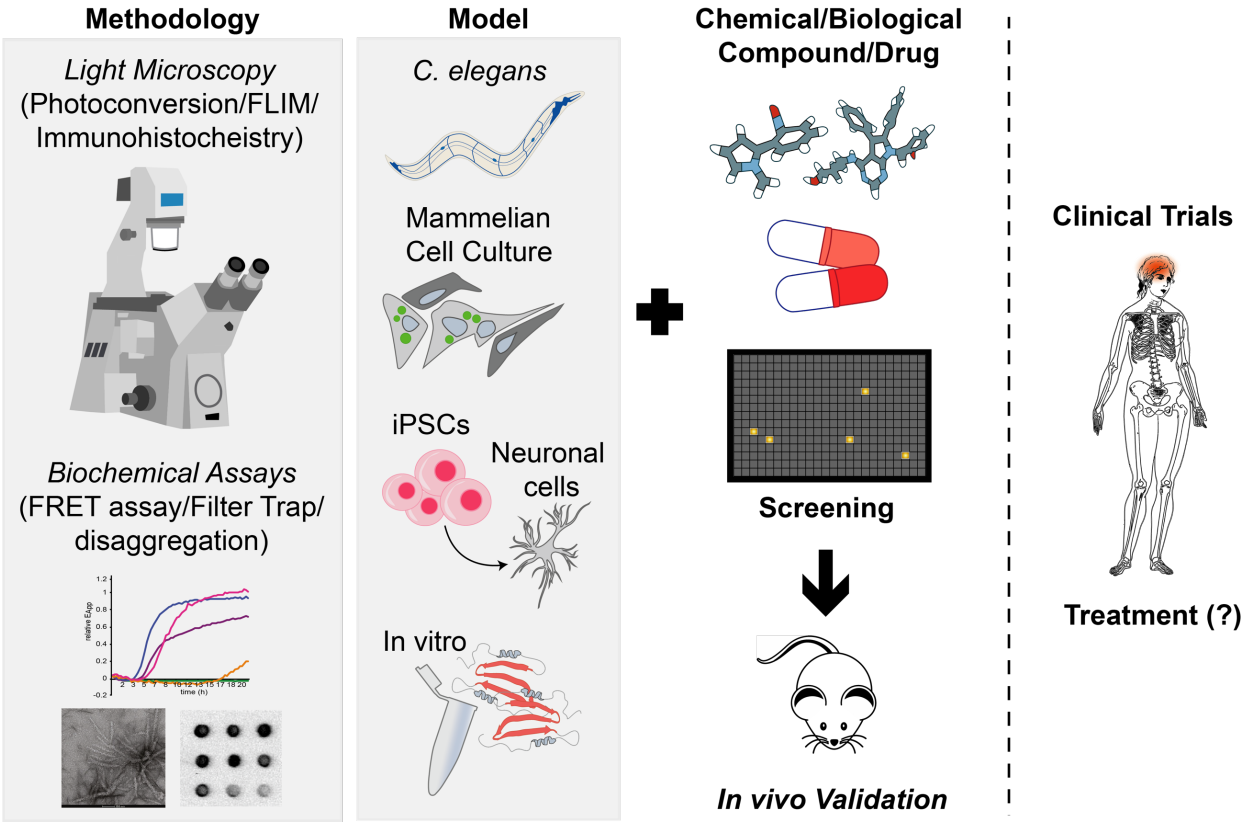


**Figure 9. Complementary methodology and model systems allow for screening of future effective treatments for neurodegenerative disorders.**
Illustration represents the potential therapeutic applications of the methodologies described in this synopsis. Novel light microscopy techniques alongside biochemical assays are combined with various *in vitro*, cellular and organismal models to screen compounds for their effectiveness. Promising targets can then be validated in higher mammals before being tested in clinical trials. Ultimately, all strategies are aimed at discovering a treatment for neurogenerative disorders.

The field of protein aggregation has developed greatly in the past 20 years and technical advancements have recently brought breakthrough in the structural characterisation of amyloid fibrils and their building block. Notwithstanding, the relationship between structure-function-pathogenesis is still poorly understood and the discovery of fibril polymorphism and related toxic species has added a layer of complexity to current understanding. Exactly how much pathology is caused by monomer, oligomers or amyloids and what is the contribution of the vasculature, microbiome or immune response is still unknown or underappreciated. Finally, just how these toxic structures interplay with and impede the proteostasis network, and how can they impact neurons selectively, in the context of an aging organism, is still unclear. All are fundamental, yet unanswered, questions towards understanding and solving the riddle of neurodegeneration.

## *IV. Personal Contribution*

The work described herein was performed throughout my years as a doctoral student in the laboratory of Prof. Dr. Janine Kirstein, under the joint supervision of Prof. Dr. Ralf Schülein at the Leibniz-Forschungsinstitut für Molekulare Pharmakologie im Forschungsverbund Berlin e.V. (FMP). The experimental work of the first publication *´In vivo quantification of protein turnover in aging C. elegans using photoconvertible Dendra2`* was entirely performed by myself, and the conception and writing of the manuscript was performed in collaboration with Janine Kirstein. The work included the creation of novel *C. elegans* lines and extensive testing and optimisation of the imaging technique. The idea behind the second publication *´Characterisation of amyloid structures in aging C. elegans using fluorescence lifetime imaging*' was conceived by Christian Gallrein, Janine Kirstein and myself; experiments and analysis were performed by the first co-authors, while the manuscript was written by me, with oversight from Janine Kirstein. The *C. elegans* FLIM technique was newly introduced and set-up at our institute after I learned it during a short fellowship at Cambridge University. Importantly, both articles are accompanied by online visual guides in the form of a video, which were scripted by me, and acted by all co-authors. Finally, the publication *´Complete suppression of HTT fibrilization and disaggregation of HTT fibrils by a trimeric chaperone complex´* was the result of an extensive inter and intra-laboratory collaboration and my contribution was mainly related to obtaining and analysing empirical data. Several questions related to this publication subsequently became part of my own doctoral investigation.

## *V. Bibliography*


[1] Prince M, Bryce R, Albanese E, Wimo A, Ribeiro W, Ferri CP. The global prevalence of dementia: A systematic review and metaanalysis. Alzheimer's Dement (2013);9:63-75.e2.

[2] Hou Y, Dan X, Babbar M, Wei Y, Hasselbalch SG, Croteau DL, Bohr VA. Ageing as a risk factor for neurodegenerative disease. Nat Rev Neurol (2019);15:565–81.

[3] Castillo X, Castro-Obregón S, Gutiérrez-Becker B, Gutiérrez-Ospina G, Karalis N, Khalil AA, Lopez-Noguerola JS, Rodríguez LL, Martínez-Martínez E, Perez-Cruz C, Pérez-Velázquez J, Piña AL, Rubio K, García HPS, Syeda T, Vanoye-Carlo A, Villringer A, Winek K, Zille M. Re-thinking the etiological framework of neurodegeneration. Front Neurosci (2019);13:1–25.

[4] Scheiblich H, Trombly M, Ramirez A, Heneka MT. Neuroimmune Connections in Aging and Neurodegenerative Diseases. Trends Immunol (2020):1–13.

[5] Cunnane SC, Trushina E, Morland C, Prigione A, Casadesus G, Andrews ZB, Beal MF, Bergersen LH, Brinton RD, de la Monte S, Eckert A, Harvey J, Jeggo R, Jhamandas JH, Kann O, la Cour CM, Martin WF, Mithieux G, Moreira PI, Murphy MP, Nave KA, Nuriel T, Oliet SHR, Saudou F, Mattson MP, Swerdlow RH, Millan MJ. Brain energy rescue: an emerging therapeutic concept for neurodegenerative disorders of ageing. Nat Rev Drug Discov (2020);19:609–33.

[6] Fu H, Hardy J, Duff KE. Selective vulnerability in neurodegenerative diseases. Nat Neurosci (2018);21:1350–8.

[7] Soto C, Pritzkow S. Protein misfolding, aggregation, and conformational strains in neurodegenerative diseases. Nat Neurosci (2018);21:1332–40.

[8] Ross CA, Poirier MA. Protein aggregation and neurodegenerative disease. Nat Med (2004).

[9] Linding R, Schymkowitz J, Rousseau F, Diella F, Serrano L. A comparative study of the relationship between protein structure and β-aggregation in globular and intrinsically disordered proteins. J Mol Biol (2004);342:345–53.

[10] Ke PC, Zhou R, Serpell LC, Riek R, Knowles TPJ, Lashuel HA, Gazit E, Hamley IW, Davis TP, Fändrich M, Otzen DE, Chapman MR, Dobson CM, Eisenberg DS, Mezzenga R. Half a century of amyloids: Past, present and future. Chem Soc Rev (2020);49:5473–509.

[11] Dobson CM. Protein folding and misfolding. Nature (2003);426:884–90.

[12] Nelson R, Sawaya MR, Balbirnie M, Madsen A, Riekel C, Grothe R, Eisenberg D. Structure of the cross-β spine of amyloid-like fibrils. Nature (2005);435:773–8.

[13] Sawaya MR, Sambashivan S, Nelson R, Ivanova MI, Sievers SA, Apostol MI, Thompson MJ, Balbirnie M, Wiltzius JJW, McFarlane HT, Madsen AØ, Riekel C, Eisenberg D. Atomic structures of amyloid cross-β spines reveal varied steric zippers. Nature (2007);447:453–7.

[14] Morris AM, Watzky MA, Finke RG. Protein aggregation kinetics, mechanism, and curve-fitting: A review of the literature. Biochim Biophys Acta - Proteins Proteomics (2009);1794:375–97.

[15] Almeida ZL, Brito RMM. Structure and Aggregation Mechanisms in Amyloids (2020).
[16] Musiek ES, Holtzman DM. Three dimensions of the amyloid hypothesis: Time, space and “wingmen.” Nat Neurosci (2015);18:800–6.
[17] Otzen D, Riek R. Functional amyloids. Cold Spring Harb Perspect Biol (2019);11.
[18] Cline EN, Bicca MA, Viola KL, Klein WL. The Amyloid-β Oligomer Hypothesis: Beginning of the Third Decade. J Alzheimer’s Dis (2018);64:S567–610.
[19] Glabe CG. Structural classification of toxic amyloid oligomers. J Biol Chem (2008);283:29639–43.
[20] Michaels TCT, Šarić A, Curk S, Bernfur K, Arosio P, Meisl G, Dear AJ, Cohen SIA, Dobson CM, Vendruscolo M, Linse S, Knowles TPJ. Dynamics of oligomer populations formed during the aggregation of Alzheimer’s Aβ42 peptide. Nat Chem (2020);12:445–51.
[21] Ciudad S, Puig E, Botzanowski T, Meigooni M, Arango AS, Do J, Mayzel M, Bayoumi M, Chaignepain S, Maglia G, Cianferani S, Orekhov V, Tajkhorshid E, Bardiaux B, Carulla N. Aβ(1-42) tetramer and octamer structures reveal edge conductivity pores as a mechanism for membrane damage. Nat Commun (2020);11:1–14.
[22] Tipping KW, van Oosten-Hawle P, Hewitt EW, Radford SE. Amyloid Fibres: Inert End-Stage Aggregates or Key Players in Disease? Trends Biochem Sci (2015);40:719–27.
[23] Brundin P, Melki R, Kopito R. Prion-like transmission of protein aggregates in neurodegenerative diseases. Nat Rev Mol Cell Biol (2010);11:301–7.
[24] Fitzpatrick AWP, Falcon B, He S, Murzin AG, Murshudov G, Garringer HJ, Crowther RA, Ghetti B, Goedert M, Scheres SHW. Cryo-EM structures of tau filaments from Alzheimer’s disease. Nature (2017);547:185–90.
[25] Guerrero-Ferreira R, Taylor NMI, Mona D, Ringler P, Lauer ME, Riek R, Britschgi M, Stahlberg H. Cryo-EM structure of alpha-synuclein fibrils. Elife (2018);7:1–18.
[26] Li D, Liu C. Hierarchical chemical determination of amyloid polymorphs in neurodegenerative disease. Nat Chem Biol (2021).
[27] Anfinsen CB. Principles that Govern the Folding of Protein Chains. vol. 181. 1973.
[28] Ellis RJ, Minton AP. Protein aggregation in crowded environments. Biol Chem (2006);387:485–97.
[29] Balchin D, Hayer-Hartl M, Hartl FU. In vivo aspects of protein folding and quality control. Science (80- ) (2016);353.
[30] Klaips CL, Jayaraj GG, Hartl FU. Pathways of cellular proteostasis in aging and disease. J Cell Biol (2018);217:51–63.
[31] Jayaraj GG, Hipp MS, Ulrich Hartl F. Functional modules of the proteostasis network. Cold Spring Harb Perspect Biol (2020);12.
[32] Taylor RC, Dillin A. Aging as an event of proteostasis collapse. Cold Spring Harb Perspect Biol (2011);3:1–17.
[33] Sala AJ, Bott LC, Morimoto RI. Shaping proteostasis at the cellular, tissue, and organismal level. J Cell Biol (2017);216:1231–41.
[34] Brehme M, Voisine C, Rolland T, Wachi S, Soper JH, Zhu Y, Orton K, Villella A,

Garza D, Vidal M, Ge H, Morimoto RI. A chaperome subnetwork safeguards proteostasis in aging and neurodegenerative disease. Cell Rep (2014);9:1135–50.
[35] Kampinga HH, Craig EA. The HSP70 chaperone machinery: J proteins as drivers of functional specificity. Nat Rev Mol Cell Biol (2010);11:579–92.
[36] Young JC, Agashe VR, Siegers K, Hartl FU. Pathways of chaperone-mediated protein folding in the cytosol. Nat Rev Mol Cell Biol (2004);5:781–91.
[37] Mannini B, Chiti F. Chaperones as Suppressors of Protein Misfolded Oligomer Toxicity. Front Mol Neurosci (2017);10:1–8.
[38] Nillegoda NB, Wentink AS, Bukau B. Protein Disaggregation in Multicellular Organisms. Trends Biochem Sci (2018);43:285–300.
[39] Nillegoda NB, Kirstein J, Szlachcic A, Berynskyy M, Stank A, Stengel F, Arnsburg K, Gao X, Scior A, Aebersold R, Guilbride DL, Wade RC, Morimoto RI, Mayer MP, Bukau B. Crucial HSP70 co-chaperone complex unlocks metazoan protein disaggregation. Nature (2015);524:247–51.
[40] Olzscha H, Schermann SM, Woerner AC, Pinkert S, Hecht MH, Tartaglia GG, Vendruscolo M, Hayer-Hartl M, Hartl FU, Vabulas RM. Amyloid-like aggregates sequester numerous metastable proteins with essential cellular functions. Cell (2011);144:67–78.
[41] Boland B, Yu WH, Corti O, Mollereau B, Henriques A, Bezard E, Pastores GM, Rubinsztein DC, Nixon RA, Duchen MR, Mallucci GR, Kroemer G, Levine B, Eskelinen EL, Mochel F, Spedding M, Louis C, Martin OR, Millan MJ. Promoting the clearance of neurotoxic proteins in neurodegenerative disorders of ageing. Nat Rev Drug Discov (2018);17:660–88.
[42] Orr H, Zoghbi H. Trinucleotide repeat disorders. Annu Rev Neurosci (2007);30:1114–22.
[43] Huntington G. On Chorea. J Neuropsychiatry Clin Neurosci (2003);15:109–12.
[44] Gusella JF, Wexler NS, Conneally PM, Naylor SL, Anderson MA, Tanzi RE, Watkins PC, Ottina K, Wallace MR, Sakaguchi AY, Young AB, Shoulson I, Bonilla E, Martin JB. A polymorphic DNA marker genetically linked to Huntington's disease. Nature (1983);306:234–8.
[45] Macdonald ME, Ambrose CM, Duyao MP, Myers RH, Lin C, Srinidhi L, Barnes G, Taylor SA, James M, Groat N, Macfarlane H, Jenkins B, Anderson MA, Wexler NS, Gusella JF, Riba-ramirer L, Shah M, Stanton VP, Strobel SA, Draths KM, Wales JL, Dervan P, Housman DE, Fielder T, Wasmuth JJ, Bates GP, Baxendale S, Hummerich H, Kirby S, North M, Youngman S, Mott R, Zehetner G, Sedlacek Z, Lehrach H, Tagle D, Valdes J, Elmer L, Allard M, Castilla L, Swaroop M, Blanchard K, Snell R, Holloway T, Gillespie K, Datson N, Shaw D, Harper PS. A novel gene containing a trinucleotide repeat that is expanded and unstable on Huntington's disease chromosomes. Cell (1993);72:971–83.
[46] Wright GEB, Black HF, Collins JA, Gall-Duncan T, Caron NS, Pearson CE, Hayden MR. Interrupting sequence variants and age of onset in Huntington's disease: clinical implications and emerging therapies. Lancet Neurol (2020);19:930–9.
[47] Jones L, Houlden H, Tabrizi SJ. DNA repair in the trinucleotide repeat disorders. Lancet Neurol (2017).

[48] Walker FO. Huntington's disease. Lancet (2007);369:218–28.
[49] Bates GP, Dorsey R, Gusella JF, Hayden MR, Kay C, Leavitt BR, Nance M, Ross CA, Scahill RI, Wetzel R, Wild EJ, Tabrizi SJ. Huntington disease. Nat Rev Dis Prim (2015);1:15005.
[50] Cattaneo E, Zuccato C, Tartari M. Normal huntingtin function: An alternative approach to Huntington's disease. Nat Rev Neurosci (2005).
[51] Barnat M, Capizzi M, Aparicio E, Boluda S, Wennagel D, Kacher R, Kassem R, Lenoir S, Agasse F, Bra BY, Liu JP, Ighil J, Tessier A, Zeitli SO, Duyckaerts C, Dommergues M, Durr A, Humbert S. Huntington's disease alters human neurodevelopment. Science (80- ) (2020);369:787–93.
[52] Zuccato C. Loss of Huntingtin-Mediated BDNF Gene Transcription in Huntington's Disease. Science (80- ) (2001);293:493–8.
[53] Saudou F, Humbert S. The Biology of Huntingtin. Neuron (2016);89:910–26.
[54] Graham RK, Deng Y, Slow EJ, Haigh B, Bissada N, Lu G, Pearson J, Shehadeh J, Bertram L, Murphy Z, Warby SC, Doty CN, Roy S, Wellington CL, Leavitt BR, Raymond LA, Nicholson DW, Hayden MR. Cleavage at the Caspase-6 Site Is Required for Neuronal Dysfunction and Degeneration Due to Mutant Huntingtin. Cell (2006);125:1179–91.
[55] Zuccato C, Valenza M, Cattaneo E. Molecular Mechanisms and Potential Therapeutical Targets in Huntington ' s Disease. Physiol Rev (2010);90:905–81.
[56] Neueder A, Dumas AA, Benjamin AC, Bates GP. Regulatory mechanisms of incomplete huntingtin mRNA splicing. Nat Commun (2018).
[57] Perutz MF, Johnson T, Suzuki M, Finch JT. Glutamine repeats as polar zippers: their possible role in inherited neurodegenerative diseases. Proc Natl Acad Sci (1994);91:5355–8.
[58] Davies SW, Turmaine M, Cozens B a, DiFiglia M, Sharp a H, Ross C a, Scherzinger E, Wanker EE, Mangiarini L, Bates GP. Formation of neuronal intranuclear inclusions underlies the neurological dysfunction in mice transgenic for the HD mutation. Cell (1997);90:537–48.
[59] Saudou F, Finkbeiner S, Devys D, Greenberg ME. Huntingtin acts in the nucleus to induce apoptosis but death does not correlate with the formation of intranuclear inclusions. Cell (1998);95:55–66.
[60] Bäuerlein FJB, Saha I, Mishra A, Kalemanov M, Martínez-Sánchez A, Klein R, Dudanova I, Hipp MS, Hartl FU, Baumeister W, Fernández-Busnadiego R. In Situ Architecture and Cellular Interactions of PolyQ Inclusions. Cell (2017).
[61] Arrasate M, Mitra S, Schweitzer ES, Segal MR, Finkbeiner S. Inclusion body formation reduces levels of mutant huntingtin and the risk of neuronal death. Nature (2004);431:805–10.
[62] Kim YE, Hosp F, Frottin F, Ge H, Mann M, Hayer-Hartl M, Hartl FU. Soluble Oligomers of PolyQ-Expanded Huntingtin Target a Multiplicity of Key Cellular Factors. Mol Cell (2016);63:951–64.
[63] Behrends C, Langer CA, Boteva R, Böttcher UM, Stemp MJ, Schaffar G, Rao BV, Giese A, Kretzschmar H, Siegers K, Hartl FU. Chaperonin TRiC Promotes the Assembly of polyQ Expansion Proteins into Nontoxic Oligomers. Mol Cell

(2006);23:887–97.
[64] Muchowski PJ, Schaffar G, Sittler A, Wanker EE, Hayer-Hartl MK, Hartl FU. Hsp70 and Hsp40 chaperones can inhibit self-assembly of polyglutamine proteins into amyloid-like fibrils. Proc Natl Acad Sci (2000);97:7841–6.
[65] Chaperone AD, Hageman J, Rujano MA, Waarde MAWH Van, Kakkar V, Dirks RP, Govorukhina N, Oosterveld-hut HMJ, Lubsen NH, Kampinga HH. Article Activities Suppresses Toxic Protein Aggregation. Mol Cell (2010);37:355–69.
[66] Tabrizi SJ, Flower MD, Ross CA, Wild EJ. Huntington disease: new insights into molecular pathogenesis and therapeutic opportunities. Nat Rev Neurol (2020);16:529–46.
[67] Pigazzini ML, Kirstein J. In Vivo Quantification of Protein Turnover in Aging C. Elegans using Photoconvertible Dendra2. J Vis Exp (2020);160:1–18.
[68] Pigazzini ML, Gallrein C, Iburg M, Kaminski Schierle G, Kirstein J. Characterization of Amyloid Structures in Aging C. Elegans Using Fluorescence Lifetime Imaging. J Vis Exp (2020);157:1–11.
[69] Scior A, Buntru A, Arnsburg K, Ast A, Iburg M, Juenemann K, Pigazzini ML, Mlody B, Puchkov D, Priller J, Wanker EE, Prigione A, Kirstein J. Complete suppression of Htt fibrilization and disaggregation of Htt fibrils by a trimeric chaperone complex. EMBO J (2018);37:282–99.
[70] Alexander AG, Marfil V, Li C. Use of C. elegans as a model to study Alzheimer's disease and other neurodegenerative diseases. Front Genet (2014).
[71] Cook SJ, Jarrell TA, Brittin CA, Wang Y, Bloniarz AE, Yakovlev MA, Nguyen KCQ, Tang LTH, Bayer EA, Duerr JS, Bülow HE, Hobert O, Hall DH, Emmons SW. Whole-animal connectomes of both Caenorhabditis elegans sexes. Nature (2019);571:63–71.
[72] Kikis EA. The struggle by Caenorhabditis elegans to maintain proteostasis during aging and disease. Biol Direct (2016);11:58.
[73] Ben-Zvi A, Miller EA, Morimoto RI. Collapse of proteostasis represents an early molecular event in Caenorhabditis elegans aging. Proc Natl Acad Sci U S A (2009);106:14914–9.
[74] Kamath RS, Martinez-Campos M, Zipperlen P, Fraser AG, Ahringer J. Effectiveness of specific RNA-mediated interference through ingested double-stranded RNA in Caenorhabditis elegans. Genome Biol (2001);2:RESEARCH0002.
[75] Breimann L, Preusser F, Preibisch S. Light-microscopy methods in C. elegans research. Curr Opin Syst Biol (2019);13:82–92.
[76] Chalfie M, Tu Y, Euskirchen G, Ward W, Prasher D. Green fluorescent protein as a marker for gene expression. Science (80- ) (1994);263:802–5.
[77] Tsien RY. the Green Fluorescent Protein. Annu Rev Biochem (1998);67:509–44.
[78] Lippincott-Schwartz J, Patterson GH. Fluorescent Proteins for Photoactivation Experiments. Methods Cell Biol (2008);85:45–61.
[79] Chudakov DM, Lukyanov S, Lukyanov KA. Tracking intracellular protein movements using photoswitchable fluorescent proteins PS-CFP2 and Dendra2. Nat Protoc (2007);2:2024–32.

[80] Gurskaya NG, Verkhusha V V., Shcheglov AS, Staroverov DB, Chepurnykh T V., Fradkov AF, Lukyanov S, Lukyanov KA. Engineering of a monomeric green-to-red photoactivatable fluorescent protein induced by blue light. Nat Biotechnol (2006);24:461–5.
[81] Zhang L, Gurskaya NG, Merzlyak EM, Staroverov DB, Mudrik NN, Samarkina ON, Vinokurov LM, Lukyanov S, Lukyanov KA. Method for real-time monitoring of protein degradation at the single cell level. Biotechniques (2007);42:446–50.
[82] Hamer G, Matilainen O, Holmberg CI. A photoconvertible reporter of the ubiquitin-proteasome system in vivo. Nat Methods (2010);7:473–8.
[83] Labbadia J, Morimoto RI. Huntington's disease: underlying molecular mechanisms and emerging concepts. Trends Biochem Sci (2013);38:378–85.
[84] Feleciano DR, Juenemann K, Iburg M, Brás IC, Holmberg CI, Kirstein J. Crosstalk between chaperone-mediated protein disaggregation and proteolytic pathways in aging and disease. Front Aging Neurosci (2019);11.
[85] Tsvetkov AS, Arrasate M, Barmada S, Ando DM, Sharma P, Shaby BA, Finkbeiner S. Proteostasis of polyglutamine varies among neurons and predicts neurodegeneration. Nat Chem Biol (2013);9:586–94.
[86] Barmada SJ, Serio A, Arjun A, Bilican B, Daub A, Ando DM, Tsvetkov A, Pleiss M, Li X, Peisach D, Shaw C, Chandran S, Finkbeiner S. Autophagy induction enhances TDP43 turnover and survival in neuronal ALS models. Nat Chem Biol (2014);10:677–85.
[87] Chudakov DM, Matz M V., Lukyanov S, Lukyanov KA. Fluorescent proteins and their applications in imaging living cells and tissues. Physiol Rev (2010);90:1103–63.
[88] Becker W. Fluorescence lifetime imaging - techniques and applications. J Microsc (2012);247:119–36.
[89] Lakowicz JR. Principles of Fluorescence Spectroscopy. Boston, MA: Springer US; 2006.
[90] Datta R, Heaster TM, Sharick JT, Gillette AA, Skala MC. Fluorescence lifetime imaging microscopy: fundamentals and advances in instrumentation, analysis, and applications. J Biomed Opt (2020);25:1.
[91] Berezin MY, Achilefu S. Fluorescence lifetime measurements and biological imaging. Chem Rev (2010);110:2641–84.
[92] Laine RF, Sinnige T, Ma KY, Haack AJ, Poudel C, Gaida P, Curry N, Perni M, Nollen EAA, Dobson CM, Vendruscolo M, Kaminski Schierle GS, Kaminski CF. Fast Fluorescence Lifetime Imaging Reveals the Aggregation Processes of α-Synuclein and Polyglutamine in Aging Caenorhabditis elegans. ACS Chem Biol (2019);14:1628–36.
[93] Kaminski Schierle GS, Bertoncini CW, Chan FTS, Van Der Goot AT, Schwedler S, Skepper J, Schlachter S, Van Ham T, Esposito A, Kumita JR, Nollen EAA, Dobson CM, Kaminski CF. A FRET sensor for non-invasive imaging of amyloid formation in vivo. ChemPhysChem (2011);12:673–80.
[94] Chan FTS, Pinotsi D, Kaminski Schierle GS, Kaminski CF. Structure-Specific Intrinsic Fluorescence of Protein Amyloids Used to Study their Kinetics of

Aggregation. Bio-nanoimaging Protein Misfolding Aggreg., 2013, p. 147–55.
[95] Li J, Le W. Modeling neurodegenerative diseases in Caenorhabditis elegans. Exp Neurol (2013);250:94–103.
[96] Moronetti Mazzeo LE, Dersh D, Boccitto M, Kalb RG, Lamitina T. Stress and aging induce distinct polyQ protein aggregation states. Proc Natl Acad Sci U S A (2012);109:10587–92.
[97] Morley JF, Brignull HR, Weyers JJ, Morimoto RI. The threshold for polyglutamine-expansion protein aggregation and cellular toxicity is dynamic and influenced by aging in Caenorhabditis elegans. Proc Natl Acad Sci U S A (2002);99:10417–22.
[98] Suhling K, Hirvonen LM, Levitt JA, Chung PH, Tregidgo C, Le Marois A, Rusakov DA, Zheng K, Ameer-Beg S, Poland S, Coelho S, Henderson R, Krstajic N. Fluorescence lifetime imaging (FLIM): Basic concepts and some recent developments. Med Photonics (2015);27:3–40.
[99] Suhling K, French MW, Phillips D. Time-resolved fluorescence microscopy† (2005);4:13–22.
[100] Becker W, Su B, Holub O, weisshart K. FLIM and FCS detection in laser-scanning microscopes: Increased efficiency by GaAsP hybrid detectors. Microsc Res Tech (2011);74:804–11.
[101] Nguyen AW, Daugherty PS. Evolutionary optimization of fluorescent proteins for intracellular FRET. Nat Biotechnol (2005);23:355–60.
[102] Rampelt H, Kirstein-Miles J, Nillegoda NB, Chi K, Scholz SR, Morimoto RI, Bukau B. Metazoan Hsp70 machines use Hsp110 to power protein disaggregation. EMBO J (2012);31:4221–35.
[103] Nikolaidis N, Nei M. Concerted and Nonconcerted Evolution of the Hsp70 Gene Superfamily in Two Sibling Species of Nematodes. Mol Biol Evol (2004);21:498–505.
[104] Christie NTM, Lee AL, Fay HG, Gray AA, Kikis EA. Novel Polyglutamine Model Uncouples Proteotoxicity from Aging. PLoS One (2014);9:e96835.
[105] The HD iPSC Consortium. Induced Pluripotent Stem Cells from Patients with Huntington's Disease Show CAG-Repeat-Expansion-Associated Phenotypes. Cell Stem Cell (2012);11:264–78.
[106] Scior A, Juenemann K, Kirstein J. Cellular strategies to cope with protein aggregation. Essays Biochem (2016).
[107] Eisele YS, Monteiro C, Fearns C, Encalada SE, Wiseman RL, Powers ET, Kelly JW. Targeting protein aggregation for the treatment of degenerative diseases. Nat Rev Drug Discov (2015);14:759–80.
[108] Wild EJ, Tabrizi SJ. Therapies targeting DNA and RNA in Huntington's disease. Lancet Neurol (2017).
[109] Balch WE, Morimoto RI, Dillin A, Kelly JW. Adapting Proteostasis for Disease Intervention. n.d.
[110] Labbadia J, Morimoto RI. The Biology of Proteostasis in Aging and Disease. Annu Rev Biochem (2015).
[111] O'Reilly LP, Luke CJ, Perlmutter DH, Silverman GA, Pak SC. C. elegans in high-throughput drug discovery. Adv Drug Deliv Rev (2014);69–70:247–53.

## 6. Statutory Declaration

"I, Maria Lucia Pigazzini, by personally signing this document in lieu of an oath, hereby affirm that I prepared the submitted dissertation on the topic '*Complementary methodologies and diverse model systems provide translational insight into the aggregation properties of neurodegenerative diseases'/* '*Komplementäre Methoden und verschiedene Modellsysteme bieten translationale Einblicke in die Aggregationseigenschaften von neurodegenerativen Erkrankungen'* independently and without the support of third parties, and that I used no other sources and aids than those stated.

All parts which are based on the publications or presentations of other authors, either in letter or in spirit, are specified as such in accordance with the citing guidelines. The sections on methodology (in particular regarding practical work, laboratory regulations, statistical processing) and results (in particular regarding figures, charts and tables) are exclusively my responsibility.

Furthermore, I declare that I have correctly marked all of the data, the analyses, and the conclusions generated from data obtained in collaboration with other persons, and that I have correctly marked my own contribution and the contributions of other persons (cf. declaration of contribution). I have correctly marked all texts or parts of texts that were generated in collaboration with other persons.

My contributions to any publications to this dissertation correspond to those stated in the below joint declaration made together with the supervisor. All publications created within the scope of the dissertation comply with the guidelines of the ICMJE (International Committee of Medical Journal Editors; www.icmje.org) on authorship. In addition, I declare that I shall comply with the regulations of Charité – Universitätsmedizin Berlin on ensuring good scientific practice.

I declare that I have not yet submitted this dissertation in identical or similar form to another Faculty.

The significance of this statutory declaration and the consequences of a false statutory declaration under criminal law (Sections 156, 161 of the German Criminal Code) are known to me."

Date Signature

## Declaration of own contribution to the publications

Maria Lucia Pigazzini contributed the following to the below listed publications:

**Publication 1: Pigazzini ML**, Kirstein J. *In vivo* quantification of protein turnover in aging *C. Elegans* using photoconvertible Dendra2. J Vis Exp (2020);160:1–18.

Contribution: Data acquisition, data analysis, statistical evaluation and preparation of all figures/graphs (Fig. 1-5) are my personal contribution. Manuscript writing and experimental design was in cooperation with Janine Kirstein.

**Publication 2: Pigazzini ML**, Gallrein C, Iburg M, Kaminski Schierle G, Kirstein J. Characterization of Amyloid Structures in Aging *C. Elegans* Using Fluorescence Lifetime Imaging. J Vis Exp (2020);157:1–11.

Contribution: Fig. 1 and 3 were the product of my experimental practice, data analysis, statistical evaluation and visual preparation. The data acquisition for figure 5 was done in collaboration with Christian Gallrein. Experimental design was in cooperation with Christian Gallrein and Janine Kirstein. The manuscript, excluding the figure legends, was written by me with the overview of Janine Kirstein.

**Publication 3:** Scior A, Buntru A, Arnsburg K, Ast A, Iburg M, Juenemann K, **Pigazzini ML**, Mlody B, Puchkov D, Priller J, Wanker EE, Prigione A, Kirstein J. Complete suppression of Htt fibrilization and disaggregation of Htt fibrils by a trimeric chaperone complex. EMBO J (2018);37:282–99.

Contribution: Acquisition and analysis of data represented in figures 5B-5C, EV1-C and EV2 D-F-G were my personal contribution. This data was obtained and analysed in cooperation with Annika Scior and Kristin Arnsburg.

_____

Signature, date and stamp of first supervising university professor / lecturer

_____

Signature of doctoral candidate

# 7. Publications

***1st Publication:***

**Pigazzini ML**, Kirstein J.

In vivo quantification of protein turnover in aging *C. Elegans* using photoconvertible Dendra2. J Vis Exp (2020);160:1–18.

## *Journal Summary List - ISI Web of Knowledge: Multidisciplinary Science (JCR Year: 2018)*

Journal Data Filtered By: **Selected JCR Year: 2018** Selected Editions: SCIE,SSCI Selected Categories: **"MULTIDISCIPLINARY SCIENCES"** Selected Category Scheme: WoS

**Gesamtanzahl: 69 Journale**

| Rank | Full Journal Title | Total Cites | Journal Impact Factor | Eigenfactor Score |
|---|---|---|---|---|
| 1 | NATURE | 745,692 | 43.070 | 1.285010 |
| 2 | SCIENCE | 680,994 | 41.037 | 1.070190 |
| 3 | National Science Review | 1,842 | 13.222 | 0.006500 |
| 4 | Science Advances | 21,901 | 12.804 | 0.110010 |
| 5 | Nature Communications | 243,793 | 11.878 | 1.103290 |
| 6 | Nature Human Behaviour | 1,230 | 10.575 | 0.006550 |
| 7 | PROCEEDINGS OF THE NATIONAL ACADEMY OF SCIENCES OF THE UNITED STATES OF AMERICA | 661,118 | 9.580 | 1.022190 |
| 8 | Science Bulletin | 3,569 | 6.277 | 0.009840 |
| 9 | Scientific Data | 3,240 | 5.929 | 0.015610 |
| 10 | Frontiers in Bioengineering and Biotechnology | 1,994 | 5.122 | 0.006540 |
| 11 | Journal of Advanced Research | 2,691 | 5.045 | 0.004780 |
| 12 | Research Synthesis Methods | 1,932 | 5.043 | 0.005420 |
| 13 | GigaScience | 2,674 | 4.688 | 0.012510 |
| 14 | Annals of the New York Academy of Sciences | 46,385 | 4.295 | 0.025840 |
| 15 | Scientific Reports | 302,086 | 4.011 | 1.061540 |
| 16 | Journal of the Royal Society Interface | 12,933 | 3.224 | 0.029190 |
| 17 | NPJ Microgravity | 203 | 3.111 | 0.000670 |
| 18 | PHILOSOPHICAL TRANSACTIONS OF THE ROYAL SOCIETY A-MATHEMATICAL PHYSICAL AND ENGINEERING SCIENCES | 19,227 | 3.093 | 0.028200 |

| Rank | Full Journal Title | Total Cites | Journal Impact Factor | Eigenfactor Score |
|---|---|---|---|---|
| 19 | FRACTALS-COMPLEX GEOMETRY PATTERNS AND SCALING IN NATURE AND SOCIETY | 1,429 | 2.971 | 0.001120 |
| 20 | Journal of Radiation Research and Applied Sciences | 860 | 2.963 | 0.001860 |
| 21 | MIT Technology Review | 929 | 2.893 | 0.001910 |
| 22 | JOURNAL OF KING SAUD UNIVERSITY SCIENCE | 1,120 | 2.835 | 0.001670 |
| 23 | PROCEEDINGS OF THE ROYAL SOCIETY A-MATHEMATICAL PHYSICAL AND ENGINEERING SCIENCES | 18,683 | 2.818 | 0.018940 |
| 24 | PLoS One | 650,727 | 2.776 | 1.706770 |
| 25 | COMPLEXITY | 2,753 | 2.591 | 0.003890 |
| 26 | Royal Society Open Science | 4,118 | 2.515 | 0.017150 |
| 27 | PeerJ | 11,911 | 2.353 | 0.045900 |
| 28 | SCIENCE AND ENGINEERING ETHICS | 1,719 | 2.275 | 0.003450 |
| 29 | INTERNATIONAL JOURNAL OF BIFURCATION AND CHAOS | 7,008 | 2.145 | 0.007390 |
| 30 | Symmetry-Basel | 2,097 | 2.143 | 0.002590 |
| 31 | SCIENTIFIC AMERICAN | 6,609 | 1.946 | 0.003540 |
| 32 | Science of Nature | 508 | 1.839 | 0.002000 |
| 33 | PROCEEDINGS OF THE JAPAN ACADEMY SERIES B-PHYSICAL AND BIOLOGICAL SCIENCES | 1,532 | 1.833 | 0.001960 |
| 34 | Journal of Taibah University for Science | 779 | 1.640 | 0.001240 |
| 35 | Frontiers in Life Science | 241 | 1.622 | 0.000500 |
| 36 | ARABIAN JOURNAL FOR SCIENCE AND ENGINEERING | 3,838 | 1.518 | 0.005840 |
| 37 | SCIENCE PROGRESS | 521 | 1.500 | 0.000400 |



Selected JCR Year: 2018; Selected Categories: “MULTIDISCIPLINARY SCIENCES”

| Rank | Full Journal Title | Total Cites | Journal Impact Factor | Eigenfactor Score |
|---|---|---|---|---|
| 38 | Proceedings of the Romanian Academy Series A-Mathematics Physics Technical Sciences Information Science | 497 | 1.402 | 0.000900 |
| 39 | SOUTH AFRICAN JOURNAL OF SCIENCE | 2,604 | 1.351 | 0.002010 |
| 40 | ISSUES IN SCIENCE AND TECHNOLOGY | 428 | 1.214 | 0.000990 |
| 41 | Jove-Journal of Visualized Experiments | 13,650 | 1.108 | 0.035180 |
| 42 | RENDICONTI LINCEI-SCIENZE FISICHE E NATURALI | 750 | 1.087 | 0.001080 |
| 43 | ENDEAVOUR | 540 | 1.068 | 0.000440 |
| 44 | DISCRETE DYNAMICS IN NATURE AND SOCIETY | 1,962 | 0.973 | 0.003690 |
| 45 | Mathematical Modelling of Natural Phenomena | 679 | 0.949 | 0.001930 |
| 46 | ANAIS DA ACADEMIA BRASILEIRA DE CIENCIAS | 2,841 | 0.938 | 0.003410 |
| 47 | Kuwait Journal of Science | 225 | 0.891 | 0.000340 |
| 48 | ADVANCES IN COMPLEX SYSTEMS | 618 | 0.867 | 0.000340 |
| 49 | JOURNAL OF THE ROYAL SOCIETY OF NEW ZEALAND | 648 | 0.774 | 0.000400 |
| 50 | CURRENT SCIENCE | 10,540 | 0.756 | 0.006420 |
| 51 | JOURNAL OF THE INDIAN INSTITUTE OF SCIENCE | 391 | 0.742 | 0.000530 |
| 52 | Iranian Journal of Science and Technology Transaction A-Science | 499 | 0.692 | 0.000460 |
| 53 | PROCEEDINGS OF THE NATIONAL ACADEMY OF SCIENCES INDIA SECTION A-PHYSICAL SCIENCES | 309 | 0.681 | 0.000400 |
| 54 | TRANSACTIONS OF THE ROYAL SOCIETY OF SOUTH AUSTRALIA | 444 | 0.667 | 0.000200 |
| 55 | DEFENCE SCIENCE JOURNAL | 928 | 0.589 | 0.000560 |
| 56 | Sains Malaysiana | 1,337 | 0.540 | 0.001320 |
| 57 | Proceedings of the Estonian Academy of Sciences | 523 | 0.510 | 0.000490 |
| 58 | AMERICAN SCIENTIST | 2,425 | 0.507 | 0.001110 |

3

Selected JCR Year: 2018; Selected Categories: “MULTIDISCIPLINARY SCIENCES”

Removed from the electronic version of this dissertation for copyright reasons.

https://doi.org/10.3791/61196

***2nd Publication:***

**Pigazzini ML**, Gallrein C, Iburg M, Kaminski Schierle G, Kirstein J. Characterization of Amyloid Structures in Aging *C. Elegans* Using Fluorescence Lifetime Imaging. J Vis Exp (2020);157:1–11.

## *Journal Summary List - ISI Web of Knowledge: Multidisciplinary Science (JCR Year: 2018)*

Journal Data Filtered By: **Selected JCR Year: 2018** Selected Editions: SCIE,SSCI Selected Categories: **"MULTIDISCIPLINARY SCIENCES"** Selected Category Scheme: WoS

**Gesamtanzahl: 69 Journale**

| Rank | Full Journal Title | Total Cites | Journal Impact Factor | Eigenfactor Score |
|---|---|---|---|---|
| 1 | NATURE | 745,692 | 43.070 | 1.285010 |
| 2 | SCIENCE | 680,994 | 41.037 | 1.070190 |
| 3 | National Science Review | 1,842 | 13.222 | 0.006500 |
| 4 | Science Advances | 21,901 | 12.804 | 0.110010 |
| 5 | Nature Communications | 243,793 | 11.878 | 1.103290 |
| 6 | Nature Human Behaviour | 1,230 | 10.575 | 0.006550 |
| 7 | PROCEEDINGS OF THE NATIONAL ACADEMY OF SCIENCES OF THE UNITED STATES OF AMERICA | 661,118 | 9.580 | 1.022190 |
| 8 | Science Bulletin | 3,569 | 6.277 | 0.009840 |
| 9 | Scientific Data | 3,240 | 5.929 | 0.015610 |
| 10 | Frontiers in Bioengineering and Biotechnology | 1,994 | 5.122 | 0.006540 |
| 11 | Journal of Advanced Research | 2,691 | 5.045 | 0.004780 |
| 12 | Research Synthesis Methods | 1,932 | 5.043 | 0.005420 |
| 13 | GigaScience | 2,674 | 4.688 | 0.012510 |
| 14 | Annals of the New York Academy of Sciences | 46,385 | 4.295 | 0.025840 |
| 15 | Scientific Reports | 302,086 | 4.011 | 1.061540 |
| 16 | Journal of the Royal Society Interface | 12,933 | 3.224 | 0.029190 |
| 17 | NPJ Microgravity | 203 | 3.111 | 0.000670 |
| 18 | PHILOSOPHICAL TRANSACTIONS OF THE ROYAL SOCIETY A-MATHEMATICAL PHYSICAL AND ENGINEERING SCIENCES | 19,227 | 3.093 | 0.028200 |

| Rank | Full Journal Title | Total Cites | Journal Impact Factor | Eigenfactor Score |
|---|---|---|---|---|
| 19 | FRACTALS-COMPLEX GEOMETRY PATTERNS AND SCALING IN NATURE AND SOCIETY | 1,429 | 2.971 | 0.001120 |
| 20 | Journal of Radiation Research and Applied Sciences | 860 | 2.963 | 0.001860 |
| 21 | MIT Technology Review | 929 | 2.893 | 0.001910 |
| 22 | JOURNAL OF KING SAUD UNIVERSITY SCIENCE | 1,120 | 2.835 | 0.001670 |
| 23 | PROCEEDINGS OF THE ROYAL SOCIETY A-MATHEMATICAL PHYSICAL AND ENGINEERING SCIENCES | 18,683 | 2.818 | 0.018940 |
| 24 | PLoS One | 650,727 | 2.776 | 1.706770 |
| 25 | COMPLEXITY | 2,753 | 2.591 | 0.003890 |
| 26 | Royal Society Open Science | 4,118 | 2.515 | 0.017150 |
| 27 | PeerJ | 11,911 | 2.353 | 0.045900 |
| 28 | SCIENCE AND ENGINEERING ETHICS | 1,719 | 2.275 | 0.003450 |
| 29 | INTERNATIONAL JOURNAL OF BIFURCATION AND CHAOS | 7,008 | 2.145 | 0.007390 |
| 30 | Symmetry-Basel | 2,097 | 2.143 | 0.002590 |
| 31 | SCIENTIFIC AMERICAN | 6,609 | 1.946 | 0.003540 |
| 32 | Science of Nature | 508 | 1.839 | 0.002000 |
| 33 | PROCEEDINGS OF THE JAPAN ACADEMY SERIES B-PHYSICAL AND BIOLOGICAL SCIENCES | 1,532 | 1.833 | 0.001960 |
| 34 | Journal of Taibah University for Science | 779 | 1.640 | 0.001240 |
| 35 | Frontiers in Life Science | 241 | 1.622 | 0.000500 |
| 36 | ARABIAN JOURNAL FOR SCIENCE AND ENGINEERING | 3,838 | 1.518 | 0.005840 |
| 37 | SCIENCE PROGRESS | 521 | 1.500 | 0.000400 |

2

Selected JCR Year: 2018; Selected Categories: “MULTIDISCIPLINARY SCIENCES”

| Rank | Full Journal Title | Total Cites | Journal Impact Factor | Eigenfactor Score |
|---|---|---|---|---|
| 38 | Proceedings of the Romanian Academy Series A-Mathematics Physics Technical Sciences Information Science | 497 | 1.402 | 0.000900 |
| 39 | SOUTH AFRICAN JOURNAL OF SCIENCE | 2,604 | 1.351 | 0.002010 |
| 40 | ISSUES IN SCIENCE AND TECHNOLOGY | 428 | 1.214 | 0.000990 |
| 41 | Jove-Journal of Visualized Experiments | 13,650 | 1.108 | 0.035180 |
| 42 | RENDICONTI LINCEI-SCIENZE FISICHE E NATURALI | 750 | 1.087 | 0.001080 |
| 43 | ENDEAVOUR | 540 | 1.068 | 0.000440 |
| 44 | DISCRETE DYNAMICS IN NATURE AND SOCIETY | 1,962 | 0.973 | 0.003690 |
| 45 | Mathematical Modelling of Natural Phenomena | 679 | 0.949 | 0.001930 |
| 46 | ANAIS DA ACADEMIA BRASILEIRA DE CIENCIAS | 2,841 | 0.938 | 0.003410 |
| 47 | Kuwait Journal of Science | 225 | 0.891 | 0.000340 |
| 48 | ADVANCES IN COMPLEX SYSTEMS | 618 | 0.867 | 0.000340 |
| 49 | JOURNAL OF THE ROYAL SOCIETY OF NEW ZEALAND | 648 | 0.774 | 0.000400 |
| 50 | CURRENT SCIENCE | 10,540 | 0.756 | 0.006420 |
| 51 | JOURNAL OF THE INDIAN INSTITUTE OF SCIENCE | 391 | 0.742 | 0.000530 |
| 52 | Iranian Journal of Science and Technology Transaction A-Science | 499 | 0.692 | 0.000460 |
| 53 | PROCEEDINGS OF THE NATIONAL ACADEMY OF SCIENCES INDIA SECTION A-PHYSICAL SCIENCES | 309 | 0.681 | 0.000400 |
| 54 | TRANSACTIONS OF THE ROYAL SOCIETY OF SOUTH AUSTRALIA | 444 | 0.667 | 0.000200 |
| 55 | DEFENCE SCIENCE JOURNAL | 928 | 0.589 | 0.000560 |
| 56 | Sains Malaysiana | 1,337 | 0.540 | 0.001320 |
| 57 | Proceedings of the Estonian Academy of Sciences | 523 | 0.510 | 0.000490 |
| 58 | AMERICAN SCIENTIST | 2,425 | 0.507 | 0.001110 |

3

Selected JCR Year: 2018; Selected Categories: "MULTIDISCIPLINARY SCIENCES"

Removed from the electronic version of this dissertation for copyright reasons.

https://doi.org/10.3791/61004

***3rd Publication:***

Scior A, Buntru A, Arnsburg K, Ast A, Iburg M, Juenemann K, **Pigazzini ML**, Mlody B, Puchkov D, Priller J, Wanker EE, Prigione A, Kirstein J.
Complete suppression of Htt fibrilization and disaggregation of Htt fibrils by a trimeric chaperone complex. EMBO J (2018);37:282–299.

## *Journal Summary List - ISI Web of Knowledge: Cell Biology (JCR Year: 2015)*

Journal Data Filtered By: **Selected JCR Year: 2015** Selected Editions: SCIE,SSCI
Selected Categories: **'CELL BIOLOGY'** Selected Category Scheme: WoS
**Gesamtanzahl: 187 Journale**

| Rank | Full Journal Title | Total Cites | Journal Impact Factor | Eigenfactor Score |
|---|---|---|---|---|
| 1 | NATURE REVIEWS MOLECULAR CELL BIOLOGY | 36,784 | 38.602 | 0.099310 |
| 2 | NATURE MEDICINE | 65,230 | 30.357 | 0.161790 |
| 3 | CELL | 202,467 | 28.710 | 0.555090 |
| 4 | CANCER CELL | 29,149 | 23.214 | 0.102440 |
| 5 | Cell Stem Cell | 18,575 | 22.387 | 0.091360 |
| 6 | NATURE CELL BIOLOGY | 35,807 | 18.699 | 0.104400 |
| 7 | Cell Metabolism | 21,343 | 17.303 | 0.088610 |
| 8 | Science Translational Medicine | 17,066 | 16.264 | 0.114890 |
| 9 | CELL RESEARCH | 10,393 | 14.812 | 0.035850 |
| 10 | MOLECULAR CELL | 53,714 | 13.958 | 0.192560 |
| 11 | NATURE STRUCTURAL & MOLECULAR BIOLOGY | 25,671 | 13.338 | 0.103970 |
| 12 | Annual Review of Cell and Developmental Biology | 8,992 | 12.755 | 0.020570 |
| 13 | TRENDS IN CELL BIOLOGY | 11,479 | 11.532 | 0.032440 |
| 14 | GENES & DEVELOPMENT | 57,109 | 10.042 | 0.117120 |
| 15 | EMBO JOURNAL | 68,016 | 9.643 | 0.106940 |
| 16 | DEVELOPMENTAL CELL | 24,023 | 9.338 | 0.083330 |
| 17 | TRENDS IN MOLECULAR MEDICINE | 7,703 | 9.292 | 0.020480 |
| 18 | Cold Spring Harbor Perspectives in Biology | 9,184 | 9.173 | 0.058550 |
| 19 | Autophagy | 10,957 | 9.108 | 0.035990 |
| 20 | CURRENT BIOLOGY | 49,471 | 8.983 | 0.141790 |
| 21 | CURRENT OPINION IN CELL BIOLOGY | 13,034 | 8.851 | 0.031840 |

Article

TRANSPARENT PROCESS

THE EMBO JOURNAL

# Complete suppression of Htt fibrilization and disaggregation of Htt fibrils by a trimeric chaperone complex

Annika Scior[1], Alexander Buntru[2], Kristin Arnsburg[1], Anne Ast[2], Manuel Iburg[1], Katrin Juenemann[1], Maria Lucia Pigazzini[1,3], Barbara Mlody[2], Dmytro Puchkov[1], Josef Priller[4], Erich E Wanker[2,*], Alessandro Prigione[2] & Janine Kirstein[1,**]

## Abstract

**Huntington's disease (HD) is a neurodegenerative disorder caused by an expanded CAG trinucleotide repeat in the huntingtin gene (*HTT*). Molecular chaperones have been implicated in suppressing or delaying the aggregation of mutant Htt. Using *in vitro* and *in vivo* assays, we have identified a trimeric chaperone complex (Hsc70, Hsp110, and J-protein) that completely suppresses fibrilization of HttExon1$Q_{48}$. The composition of this chaperone complex is variable as recruitment of different chaperone family members forms distinct functional complexes. The trimeric chaperone complex is also able to resolubilize Htt fibrils. We confirmed the biological significance of these findings in HD patient-derived neural cells and on an organismal level in *Caenorhabditis elegans*. Among the proteins in this chaperone complex, the J-protein is the concentration-limiting factor. The single overexpression of DNAJB1 in HEK293T cells is sufficient to profoundly reduce HttExon1$Q_{97}$ aggregation and represents a target of future therapeutic avenues for HD.**

**Keywords** disaggregation; HttpolyQ; molecular chaperones; NPCs; suppression

**Subject Categories** Molecular Biology of Disease; Neuroscience; Protein Biosynthesis & Quality Control

**DOI** 10.15252/embj.201797212 | Received 25 April 2017 | Revised 19 October 2017 | Accepted 26 October 2017 | Published online 6 December 2017

**The EMBO Journal (2018) 37: 282–299**

## Introduction

Huntington's disease (HD) is caused by a CAG trinucleotide repeat expansion in the first exon of the Huntingtin gene (*HTT*), which renders N-terminal fragments of the protein ($HttQ_n$) aggregation-prone and ultimately results in β-sheet formation and amyloid fibrilization. The pathogenic threshold of the polyQ expansion in HTT is 35, and the aggregation propensity correlates with the number of glutamine residues (Scherzinger *et al*, 1999; Gusella & MacDonald, 2000). The aggregation of $HttQ_n$ is proteotoxic and is associated with cellular dysfunction and neuronal degeneration (Hoffner *et al*, 2007). Consequently, the search for factors that interfere with the amyloid formation in particular by suppressing the formation of toxic oligomeric and high molecular weight aggregates such as amyloid fibrils represents an attractive therapeutic strategy. Commonly, in response to protein misfolding and aggregation the cell induces the expression of the proteostasis network (PN) that is composed of proteases, molecular chaperones, and many other proteins (Balch *et al*, 2008). However, the expression of polyQ proteins fails to induce this network (Bersuker *et al*, 2013). The expression of $HttQ_n$ triggers a protein aggregation cascade. Oligomers and protofibrils can act as nuclei (seeds) that induce a conformational switch in soluble monomeric $HttQ_n$ molecules by primary and secondary nucleation events (Scherzinger *et al*, 1999; Wetzel, 2012; Kakkar *et al*, 2016). Moreover, $HttQ_n$ fibrils sequester aggregation-prone endogenous proteins and molecular chaperones and also inhibit the ubiquitin proteasome system (Olzscha *et al*, 2011; Hipp *et al*, 2012; Kirstein-Miles *et al*, 2013; Kim *et al*, 2016). Such an impairment of the PN leads to further accumulation of misfolded and aggregated proteins that ultimately results in degeneration of the affected neuronal cells (Cicchetti *et al*, 2011).

Molecular chaperones represent an attractive target to prevent the accumulation of proteotoxic amyloid proteins such as $HttQ_n$ as demonstrated by recent findings. The first observations that chaperones can to a certain extent decrease the aggregation propensity of $HttQ_n$ in *in vitro* assays were obtained using bacterial or yeast Hsp70 and Hsp40 (J-protein) chaperones, respectively (Muchowski *et al*, 2000). *In vivo*, overexpression of Hsp70, J-protein, Hsp110, or TRiC reduces the aggregation toxicity of Htt in cultured cells, flies, and HD mouse models (Chan *et al*, 2000; Tam *et al*, 2006; Kuo *et al*,

1 Leibniz-Institute for Molecular Pharmacology (FMP) im Forschungsverbund Berlin, Berlin, Germany
2 Max Delbrueck Center for Molecular Medicine, Berlin, Germany
3 Charité – Universitätsmedizin and NeuroCure Cluster of Excellence, Berlin, Germany
4 Department of Neuropsychiatry and Laboratory of Molecular Psychiatry, Charite Universitätsmedizin Berlin, Berlin, Germany
*Corresponding author. Tel: +49 30 9406 2157; E-mail: ewanker@mdc-berlin.de
**Corresponding author. Tel: +49 30 94793250; E-mail: kirstein@fmp-berlin.de

2013; Monsellier *et al*, 2015; Kakkar *et al*, 2016). It was also observed that expression of two chaperones (Hsp70/J-protein or Hsp110/J-protein) synergistically suppressed Htt aggregation (Kuo *et al*, 2013). These findings are in agreement with previous reports indicating that these chaperones form functional complexes (Rampelt *et al*, 2012; Nillegoda *et al*, 2015) and suggest that they cooperate *in vivo* to prevent or reverse polyQ aggregation (Chan *et al*, 2000; Kuo *et al*, 2013). Despite these efforts, many open questions remain. Are there specific chaperones or chaperone complexes that recognize distinct moieties of misfolded and aggregated Htt? The diversity within the chaperone families increased in the course of evolution (Brehme *et al*, 2014). A pronounced expansion in the number of distinct chaperones occurred, for example, within the J-protein family, suggesting an increased functional specialization of chaperones. Do chaperones interfere with the nucleation events of beta-sheet formation or influence seeding activities? Can chaperones resolubilize Htt once it is assembled into amyloid fibrils?

To address these questions, we set out to gain mechanistic insights into how chaperones maintain and restore the solubility of $HttQ_n$ *in vitro* and *in vivo*. In this study, we demonstrate that a trimeric chaperone complex composed of a member each of the Hsp70, Hsp110, and type B J-protein family can completely suppress the amyloid fibril formation of $HttExon1Q_{48}$ and almost completely the fibrilization of $HttExon1Q_{75}$. We also demonstrate for the first time the disaggregation of $HttExon1Q_{48}$ fibrils by this trimeric chaperone complex. The composition of the chaperone complex is variable. The combination of different Hsp70 and J-protein chaperones together with Hsp110 leads to distinct chaperone complexes that exhibit different suppression and disaggregation activities. Depletion of these chaperones in HD patient-derived neural progenitor cells (NPCs) leads to a pronounced increase in Htt protein aggregates ($Q_{44}$). We could confirm the importance of Hsc70, HSP-110, and the J-protein to maintain the solubility of $HttQ_n$ and related polyQ proteins on an organismal level in *Caenorhabditis elegans*. We can show that the J-protein is the chaperone component whose concentration is most critical in the *in vitro* assays and exhibited the strongest effect on $HttQ_{44}$ upon knockdown in the NPCs. Accordingly, overexpression of a specific J-protein (DNAJB1) can ameliorate the aggregation of $HttExon1Q_{97}$ in human cell culture.

## Results

### FRET-based assay to monitor the fibrilization of $HttExon1Q_{48}$

To gain mechanistic insight into how molecular chaperones maintain Htt protein species in a soluble state and prevent their self-assembly into amyloid fibrils, we employed a FRET-based HttExon1 aggregation assay. The assay is based on GST-$HttExon1Q_{48}$ that is fused at the C-terminus to either CyPet or YPet (Nguyen & Daugherty, 2005). These fluorescent proteins represent a potential FRET pair with CyPet being the donor and YPet the acceptor molecule. The globular GST tag fused to the N-terminus inhibits the fibril formation of the pathogenic polyQ stretch in the HttExon1 fragment. The cleavage of this tag with the PreScission protease (PreSP) liberates the $HttExon1Q_{48}$-CyPet/YPet (from now on referred to as $HttExon1Q_{48}$) protein and initiates its self-assembly into fibrils (Fig 1A). In this fibrilized form, the fluorescent fusion proteins come into close proximity that enables the energy transfer from CyPet to YPet. Thus, the FRET efficiency between CyPet and YPet reports on the aggregation status of $HttExon1Q_{48}$ (Fig 1A).

We additionally used transmission electron microscopy (TEM) analysis to monitor the aggregation of the $HttExon1Q_{48}$ proteins *in vitro*. Images taken 24 h post-PreSP treatment of tagged and untagged $HttExon1Q_{48}$ proteins show fibrilization of the Htt proteins and validate amyloid formation. Furthermore, they demonstrate that the fluorescent tags do not interfere with amyloid formation (Figs 1B and EV1A). Using the FRET-based Htt fibrilization assay, we

**Figure 1. Trimeric human chaperone complex can suppress the fibrilization of $HttExon1Q_{48}$ and resolubilize $HttExon1Q_{48}$ fibrils.**

A Scheme of experimental FRET-based assay for the analysis of fibrilization of $HttExon1Q_{48}$. In all FRET assays, we use the fluorescently tagged $HttExon1Q_{48}$-YPet/CyPet proteins yet refer to them as $HttExon1Q_{48}$ for clarity.

B TEM images of $HttExon1Q_{48}$ fibrils at time points 0 and 24 h after addition of PreSP. Analysis of the sedimentation by ultracentrifugation of $HttExon1Q_{48}$ 24 h post-PreSP treatment is depicted below. The supernatant represents the soluble species and the pellet the insoluble $HttExon1Q_{48}$ protein. The total depicts a sample before the centrifugation step. Scale bars: 200 nm.

C FRET analysis of $HttExon1Q_{48}$ fibrilization. The black curve represents the $HttExon1Q_{48}$-YPet/CyPet mixtures alone (no chaperone control) in all figures. The relative concentrations of $HttExon1Q_{48}$ and the chaperones are indicated as ratios in brackets. The first number always refers to $HttExon1Q_{48}$. The chaperones were added at time point 0 together with $HttExon1Q_{48}$ and PreSP. The addition of Hsc70, Apg2, and DNAJB1 completely suppresses the fibrilization of $HttExon1Q_{48}$ (bright red curve). The effect of individual chaperones and chaperone mixtures on the $HttExon1Q_{48}$ fibrilization is indicated in the figure. The non-pathogenic $HttExon1Q_{23}$-YPet/CyPet mixtures display no FRET post-PreSP treatment even upon doubling their concentration (dark blue and turquoise curves).

D TEM analysis of the suppression of $HttExon1Q_{48}$ fibrilization by Hsc70, Apg2, and DNAJB1. A scheme of the experimental outline is depicted on the right. The red arrow refers to the time point of sample analysis. Scale bar: 100 nm.

E Suppression of $HttExon1Q_{48}$ fibrilization by sedimentation analysis in the absence or presence of Hsc70, Apg2, DNAJB1, and ATP. The values refer to the ratio between the fluorescent signal of $HttExon1Q_{48}$-CyPet in the supernatant (soluble) and pellet (aggregated moiety) fraction. Depicted is the average of three independent experiments with error bars representing the standard deviation.

F Sedimentation analysis of the disaggregation of $HttExon1Q_{48}$ by Hsc70, Apg2, and DNAJB1 in the presence or absence of ATP. Depicted are the ratios of supernatant (soluble) to pellet (aggregated $HttExon1Q_{48}$). Depicted is the average of three independent experiments with error bars representing the standard deviation.

G TEM analysis of disaggregation of $HttExon1Q_{48}$ fibrils by Hsc70, Apg2, and DNAJB1. The top left image depicts fibrils after 24 h post-PreSP treatment and the top right after an additional 20 h without addition of chaperones. The bottom row depicts images of $HttExon1Q_{48}$ fibrils 24 h post-PreSP + 1 h (left), 4 h (middle), and 20 h (right) in the presence of Hsc70, Apg2, DNAJB1, and ATP. A scheme of the experimental outline is depicted on the right. The red arrow refers to the time point of sample analysis. Scale bar: 100 nm.

H Filter retardation analysis of $HttExon1Q_{97}$-HA aggregates. Lysates of HEK293T cells expressing $HttExon1Q_{97}$-HA were probed on the filter membrane with antibodies against HA ($HttExon1Q_{97}$), DNAJB1, Apg2 (Hsp110), and Hsc70 to detect their association with the respective chaperones (second to fourth membranes) and to confirm the presence of the $HttExon1Q_{97}$ aggregates (first membrane). Lysates were spotted on the filter in duplicates, and the bottom row depicts the control (cells that do not express $HttExon1Q_{97}$-HA).

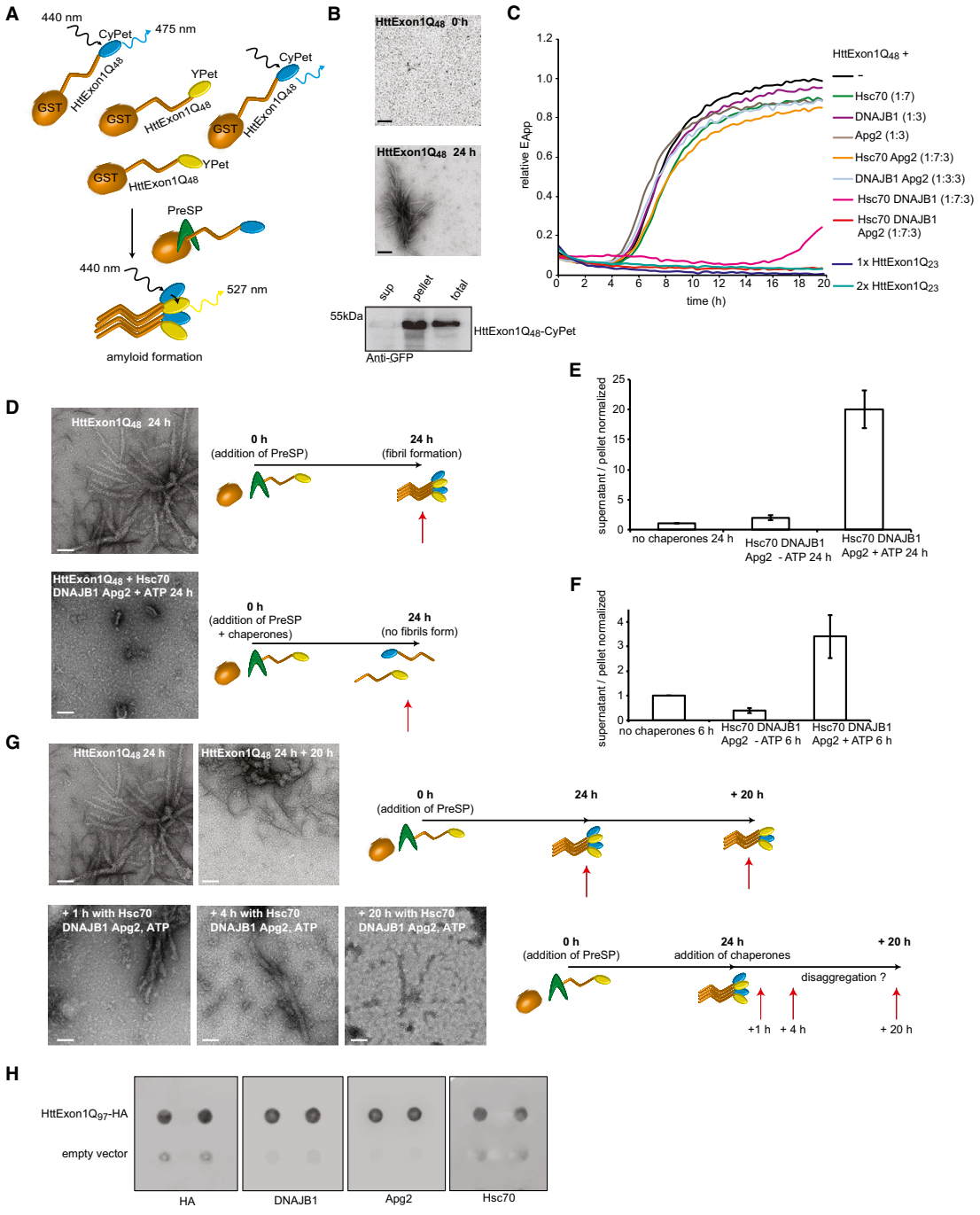


**Figure 1.**

 

observed an initial decrease in FRET efficiency that accounts for the monomerization of the GST-tagged Htt proteins. After a lag phase of about 3 h, the FRET efficiency sharply increases, reflecting the fibrilization process (elongation phase). The FRET signal reaches a plateau within the next 2 h and remains there for the entire duration of the experiment (Fig 1C; black curve). TEM analysis of samples of the plateau phase shows only fibrilized Htt that can be sedimented with ultracentrifugation (Fig 1B), indicating that HttExon1$Q_{48}$ is converted into amyloid fibrils. We used a sedimentation approach to further validate the time course of fibrilization. For that, we used the CFP fluorescence of HttExon1$Q_{48}$-CyPet as readout for the abundance of the protein in the soluble and insoluble fractions and could confirm the aggregation of HttExon1$Q_{48}$ at the respective time points post-PreSP treatment (Fig EV1B), mirroring the FRET fibrilization curve (Fig 1C; black curve). As a control, we employed HttExon1$Q_{23}$-CyPet/YPet constructs whose polyQ length is below the pathogenic threshold of 35Q residues required to form Htt fibrils. As expected, the HttExon1$Q_{23}$-CyPet/YPet proteins do not exhibit any FRET upon PreSP treatment even when we doubled the HttExon1$Q_{23}$ concentration (Fig 1C; dark blue and turquoise curves). Taken together, we conclude that the FRET assay provides a quantitative and reliable method to monitor the fibrilization of HttExon1$Q_{48}$.

#### A distinct trimeric chaperone complex completely suppresses and reverses HttExon1$Q_{48}$ fibril formation

Recently, a metazoan disaggregation complex was identified that has the capacity to disaggregate amorphous aggregates as well as α-synuclein fibrils *in vitro* (Rampelt *et al*, 2012; Gao *et al*, 2015; Nillegoda *et al*, 2015). Disaggregation in higher eukaryotes requires a member of the Hsp70 chaperone family, a corresponding J-protein and a member of the Hsp110 protein family (Rampelt *et al*, 2012). Complete suppression of amyloid fibril formation has not been demonstrated yet. Therefore, we set out to first test the ability of human chaperones to suppress the formation of HttExon1$Q_{48}$ amyloid fibrils by using the aforementioned FRET-based aggregation assay. First, we analyzed human chaperones that exhibited *in vitro* disaggregation activity for α−synuclein fibrils (Gao *et al*, 2015). This included the constitutive Hsc70 protein, the Hsp110 protein Apg2, and the class B J-protein DNAJB1. All chaperones were purified without additional tags. The purities of all chaperones and HttExon1$Q_n$ variants used in this study were assessed by SDS–PAGE and Coomassie staining (Fig EV1D). We then mixed HttExon1$Q_{48}$ with the respective chaperones just prior to PreSP treatment. The addition of individual chaperones did not affect the fibrilization kinetics of HttExon1$Q_{48}$ (Fig 1C). The proteins Hsc70 and DNAJB1 together, however, suppressed the aggregation of HttExon1$Q_{48}$ for about 15 h. The additional presence of Apg2 (Hsp110) led to a complete suppression of HttExon1$Q_{48}$ fibrilization for the entire duration of the experiment (20 h; red curve). We refer from now on only to a complete suppression if the chaperones fully inhibit any FRET signal of the HttExon1$Q_{48}$-CyPet/YPet pair over the complete time period of the experiment that lasts usually between 20 and 30 h. The three chaperones functionally cooperate to suppress the HttExon1$Q_{48}$ fibrilization and are from now on referred to as chaperone complex. The full suppression of aggregation required ATP and a sevenfold excess of Hsc70 over HttExon1$Q_{48}$ protein. The ideal ratio between the chaperones Hsc70:DNAJB1:Apg2 for this activity is 2:1:1 (Fig 1C and data not shown). We confirmed the suppression of fibrilization by TEM and sedimentation analyses (Fig 1D and E). We analyzed the GST-cleavage reaction in a time course reaction in the presence and absence of the chaperones to exclude the possibility that the addition of the chaperones might inhibit or delay the PreSP cleavage reaction that liberates the HttExon1$Q_{48}$ from the GST tag. Importantly, we did not observe an adverse effect of the chaperones on the GST-cleavage reaction (Fig EV1C). Next, we asked if the same chaperone complex could also disaggregate preformed HttExon1$Q_{48}$ fibrils. We incubated Hsc70, Apg2, and DNAJB1 and ATP with HttExon1$Q_{48}$ fibrils and analyzed samples after 1, 4, and 20 h by TEM. As can be seen in Fig 1G, the addition of the chaperones results in a decrease in fibrils over time. No fibrillar structures were visible at the 20-h time point. We confirmed the TEM data of the disaggregation using first a sedimentation analysis of HttExon1$Q_{48}$ in the presence or absence of chaperones and ATP (Fig 1F) and second by using a filter retardation analysis that allows the detection of SDS-resistant amyloid proteins (Fig 4E). Taken together, these studies show that the chaperone complex Hsc70, Apg2, and DNAJB1 can suppress and reverse the aggregation of HttExon1$Q_{48}$ *in vitro*. To demonstrate a physical interaction of all three chaperones with the aggregated Htt moiety, HttExon1$Q_{97}$-HA aggregates from HEK293T cells were isolated via a filter retardation assay and probed with antibodies against Hsc70 (HSPA8), DNAJB1 and Apg2 (HSPA4). All three chaperones were found to be associated with the aggregated HttExon1$Q_{97}$-HA moiety isolated from HEK293T cells (Fig 1H).

#### Suppression of HttExon1$Q_{48}$ fibrilization is conserved in metazoan

For the subsequent studies, we employed the *C. elegans* orthologs of the three human chaperones HSP-1 (Hsc70), HSP-110 (Apg2), and DNJ-13 (DNAJB1) as these proteins allow us to complement the *in vitro* data with *in vivo* analyses of suppression and disaggregation of $HttQ_n$ in a living animal. This is of particular importance as Huntington's disease is a late onset neurodegenerative disease and the chaperone capacity to maintain Htt proteins soluble can be studied in an aging animal model such as *C. elegans* (Morley *et al*, 2002; Kirstein *et al*, 2015). The chaperome of *C. elegans* is of similar complexity as the human chaperone, yet has the advantage of encoding only one cytosolic HSP-110 protein that allows depletion of disaggregase activity by RNAi-mediated knockdown of a single gene (Table EV1; Nikolaidis & Nei, 2004; Rampelt *et al*, 2012; Brehme *et al*, 2014).

As observed for the human chaperones (Fig 1C), incubation of HttExon1$Q_{48}$ with the individual nematode orthologous chaperones, HSP-1 (Hsc70), HSP-110 (Apg2), and DNJ-13 (DNAJB1) alone, did not affect the aggregation kinetics (Fig 2A). However, when HSP-1 and DNJ-13 were added together to HttExon1$Q_{48}$ monomers, we detected a strong delay and overall decrease in fibrilization. The additional presence of HSP-110 led to a complete suppression of HttExon1$Q_{48}$ fibrilization (Fig 2A) similar to the human proteins (Fig 1C). The suppression requires an excess of chaperones over HttExon1$Q_{48}$ proteins and complete suppression could be observed at a HSP-1:HttExon1$Q_{48}$ (monomer) 3.5:1 ratio or higher and is thus more efficient compared to the human chaperones that require an excess of Hsc70:HttExon1$Q_{48}$ of 7:1 (Figs 1C, and 2A and B). The

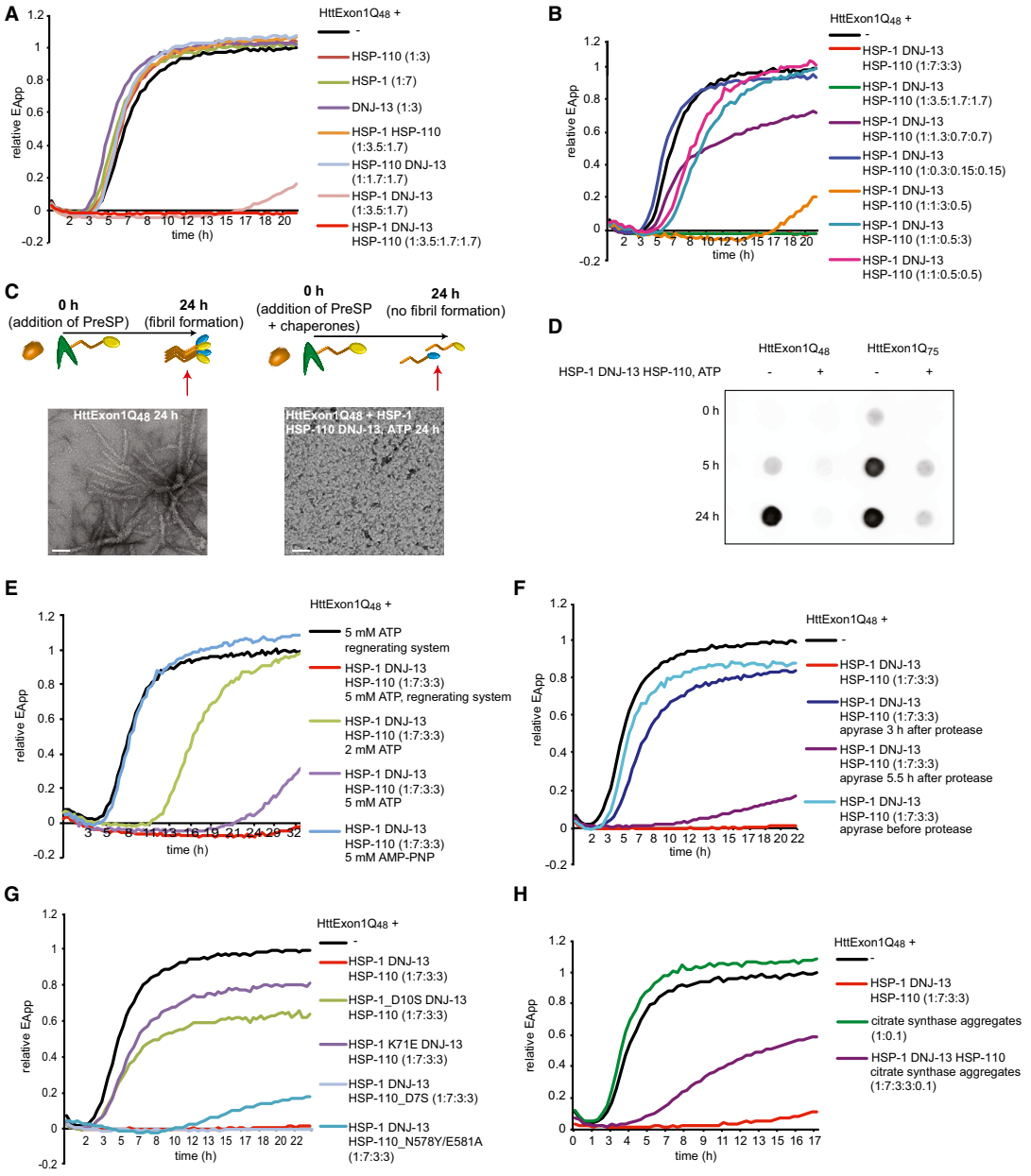


**Figure 2.**

optimal ratio between the chaperones HSP-1:DNJ-13:HSP-110 is 2:1:1 (Fig 2B). Interestingly, sub-stoichiometric chaperone concentrations of HSP-1 and HSP-110 can be tolerated if DNJ-13 is present in excess (Fig 2B; compare orange with pink curve). TEM analysis revealed that in the presence of HSP-1, HSP-110, DNJ-13, and ATP, no fibrils or any other larger assemblies can be detected, which confirms the data obtained with the FRET assay (Fig 2A and C). Next, we wanted to test if the three chaperones could also suppress the aggregation of HttExon1 harboring a longer polyQ stretch. For that, we analyzed the aggregation of HttExon1$Q_{75}$ in the presence and

 

**Figure 2. Mechanistic insights into the chaperone-mediated suppression of HttExon1$Q_{48}$ fibrilization by nematode chaperones.**

A FRET analysis of the suppression activity of individual nematode chaperones and chaperone complexes of the fibrilization of HttExon1$Q_{48}$. HSP-1, HSP-110, and DNJ-13 completely suppress the fibrilization analogous to the human orthologs (bright red curve; compare with Fig 1C).

B Analysis of various chaperone:HttExon1$Q_{48}$ ratios and effect on suppression efficiency.

C TEM analysis of suppression of HttExon1$Q_{48}$ fibrilization by HSP-1, HSP-110, and DNJ-13 taken 24 h post-PreSP treatment (right image; same as image depicted in Fig 1D). The control in the absence of chaperones is shown on the left. A scheme of the experimental outline is depicted above, and the red arrow refers to the time point of sample analysis. Scale bars: 100 nm.

D Analysis of chaperone-mediated suppression of HttExon1$Q_{48}$ (left) and HttExon1$Q_{75}$ (right) by a filter retardation analysis using an Htt antibody. Time points of analysis are indicated on the left and the absence or presence of chaperones on top of the filters.

E Analysis of the effect of varying concentrations of ATP and the non-hydrolyzable analog, AMP-PNP on the chaperone-mediated suppression of the fibril formation of HttExon1$Q_{48}$.

F Addition of apyrase inhibits the suppression activity of the chaperones in a time-dependent manner. Addition of apyrase before PreSP treatment (light blue), 3 h (dark blue), or 5.5 h (purple) after PreSP treatment affects the chaperone-mediated suppression to a different extent.

G Single point mutations in HSP-1 that diminish the ATPase activity, D10S (green curve), and K71E (purple), yet not in HSP-110_D7S (light blue) negatively affect the suppression activity. The NEF mutant: HSP-110_N578/E581A (turquoise) negatively affects the suppression activity of the chaperones.

H Analysis of chaperone-mediated suppression of HttExon1$Q_{48}$ fibrilization in the presence of citrate synthase (CS) aggregates. The addition of CS aggregates to the HttExon1$Q_{48}$ proteins alone depicted in green does not affect the fibrilization kinetics of HttExon1$Q_{48}$. Yet, the addition of CS to a sample containing HttExon1$Q_{48}$ and HSP-1, HSP-110$^{+}$ DNJ-13 diminishes the suppression activity of the chaperones (purple curve). The sample containing the chaperone mixture with HttExon1$Q_{48}$ is depicted in red.

absence of the three chaperones over a time course of 0, 5, and 24 h using a filter retardation assay as readout. Indeed, HSP-1, DNJ-13, and HSP-110 could in addition to HttExon1$Q_{48}$ also almost completely suppress the aggregation of HttExon1$Q_{75}$ (Fig 2D).

### Suppression of HttExon1$Q_{48}$ requires ATP hydrolysis by HSP-1 and the NEF activity of HSP-110

The observation that HSP-110 is required for a complete suppression argues for an ATPase cycle-dependent chaperone activity to suppress the fibril formation of HttExon1$Q_{48}$. Thus, we analyzed the suppression of HttExon1$Q_{48}$ in the presence of either ATP or the non-hydrolyzable ATP analog AMP-PNP. AMP-PNP binding locks Hsp70 in an open conformation with a high on and off rate for substrate binding yet prevents ATP-hydrolysis reactions (Gao *et al*, 1994). Notably, AMP-PNP did not support the suppression arguing for an ATP-hydrolysis-dependent mechanism (Fig 2E; light blue curve).

Next, we titrated the amount of ATP and used either 2 or 5 mM with an ATP regeneration system (PK and PEP) to replenish converted ATP (to ADP) back to ATP. The presence of 2 mM ATP supported the HSP-1/HSP-110/DNJ-13-mediated suppression of HttExon1$Q_{48}$ for 11 h, and the addition of 5 mM for 24 h and the additional presence of the regeneration system extended the suppression period to 30 h (Fig 2E; compare green, purple and red curves). These findings indicate that chaperone-mediated suppression of polyQ-mediated Htt fibril formation requires the consumption of ATP.

We then analyzed the suppression activity in the presence of apyrase that hydrolyzes ATP to AMP and inorganic phosphate and thereby immediately depletes the ATP pool. Addition of apyrase before initiating the Htt fibrilization by adding PreSP immediately before adding the chaperones completely prevents any suppression activity (Fig 2F; light blue). Addition of apyrase 3 h after the treatment with PreSP almost completely abolished the suppression activity of the chaperones (Fig 2F; dark blue). This is the critical time point of the transition between the lag and the log phase of the fibrilization kinetics (Fig 2A). The addition of apyrase at a later time point (5 h), when the chaperones are probably completely bound to the HttExon1$Q_{48}$ moiety and suppressed the fibrilization, however only delayed a regain of FRET efficiency and kept it at low levels (0.2 relative $E_{App}$; purple curve in Fig 2F). The availability of ATP is thus a time-critical variable in the chaperone-mediated suppression of Htt amyloid formation. To further analyze the ATP requirements, we created point mutations in HSP-1 and HSP-110 that abrogate or reduce ATP-hydrolysis rates in the respective chaperone (Wilbanks *et al*, 1994; O'Brien *et al*, 1996). We confirmed the diminished ATPase activity in ATPase assays (Fig EV1G) and demonstrate that the point mutations do not affect the fold/secondary structure of the proteins as assessed by circular dichroism (CD) analysis (Fig EV1E and F). Interestingly, both point mutations of HSP-1 (D10S and K71E) were severely impaired in the suppression of HttExon1$Q_{48}$ fibril formation, whereas the ATPase mutant D7S of HSP-110 did not affect the suppression of HttExon1$Q_{48}$ amyloid formation (Fig 2G). Thus, we conclude that the ATP consumption is due to the ATPase activity of HSP-1 and that the ATPase activity of HSP-110 (Fig EV1G) does not contribute to the chaperone activity of the HSP-1/HSP-110/DNJ-13 protein complex in suppressing Htt fibril formation. Mutating the nucleotide exchange factor (NEF) function of HSP-110 (HSP-110_N578Y/E581A) leads to an incomplete suppression that resembles the suppression of Htt fibrilization by HSP-1 and DNJ-13 alone (Fig 2A, light red and G, blue). Thus, the NEF activity of HSP-110 is essential for the suppression of Htt fibrilization together with HSP-1 and DNJ-13.

### Competition with other chaperone substrates reduces suppression efficiency

Our findings of the concentration-dependent suppression of HttExon1$Q_{48}$ fibril formation (Fig 2B) suggest that available cellular chaperone concentrations are critical and might become limiting under conditions that cause endogenous proteins to unfold or misfold such as aging or proteotoxic stress. To test chaperone competition in the *in vitro* FRET assay, we used aggregated citrate synthase (CS) as model chaperone substrate as the aggregates are of amorphous nature and therefore resemble protein aggregates formed in response to stress (Buchner *et al*, 1998). First, we established that the presence of CS aggregates does not interfere with the fibrilization of HttExon1$Q_{48}$ (Fig 2H; green vs. black curve). Yet, the additional presence of CS aggregates in the sample containing the

chaperone mixture showed that the chaperones were severely affected in the suppression of HttExon1$Q_{48}$ fibrilization (Fig 2H; purple vs. red curve). These data suggest that indeed the chaperones are titrated away by the CS aggregates and become limiting to attend to the aggregation-prone HttExon1$Q_{48}$ protein moiety.

### Hsc70 chaperone complexes are more potent in the suppression of HttExon1$Q_{48}$ fibrilization than HSP-70 chaperone complexes

The genome of *C. elegans* harbors genes encoding for four HSP-70, one HSP-110, but 25 J-proteins for expression in the cytosol alone (Table EV1). The high abundance of HSP-70 proteins and in particular of J-proteins poses the question as to which chaperones cooperate to support the suppression of HttExon1$Q_{48}$ fibril formation. We first set out to test all three stress-inducible HSP-70 proteins in combination with HSP-110 and DNJ-13 in comparison with the constitutive Hsc70 (HSP-1) protein. Surprisingly, we did not observe suppression activity of the stress-inducible HSP-70s that even remotely resemble the activity by the constitutive Hsc70 (HSP-1; Fig 3A). We, however, detected a slight shift to the right for F44E5.4 (blue), suggesting a delay of fibril formation and wondered if higher chaperone concentrations could further delay or even suppress the

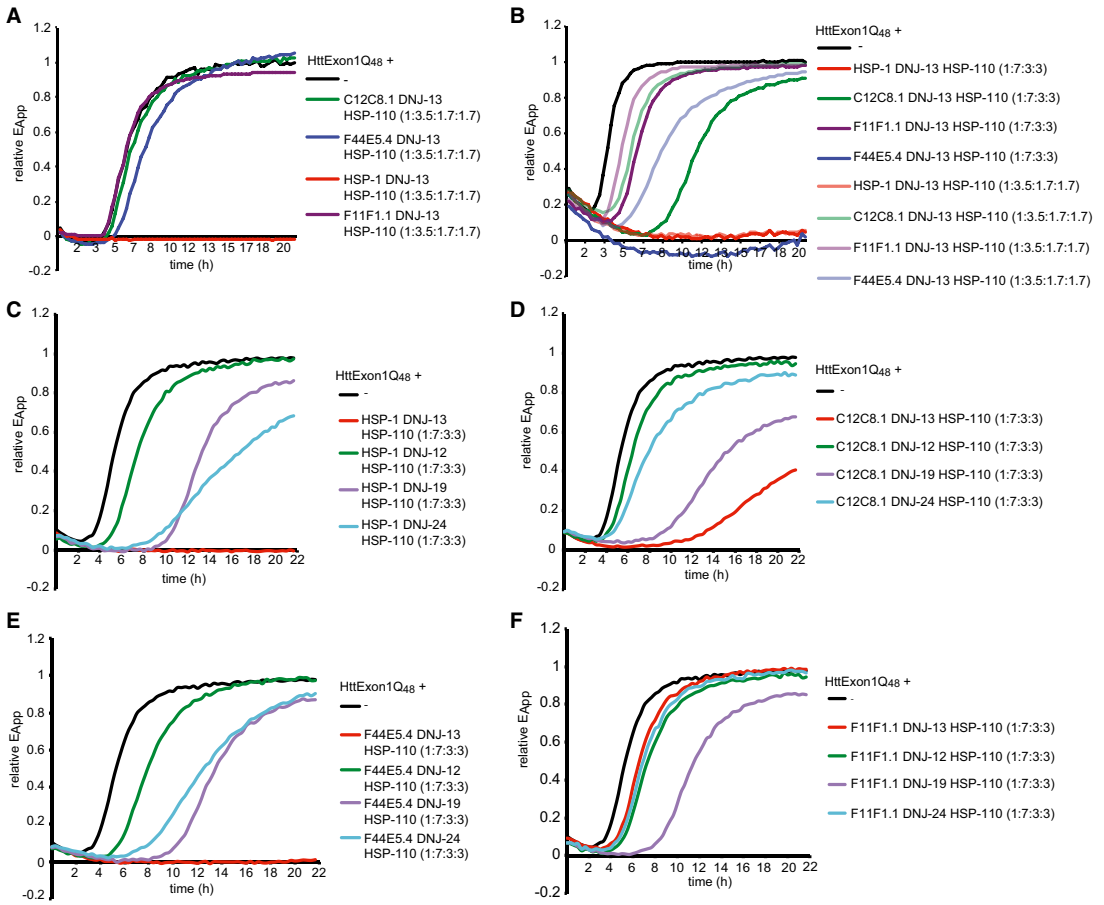


**Figure 3. Constitutive Hsc70 is more potent than the inducible Hsp70s in the suppression of HttExon1$Q_{48}$ fibrilization.**

A FRET assay of varying HSP-70 combinations. HSP-110 and DNJ-13 are kept constant in all samples and the addition of HSP-1 (red) shows complete suppression, whereas in combination with C12C8.1 (green) or F11F1.1 (purple) no suppression occurs and only a slight delay of fibril formation in combination with F44E5.4 (blue).

B FRET assay using two different ratios between HttExon1$Q_{48}$ and the chaperones. Chaperones were either used in the ratios as in Figs 1C and 2A (HttExon1$Q_{48}$:HSP-1/HSP-70s:DNJ-13:HSP-110 = 1:3.5:1.7:1.7) and represented in light colors or used in double concentrations (1:7:3:3) represented in dark colors. HSP-110 and DNJ-13 in combination with HSP-1 (red) with F44E5.4 (blue), C12C8.1 (green), and F11F1.1 (purple).

C–F FRET analysis of HttExon1$Q_{48}$ fibrilization with varying J-protein combinations of HSP-1 (C), C12C8.1 (D), F44E5.4 (E), and F11F1.1 (F) with HSP-110. Additions of J-proteins are depicted in all graphs as follows: DNJ-13 (red), DNJ-24 (light blue), DNJ-19 (purple), and DNJ-12 (green).

HttExon1$Q_{48}$ fibril formation. Upon doubling the chaperone concentrations (for all three chaperones) to achieve a ratio of HttExon1$Q_{48}$: HSP-70:DNJ-13:HSP-110 = 1:7:3:3, we could indeed observe a complete suppression of HttExon1$Q_{48}$ fibril formation for the inducible HSP-70 protein F44E5.4 together with HSP-110 and DNJ-13 (Fig 3B; compare light with dark blue curve). For the other two inducible HSP-70s, C12C8.1 and F11F1.1, we could observe a pronounced shift of the FRET curves to the right, demonstrating a delay in the fibril formation with the higher chaperone concentration (Fig 3B; compare light with corresponding dark colored curves). Thus, the inducible HSP-70s can promote the suppression of Htt fibrilization if they are provided in excess.

#### Preference for a specific J-protein partner by HSP-70s

As demonstrated in Fig 2B, the J-protein is the limiting chaperone in the suppression of HttExon1$Q_{48}$ fibrilization. We thus wondered which J-protein is the preferred cochaperone for each of the HSP-70s in supporting the suppression of HttExon1$Q_{48}$ fibrilization. To address this question, we systematically analyzed combinations of the HSP-70 proteins HSP-1, F44E5.4, C12C8.1, and F11F1.1 with members of the class A (DNJ-12 and DNJ-19 that represent all cytosolic class A J-proteins) and two class B (DNJ-13 and DNJ-24) J-proteins. *C. elegans* encodes for only one HSP-110 protein in the cytosol, which was thus kept constant in all experiments. Interestingly, each HSP-70 protein displays a preference for its cooperation with a J-protein in the suppression assay (Fig 3C–F). The proteins HSP-1 and HSP-110 together with DNJ-13 completely suppressed HttExon1$Q_{48}$ fibril formation. However, HSP-1 and HSP-110 together with DNJ-24, DNJ-19, or DNJ-12 could only delay fibril formation (Fig 3C). The stress-inducible F44E5.4 protein is the only other HSP-70 that, together with DNJ-13 and HSP-110, can fully suppress HttExon1$Q_{48}$ fibril formation (Fig 3E). Interestingly, the preference of the HSP-70s for a partner J-protein in the suppression of Htt amyloid formation differs among the HSP-70s. For instance, whereas DNJ-13 is the preferred J-protein for HSP-1, F44E5.4, and C12C8.1, it does not seem to support F11F1.1 in its chaperone activity to affect HttExon1$Q_{48}$ fibrilization (Fig 3C–F). We wondered if the basis for the preferred J-protein partner for each of the HSP-70s is attributed to the induction of the ATPase activity by the different J-proteins. The ATPase activity of all HSP-70s is induced by any of the tested J-proteins *in vitro* (Fig EV1H). We analyzed various combinations and observed no major differences of the stimulation of the ATP-hydrolysis rate of the HSP-70s by the J-proteins DNJ-12, DNJ-13, DNJ-19, or DNJ-24 (Fig EV1H). The ATPase activity is further stimulated by the presence of HSP-110. To exclude that the ATPase activity of HSP-110 itself accounts for the increase in ATP hydrolysis, we analyzed the basal ATPase activity of HSP-110 and upon addition of the J-proteins. However, we observed only a slight induction of the very low basal ATPase activity of HSP-110 (Fig EV1G and data not shown). Notably, we did not observe a stimulation of the HSP-70 ATP-hydrolysis rate in the presence of the Htt fibrils (data not shown). Importantly, although all tested J-proteins can stimulate the ATPase activity of all HSP-70s, the rates differ substantially. The steady state ATP-hydrolysis rate of HSP-1, HSP-110, and any J-protein is with 200 pmol ATP/μM HSP-1/min on average twice as high as those of the stress-inducible HSP-70s in combination with a J-protein and HSP-110. (Fig EV1H). This difference in ATP hydrolysis might account for the observed variations in the HttExon1$Q_{48}$ suppression efficiencies (Fig 3A and B). Taken together, the composition of chaperone complexes that can suppress Htt amyloid formation is very variable and also stress-inducible HSP-70s can, if provided in excess and with a specific J-protein partner, suppress the fibrilization of Htt.

#### Suppression of HttExon1$Q_{48}$ fibrilization in the presence of seeds

Previously, it was shown that fragments of Htt fibrils can act as seeds and nucleate the fibrilization of still monomeric Htt proteins and thereby accelerate their aggregation (Scherzinger *et al*, 1999; Bhattacharyya *et al*, 2005). We also observed this phenomenon by spiking the FRET assay at time point zero with a small volume (10% v/v) of a 24 h fibril sample that was sonicated beforehand in order to break the fibrils and to create seeding-competent Htt moieties. The addition of the seeds accelerated the fibrilization to the point that the lag phase was almost non-existent (Fig 4A; compare blue with black curve). Next, we tested whether the chaperone mixtures could still suppress the Htt fibril formation in the

**Figure 4. Colocalization of chaperones with HttExon1$Q_{48}$ aggregates *in vitro* and *in vivo*.**

A A scheme of the experimental outline is depicted on the left. On the right, FRET assay of Htt fibrilization in the presence of Htt seeds (blue), in the presence of Htt seeds + HSP-1, HSP-110, and DNJ-13 (red) and the control (black).

B TEM analysis of (A). Scale bars: 100 nm.

C A scheme of the experimental outline is depicted on the left. On the right, FRET assay of suppression of fibrilization in the presence of seeds (blue) and seeds that were incubated with the chaperones for 5 h prior to initiation of FRET assay (red). The control is depicted in black.

D TEM analysis of disaggregation of HttEx1$Q_{48}$ fibrils. On the left: HttExon1$Q_{48}$ fibrils 24 h post-PreSP treatment ($t$ = 0 h; same image as depicted in Figs 1D and G, and 2C); middle: HttExon1$Q_{48}$ fibrils at $t$ = 20 h; right: disaggregation of HttExon1$Q_{48}$ fibrils by nematode chaperones (HSP-1, HSP-110, DNJ-13, ATP) $t$ = 20 h. A scheme of the experimental outline is depicted below. Scale bars: 100 nm.

E Filter retardation analysis of the disaggregation of HttExon1$Q_{48}$ fibrils by human (Hsc70, DNAJB1, Apg2; middle row) and nematode chaperones (HSP-1, DNJ-13, HSP-110; right row). The control (absence of chaperones) is depicted on the left. The time points of analysis are indicated on the left side. A quantification of the disaggregation reaction is depicted in the graph on the right ($N$ = 3). All signals were normalized to the control. Error bars represent the standard deviation.

F Disaggregation analysis of HttExon1$Q_{48}$ fibrils by a sedimentation analysis using the CyPet signal as readout for the moieties of the supernatant and pellet fraction. All data were normalized to the control (absence of chaperones). The chaperone mixtures that were analyzed are indicated on the $x$-axis ($N$ = 5). Error bars represent the standard deviation.

G TEM analysis of the interaction of individual chaperones with HttExon1$Q_{48}$ fibrils by immunostaining. HttExon1$Q_{48}$ fibrils were incubated for 1 h with the individual chaperones, and the interaction of the chaperones was analyzed by immunostaining using the respective antibodies; left: DNJ-13, middle: HSP-1, and right: HSP-110. Scale bars: 50 nm. The red arrows mark the positive immunogold labeling.

H *In vivo* colocalization of DNJ-13, HSP-1, and HSP-110 with Htt513$Q_{128}$-YFP. Htt513$Q_{128}$-YFP-expressing nematodes were immunostained with the antibodies against DNJ-13 (top row), HSP-1 (middle row), and HSP-110 (bottom row). Depicted are head regions of the nematode. Scale bars: 20 μm.

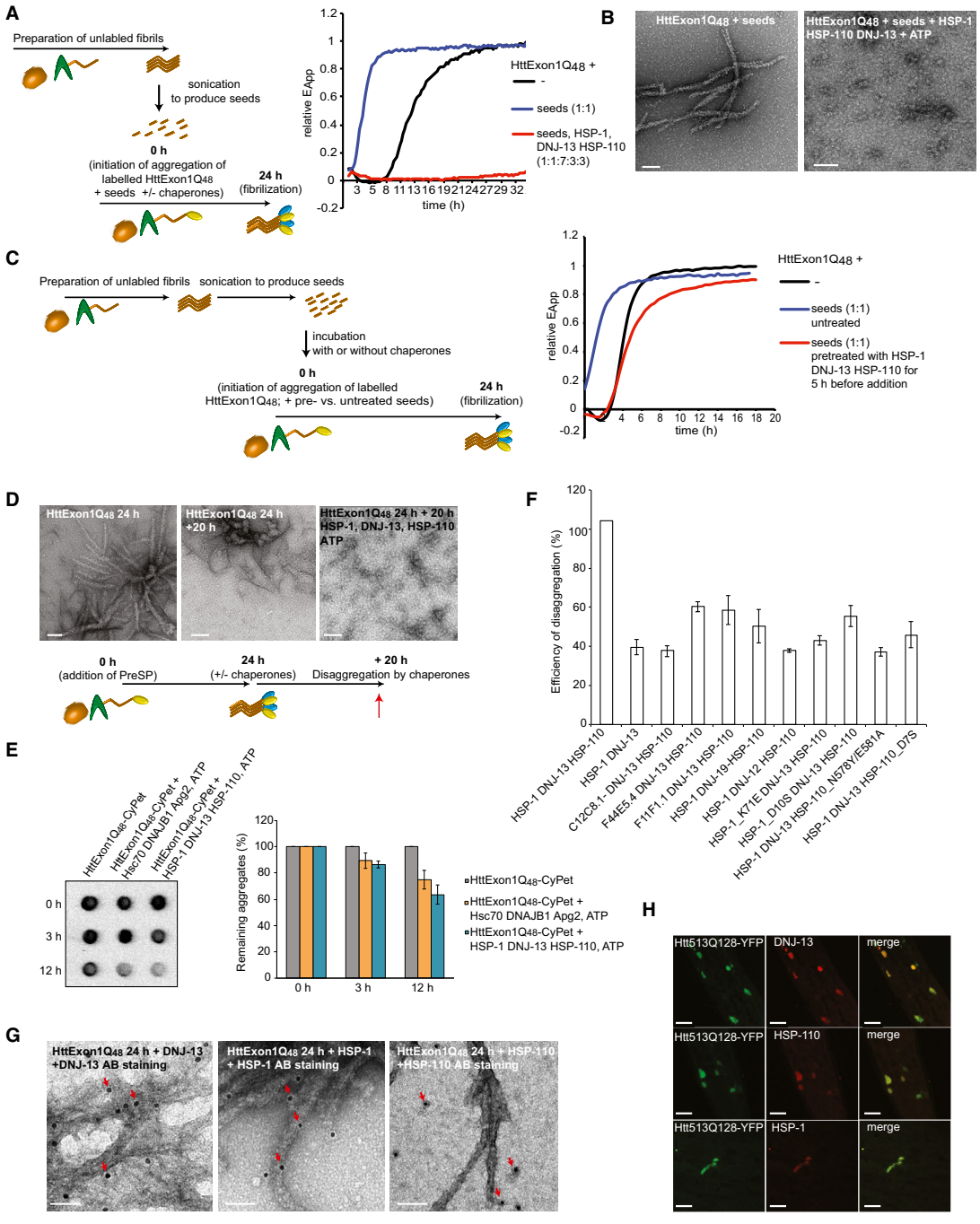


**Figure 4.**

presence of seeds. Indeed, the chaperones could still potently suppress the fibrilization for about 20 h followed by only a slight increase in FRET over a time course of 32 h ($E\Delta_{App}$ increase of < 0.1; Fig 4A). TEM analysis confirms this observation. In the presence of seeds, but absence of chaperones, we can detect HttExon1$Q_{48}$ fibrils whose morphology differs from the fibrils generated without seeds (compare Figs 4A and 1D). In the presence of the chaperone mixture, no fibrils could be detected after 24 h. Some smaller structures were visible, which might account for the weak FRET signal. Taken together, the chaperones can successfully suppress the activity of seeds in promoting HttExon1$Q_{48}$ fibrilization (Fig 4A and B).

#### A distinct chaperone complex disaggregates HttExon1$Q_{48}$ fibrils

We employed the seeding assay to test whether chaperone-treated samples could still seed the fibrilization of HttExon1$Q_{48}$ proteins. Incubation of HttExon1$Q_{48}$ seeds with HSP-1, HSP-110, and DNJ-13 for 5 h abrogated their seeding capacity (Fig 4C). One explanation for this observation is a disaggregation of the Htt seeds by the chaperone mixture that consequently diminishes the seeding competence. Analogous to the data obtained with the human chaperones, we could also observe disaggregation of HttExon1$Q_{48}$ fibrils by the nematode chaperones: HSP-1, DNJ-13, and HSP-110. TEM analysis showed that an incubation of the chaperone mixture and ATP with the fibrils resulted in resolubilization of the HttExon1$Q_{48}$ aggregates (Fig 4D). We then confirmed the TEM data by filter retardation analysis for the human and nematode chaperone mixtures (Fig 4E) and sedimentation analysis analogous to the assay with the human chaperones depicted in Fig 1F. We normalized the disaggregation activities (supernatant to pellet ratios) to the control sample that did not contain chaperones. The ratios of supernatant to pellet significantly increased for the chaperone complex HSP-1, HSP-110, and DNJ-13 in the presence of ATP (Fig EV1I). We then compared the disaggregation activities of various chaperone mixtures to HSP-1, HSP-110, and DNJ-13. As depicted in Fig 4F, the inducible HSP-70s, C12C8.1, F44E5.4, and F11F1.1, together with HSP-110 and DNJ-13, exhibited weaker disaggregation activities. Notably, both type A J-proteins (DNJ-12 and DNJ-19) were less active than DNJ-13 in the Htt disaggregation with HSP-1 and HSP-110 (Fig 4F). We then tested the contribution of the ATPase activity of HSP-1 and HSP-110 by employing the point mutations that abrogate or reduce their ATPase activity (Fig EV1G). Both HSP-1 ATPase mutants displayed a reduced disaggregation activity. Notably, the disaggregation activity of the HSP-110 ATPase mutant HSP-110_D7S is reduced to a similar extend as the ATPase mutants of HSP-1, suggesting that the ATPase activity of HSP-110 is also required for efficient disaggregation. Mutation of the NEF activity of HSP-110 reduces the disaggregation activity even further (Fig 4F), which is in agreement with previous data on the role of HSP-110 in the disaggregation of amorphous luciferase aggregates (Rampelt *et al*, 2012). We then analyzed whether the chaperones could also disaggregate HttExon1$Q_{75}$ fibrils. As depicted in Fig EV2E, no disaggregation could be observed within a time frame of 12 h indicating that the fibrils formed by the longer polyQ stretch are more inert for a chaperone-mediated remodeling.

Taken together, the constitutive Hsc70 (HSP-1) protein together with HSP-110 and the type B J-protein DNJ-13 constitutes the most active disaggregase for the resolubilization of Htt fibrils. Disaggregation of Htt fibrils requires ATPase activity of Hsc70 (HSP-1) and HSP-110 as well as the NEF activity of HSP-110.

#### J-proteins and HSP-70s both bind to Htt fibrils

We then wondered which chaperone might interact directly with the Htt fibrils and which requires recruitment by another chaperone for the disaggregation reaction. To address this question, we generated HttExon1$Q_{48}$ fibrils and incubated them with the individual chaperones for 1 h and then performed immunogold labeling using antibodies against DNJ-13, HSP-1, or HSP-110 that were generated in this study. In the samples containing Htt fibrils and chaperones, immunogold staining was only detected in the presence of both, primary and secondary, antibodies (Figs 4G and EV2A). Interestingly, DNJ-13 was only detected on the fibrils. HSP-1 was mainly detected on the fibrils, but a few gold particles were also detected outside of the fibrils. Notably, HSP-110 did not at all bind to the fibrils (Fig 4G). From these results, we conclude that DNJ-13 and to a lesser extent also HSP-1 can bind to Htt fibrils and are probably also recruiting HSP-110 to these structures. These observations are in agreement with previous data on the interaction of chaperones with α-synuclein fibrils (Gao *et al*, 2015).

Next, we wanted to analyze the association of the chaperones that constitute the active chaperone complex with the Htt aggregates *in vivo* by immunostaining of nematodes expressing aggregation-prone HttpolyQ proteins. For that, we used a nematode model that expresses Htt513$Q_{128}$-YFP in muscle cells that shows a very robust aggregation phenotype (Fig EV2C). Immunostaining, using the respective antibodies against DNJ-13, HSP-1, and HSP-110, showed clear colocalization for all chaperones with the HttpolyQ aggregates (Fig 4H). These data demonstrate that all three chaperones interact *in vivo* with Htt aggregates and confirm our previous observation of the association of the human orthologous chaperones with HttExon1$Q_{97}$ aggregates (Fig 1H).

Interestingly, although only the chaperone complex HSP-1, HSP-110, and DNJ-13 can disaggregate HttExon1$Q_{48}$ fibrils, all studied J-proteins and HSP-70s can bind *in vitro* to the HttExon1$Q_{48}$ fibrils (Fig EV2B). Thus, the ability to recognize amyloid proteins is not sufficient to resolubilize preformed fibrils.

#### Knockdown of *hsp-1*, *hsp-110*, and *dnj-13* results in enhanced polyQ aggregation in multiple *C. elegans* models

Next, we set out to analyze the contribution of the chaperones in maintaining the solubility of polyQ proteins *in vivo*. For that, we employed four different *C. elegans* polyQ models that differ in the protein context (flanking regions) of the polyQ stretch and the length of the polyQ stretch (Morley *et al*, 2002; Christie *et al*, 2014). We tested the effects of the RNAi-mediated knockdown of the chaperones that showed the strongest effect in suppression and disaggregation activities *in vitro: hsp-1*, *hsp-110*, and *dnj-13* in *C. elegans* lines that express Q35-YFP, Htt513$Q_{15}$-YFP, or the disease-relevant C-terminal domain of ataxin-3 with either 45 or 63 glutamine residues (AT3CT$Q_{45}$-YFP and AT3CT$Q_{63}$-YFP) in the body wall muscle. Importantly, depletion of these chaperones results in all models in an increase in aggregation (Fig 5A). Notably, the Htt513$Q_{15}$-YFP model does not show any aggregation under the control conditions as the polyQ length is below the aggregation and pathogenic

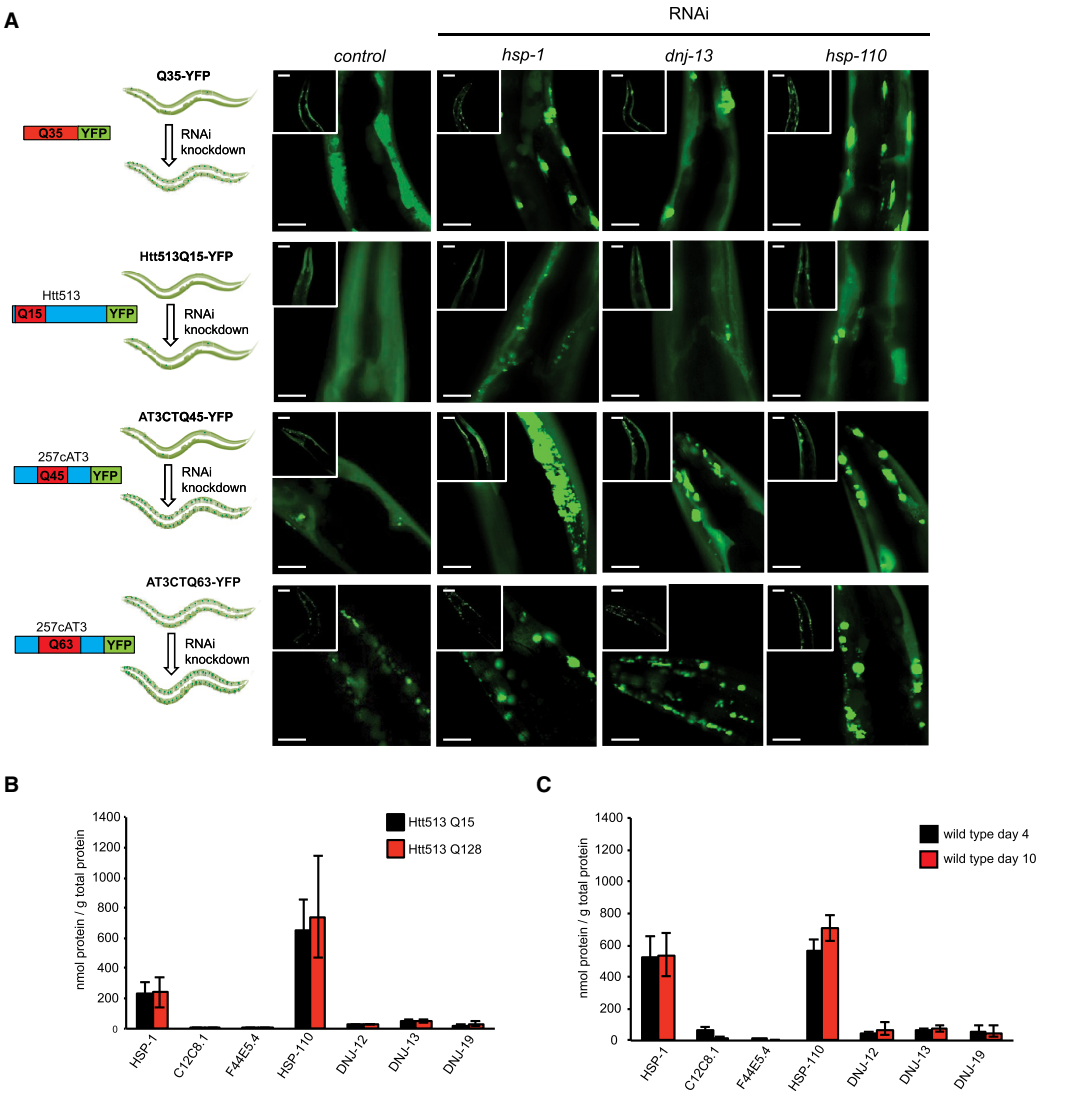


**Figure 5. Depletion of chaperones leads to enhanced aggregation of $Q_n$, $Htt Q_n$ and $ATC3Q_n$ *in vivo*.**

A RNAi-mediated knockdown of *hsp-1*, *dnj-13*, *hsp-110*, and control (empty RNAi vector L4440) in *Caenorhabditis elegans* polyQ models. first row: $Q_{35}$-YFP, second row: $Htt513Q_{15}$-YFP, third row: $ATC3Q_{45}$-YFP, and fourth row: $ATC3Q_{63}$-YFP. Twenty animals per condition were analyzed. Representative images of the head regions are shown for each knockdown. Scale bars: 50 μm.

B Analysis of protein levels of HSP-70s (HSP-1, C12C8.1, and F44E5.4), HSP-110 and J-Proteins (DNJ-12, DNJ-13, and DNJ-19) in 4-day-old animals expressing $Htt513Q_{15}$-YFP (black) or $Htt513Q_{128}$-YFP (red). Depicted is the average of three independent analyses. Error bars represent the standard deviation.

C Analysis of protein levels of DNJ-12, DNJ-19, DNJ-13, HSP-1, C12C8.1, and HSP-110 in young adults (4-day-old nematodes, black) and old (10-day-old, red) nematodes. We do not have an explanation for the higher HSP-1 protein levels in the wild-type N2 animals compared to the $Htt513Q_{15/128}$-expressing animals (Fig 5B). Depicted is the average of three independent analyses with error bars representing the standard deviation.

threshold especially given the rather long flanking region (Havel *et al*, 2009). However, depletion of *hsp-1*, *hsp-110,* and *dnj-13* leads to formation of protein aggregates in this model. These findings suggest that the chaperones are actively involved in maintaining the solubility of the $Htt513Q_{15}$-YFP proteins. From this *in vivo* analysis, we conclude that *hsp-1*, *dnj-13*, and *hsp-110* are crucial chaperones

 

to cope with the aggregation propensity of polyQ proteins in nematodes.

#### HttpolyQ aggregation does not lead to an induction of chaperone levels

The knockdown data suggest a vital role of the specific chaperones HSP-1, HSP-110, and DNJ-13 in the maintenance of the solubility of all polyQ proteins. Although it has been shown that the expression of HSF-1, the master regulator of the heat-shock response, is not activated in $HttQ_{91}$-expressing mammalian cells (Bersuker *et al*, 2013), we wondered whether specific chaperones are induced in response to polyQ expression in the nematode. For such an analysis, we quantified the protein levels of a selected set of chaperones: three cytosolic HSP-70s (HSP-1, F44E5.4, and C12C8.1), HSP-110, and the J-proteins DNJ-12, DNJ-13, and DNJ-19 in young adult (4-day-old) animals expressing soluble $Htt513Q_{15}$ and highly aggregation-prone $Htt513Q_{128}$ proteins. Importantly, we observed no significant induction for either of the investigated chaperones (Figs 5B and EV2D).

#### Chaperone levels do not change with age

Huntington's disease is a late age of onset disease (Lipe & Bird, 2009). Thus, we wondered how much the chaperone levels change with the progression of aging. We quantified the same selected set of chaperones as before in young (4-day-old) and old wild-type animals (10-day-old). Notably, the protein levels of the J-proteins, DNJ-12, DNJ-13, and DNJ-19, as well as of the HSP-70s, HSP-1, and C12C8.1, and of HSP-110 do not significantly change with aging (Figs 5C and EV2D).

#### Knockdown of DNAJB1 and Apg2 leads to Htt aggregation in neural progenitor cells (NPCs) derived from a HD patient

To validate our observations in a clinically relevant model, we employed neural progenitor cells (NPCs) derived from induced pluripotent stem cells (iPSCs) that were generated from a HD patient carrying a polyQ stretch of 44 residues within the huntingtin protein ($HttQ_{44}$; patient CH4). The derived NPC line, defined as NICH4, showed the expression of the correct NPC-specific markers at the protein and mRNA levels (Fig 6A and B). The neural induction was slightly less efficient in HD NPCs compared to control NPCs (Fig 6B), which is in agreement with recent findings (Kirstein *et al*, 2017). NICH4 cells were then transfected with siRNAs directed against transcripts encoding the human chaperones Hsc70, DNAJB1 (J-protein), and Apg2 (Hsp110).

We used a filter retardation assay to monitor the aggregation propensity of endogenous Htt. Under control conditions, we could only detect a weak signal for Htt on filter membranes (Fig 6C), indicating that the protein is not aggregated. Accordingly, although NPCs derived from HD patients have been found to exhibit bioenergetic abnormalities, Htt aggregation phenotypes have yet to be reported (Consortium, 2012; Kirstein *et al*, 2017). Importantly, however, upon siRNA-mediated knockdown of DNAJB1 and Apg2, we could detect pronounced aggregation of Htt (Fig 6C). This is the first demonstration of aggregation of the endogenous Htt protein with an expanded polyQ stretch in HD patient-derived neural cells. This observation confirms the *in vitro* data of the suppression of aggregation and disaggregation of Htt protein by these chaperones. Surprisingly, depletion of Hsc70 did not result in an increased aggregation of Htt (Fig 6C). The remaining protein levels of the chaperones upon knockdown were still between 54 and 75% of the control with Hsc70 displaying the highest remaining level (Fig 6D). Moreover, other members of the Hsp70 family could also substitute the constitutive Hsc70, as observed *in vitro* (Fig 3B). Nevertheless, a reduction in protein levels of DNAJB1 and Apg2 clearly affects the aggregation propensity of endogenous HttQ44. These findings are in complete agreement with the RNAi-mediated chaperone knockdown experiments in nematode polyQ models (Fig 5). To rule out that RNAi-mediated knockdown of chaperones could simply result in an increase in the overall levels of Htt by, for example, inhibiting targeting to the proteasome and thereby enhancing their aggregation propensity, we analyzed the $HttExon1Q_{97}$ levels in HEK293T cells upon siRNA treatment (Fig EV2E). We observed a shift of $HttExon1Q_{97}$ from the soluble to the insoluble fraction in particular upon depletion of DNAJB1 as expected from our previous observations (Figs EV2F, 5A and 6C). Importantly, however, we did not detect changes in the overall levels of $HttExon1Q_{97}$ upon knockdown of the chaperones (Fig EV2F and G).

#### Overexpression of DNAJB1 in mammalian cell culture reduces $HttExon1Q_{97}$ aggregation

Finally, we wanted to test if we could rescue the aggregation of Htt by overexpression of chaperones. For that, we chose to analyze HEK293T cells expressing $HttExon1Q_{97}$-GFP, which show robust aggregation under control conditions and enable us to analyze a potential rescue effect upon overexpression of a chaperone. We chose to test the effect of overexpression of DNAJB1 based on our previous findings: (i) siRNA-mediated depletion of DNAJB1 showed the strongest effect on the aggregation propensity of endogenous $HttQ_{44}$ of the patient-derived NPCs (Fig 6C), (ii) the J-protein directly interacts with $HttExon1Q_{48}$ fibrils (Fig 4G), and (iii) the J-protein is the chaperone whose concentration is most critical for the suppression of Htt fibril formation (Fig 2B). Overexpression of DNAJB1 in the $HttExon1Q_{97}$-GFP-expressing HEK 293T cells did indeed reduce the aggregation of Htt by ~50% as judged by a filter retardation assay. This finding demonstrates that the overexpression of a single and *in vivo* probably limiting chaperone can ameliorate Htt protein aggregation (Fig 6E–G).

## Discussion

In this study, we demonstrate for the first time a complete suppression of amyloid formation of $HttExon1Q_{48}$, a near complete suppression of $HttExon1Q_{75}$ aggregation and disaggregation of preformed amyloid $HttExon1Q_{48}$ fibrils. The suppression and disaggregation activities are mediated by distinct chaperone complexes, which are composed of members of the Hsp70, Hsp110, and J-protein families. We could demonstrate the suppression of $HttExon1Q_n$ fibrilization *in vitro* by employing a novel FRET fibrillization assay and complementary TEM and filter retardation analyses using purified human and *C. elegans* chaperones. Analysis of the kinetics of the FRET curves suggests that the chaperones suppress the fibrilization of $HttExon1Q_{48}$ by primary and secondary nucleation events as well as

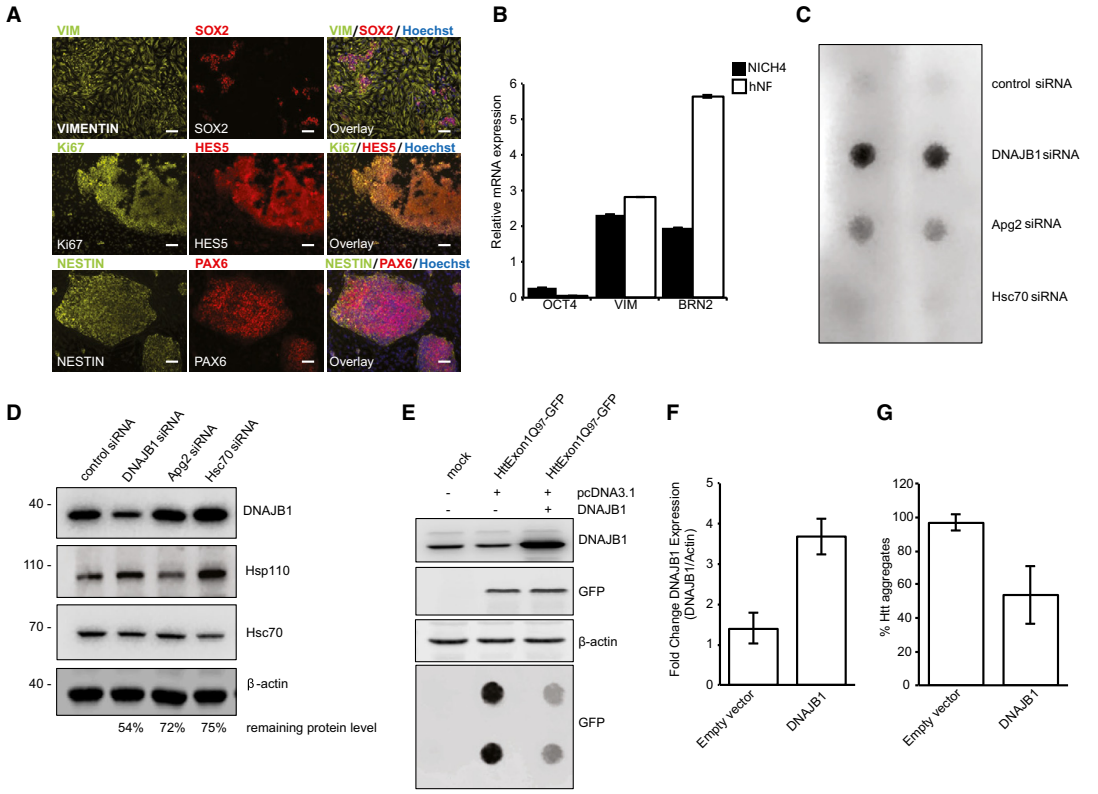


**Figure 6. Depletion of chaperones leads to an increase in Htt aggregation in NPCs and overexpression of DNAJB1 ameliorates HttExon1Q$_{97}$ aggregation in HEK 293T cells.**

A Characterization of NICH4. The neural progenitor cell (NPC) line NICH4 was differentiated from HD patient-derived iPSCs. NICH4 exhibit typical NPC morphology and grew as cellular monolayer on Matrigel-coated dishes. NICH4 expressed the NPC-specific protein markers VIMENTIN (VIM), SOX2, HES5, NESTIN, and PAX6, and the proliferation marker Ki67. Scale bars: 100 μm.

B Quantitative real-time PCR (qPCR) confirmed the transcriptional down-regulation of the pluripotency marker *OCT4* and the up-regulation of NPC-specific markers *VIMENTIN* (*VIM*) and *BRN2* in NICH4 HD NPCs compared to undifferentiated H9 hESCs, in a similar fashion as the control line hNP1 (purchased from Aruna Biomedicals). Control NPCs showed increased BRN2 expression indicative of a slightly more efficient neural induction compared to HD NPCs. Error bars represent the standard deviation ($N = 3$).

C Filter retardation assay for the analysis of the aggregation propensity of endogenous Htt in NPCs (NICH4) upon siRNA-mediated knockdown of DNAJB1, Apg2 (Hsp110), Hsc70, and the control (non-targeting siRNA). The filter trap shows duplet spots for each condition.

D Western blot depicts the knockdown efficiency of the siRNA-mediated knockdown of the chaperones in the NICH4 cells. The protein levels of the chaperones normalized to the control and β-actin levels are depicted below the blot.

E Western blot and filter retardation analysis of the aggregation propensity of HttExon1Q$_{97}$ upon overexpression of DNAJB1. The protein levels of DNAJB1 are depicted in the top blot, and overexpression of DNAJB1 (right column) does not affect the HttExon1Q$_{97}$ levels (GFP signal of middle blot). The filter trap assay (bottom blot) depicts the aggregation propensity of HttExon1Q$_{97}$ upon overexpression of DNAJB1 and is analyzed in duplets.

F Quantification of the overexpression of DNAJB1 of the Western blot shown in (E). Error bars represent the standard deviation ($N = 3$).

G Quantification of the aggregation propensity of HttExon1Q$_{97}$ upon overexpression of DNAJB1 of the filter retardation analysis depicted in (E). Error bars represent the standard deviation ($N = 3$).

by inhibiting the elongation process (Arosio *et al*, 2014). We could further establish that the same chaperone composition can resolubilize preformed HttExon1Q$_{48}$ fibrils. Both chaperone activities are ATP dependent. We could demonstrate that the suppression of HttExon1Q$_{48}$ fibrilization requires the ATPase activity of HSP-1 (Hsc70), but not of HSP-110. Yet the NEF activity of HSP-110 was essential to suppress amyloid formation. The suppression of fibrilization is therefore not mediated by a single ATPase cycle to, for example, initiate substrate engagement by the chaperones, but requires constant ATPase cycles and suggests a binding-release model of action. Notably, disaggregation requires the ATPase activities of both, HSP-1 (Hsc70) and HSP-110, as well as the NEF activity of HSP-110. Thus, the mechanism differs substantially from the suppression of fibrilization activity.

Interestingly, the constitutive Hsc70 (HSP-1), HSP-110, and the type B J-protein DNJ-13 showed the strongest suppression of Htt fibrilization. However, the stress-inducible HSP-70s could substitute for Hsc70, yet require higher chaperone:Htt ratios. Notably, all HSP-70s exhibit varying efficiencies in the suppression of Htt fibrilization depending on the partner J-protein.

The basal ATPase rates of the inducible Hsp70s are with the exception of F11F1.1 similar to the rate of the constitutive HSP-1 (30 pmol ATP/μM/min). Although each of the Hsp70s is induced by any analyzed J-protein *in vitro*, the final ATP-hydrolysis rates are about 50% of the one of the activated constitutive HSP-1 (up to 200 pmol ATP/μM/min) that can rely on the energy of twice as much ATP for its remodeling activities to suppress Htt fibrilization. This is in agreement with our observation that doubling the amount of the chaperone complexes harboring the inducible Hsp70s can boost their activities in the suppression of Htt fibrilization activities and matches those of HSP-1 (Fig 3B).

Disaggregation of Htt fibrils is mediated by Hsc70/HSP-1, Apg2/HSP-110, and DNAJB1/DNJ-13—the very same chaperone complex that exhibits the highest efficiency for the suppression of Htt fibrilization. We observed a decreased disaggregation by a type A J-protein (e.g., DNJ-12) together with HSP-1 and HSP-110, which is in agreement with the observations made for the depolymerization of α-synuclein fibrils (Gao *et al*, 2015). Notably, we did also not detect a synergistic activity when mixed-class J-proteins were provided for either suppression or disaggregation of Htt fibrils, which was also not observed for the disaggregation of α-synuclein fibrils (Gao *et al*, 2015). The resolubilization of amyloid fibrils thus only requires the action of a single type B J-protein as opposed to amorphous aggregates such as luciferase or MDH (Nillegoda *et al*, 2015; Kirstein *et al*, 2017). Perhaps the association and required remodeling activities differ substantially between structured amyloid fibrils and amorphous aggregates (Scior *et al*, 2016). Interestingly, the preference for a type B J-protein is not based on the substrate recognition as we could detect binding of the HttExon1$Q_{48}$ fibrils for DNJ-13 (type B) as well as for both type A J-proteins DNJ-12 and DNJ-19. The disaggregation activities of the inducible HSP-70s are reduced compared to the constitutive HSP-1 despite their ability to bind to HttExon1$Q_{48}$ fibrils.

We could confirm our *in vitro* data on the chaperone-mediated suppression and disaggregation of Htt fibrils by employing *in vivo* nematode models that express polyQ ($Q_n$) proteins with different flanking regions and a varying degree of polyQ expansion (Fig 5A and B). Moreover, using patient-derived neural progenitor cells, we could demonstrate a sharp increase in the aggregation of the endogenous Htt protein (Q44) upon knockdown of DNAJB1 (DNJ-13 ortholog) and Apg2 (HSP-110; Fig 6C and D). Consequently, overexpression of DNAJB1 in HEK 293T cells expressing the highly aggregation-prone HttExon1$Q_{97}$ significantly reduced the aggregation (Fig 6E–G). Thus, the induction of a single chaperone can combat the aggregation propensity of Htt. Our observations that the concentration of the J-protein appears to be the most critical of all three chaperones in the *in vitro* suppression assay, its strong interaction with the Htt fibrils together with the *in vivo* data where a depletion of the J-protein provoked the strongest aggregation effect in *C. elegans* $Q_n$ models and patient-derived NPCs as well as the rescue properties upon overexpression, suggest that the J-protein is a very attractive therapeutic target to suppress and resolubilize Htt fibrils.

We could demonstrate that an excess of chaperones is required to fully suppress the formation of amyloid fibrils. This poses the question of the *in vivo* chaperone concentration and their capacity in particular with the progression of aging as HD is a late age of onset disease (Lipe & Bird, 2009). Surprisingly, we observed that the protein levels of a subset of chaperones we analyzed *in vitro* and *in vivo* do not significantly change with aging or upon expression of polyQ proteins (Fig 5B and C). This observation is in agreement with a previously published proteome study of young adults and aged nematodes (Liang *et al*, 2014). Yet, it is well established that misfolded and aggregated proteins accumulate with the progression of aging (David, 2012). In addition, the suppression and disaggregation reactions consume substantial amounts of ATP. ATP levels decline with aging and might become a limiting factor for the activity of the chaperones and in turn lead to more aggregation (Navarro *et al*, 2002; Miyoshi *et al*, 2006; Simsek-Duran *et al*, 2013). Moreover, molecular chaperones are involved in numerous cellular processes and might simply be overwhelmed with the increasing load of misfolded proteins in aged animals (Balchin *et al*, 2016; Scior *et al*, 2016). We could mimic such a scenario by adding aggregated citrate synthase to the *in vitro* HttExon1$Q_{48}$ suppression assay and could indeed show that the efficiency of the chaperones to suppress fibril formation of Htt is impaired in the presence of additional chaperone substrates. In line with that, protein aggregates, which accumulate in response to proteotoxic conditions or with aging, sequester chaperones that are consequently depleted from the soluble proteome and thus the available chaperone pool (Kirstein-Miles *et al*, 2013).

Htt protein levels have been measured in various cell types and tissues, and the concentration of Htt was on average 171 nmol/g total protein in postmortem cortex homogenates of HD patients (Macdonald *et al*, 2014). We quantified the protein levels of a selected set of chaperones in this study. The concentration of HSP-1 (Hsc70) in *C. elegans* is about 250 nmol/g total protein in nematodes expressing Htt513$Q_{128}$. Although the quantifications were obtained from two very different biological samples, it nevertheless might provide a rough estimate that Hsc70 is only present in a ~1.5-fold excess over Htt in the brain homogenate. Given that Hsc70 has numerous roles in the maintenance of cellular proteostasis, the effective chaperone concentration that could suppress Htt fibrilization is probably limiting, especially given that a minimum of 3.5-fold excess of Hsc70 is required for a complete suppression. Although we cannot exclude that other J-proteins apart from DNJ-13 (DNAJB1) contribute to the suppression and disaggregation of Htt fibrils, the concentration of the J-protein DNJ-13 is sub-stoichiometric compared to the Htt moiety. In fact, all three analyzed J-proteins are present in similar and thus sub-stoichiometric amounts in comparison with Htt. J-proteins can act also independently of Hsc70 as has been demonstrated for DNAJB6. DNAJB6 can suppress the fibrillization of Htt via a S/T-rich region within the chaperone (Kakkar *et al*, 2016). Disaggregation of Htt fibrils, however, requires a chaperone complex composed of Hsc70, Hsp110, and a J-protein. Transient interaction of soluble oligomeric HttpolyQ species was recently reported for the J-proteins: DNAJA1, DNAJA2, DNAJB6, and DNAJB12 (Kim *et al*, 2016). Whether these J-proteins directly interact with HttpolyQ or are a part of a protein complex is not known yet, but suggests the formation of very dynamic chaperone complexes that attend to HttpolyQ proteins to maintain their solubility.

Further studies are required to gain more mechanistic insight into the mode of action of the chaperone-mediated suppression of Htt fibrilization and disaggregation of these amyloid fibrils. Do Hsp70, Hsp110, and the J-protein form a physical complex at any time of their course of action or do they bind and act sequentially? Our data suggest that the J-protein probably initiates the binding to the substrate and recruits Hsp70. It is not known yet whether the J-protein dissociates upon activation of the ATPase activity of Hsp70. Hsp110 could interact with Hsp70 in its ADP-bound form in its role as NEF to complete the ATPase cycle. We could not detect an interaction of HSP-110 alone with the $HttExon1Q_{48}$ fibrils, yet we could demonstrate an interaction of HSP-110 with $Htt513Q_{128}$ aggregates *in vivo*. We thus hypothesize that HSP-110 is recruited to the Htt aggregates by Hsc70 or the J-protein. An interaction between the J-protein and HSP-110 is possible as we also observed a slight induction of the ATPase activity of HSP-110 by a J-protein. A clamping-and-walking model of disaggregation by Hsp70-Hsp110 was recently proposed and the role of the J-proteins is here limited to initial substrate recognition and stimulation of the ATPase of Hsp70 and Hsp110 (Mattoo *et al*, 2013). Our observation that the ATPase activity of HSP-110 was required for sufficient disaggregation and the high abundance of HSP-110, whose protein levels exceed those of Hsc70 *in vivo* argues for a more central role of HSP-110 in chaperone activities besides its described role as NEF.

## Materials and Methods

#### Plasmid cloning and protein purification

Please see Appendix.

#### CD spectra of HSP-1 and HSP-110 variants

The mutagenized proteins were prepared as described, concentrated in centrifugal filters [Amicon Ultra-0.5 Centrifugal Filter Devices, 10 kDa MWCO (Merck Millipore, Germany)] to a volume of no more than 100 µl and diluted with CD buffer (10 mM sodium phosphate, 100 mM NaF, pH 7.4) to a volume of 500 µl. This process was repeated eight times to ensure the buffer was exchanged, after which samples were centrifuged at 100,000 *g* for 1 h. CD spectra were obtained in a Jasco J-720 spectropolarimeter (Jasco, Gross-Umstadt, Germany) with 10 accumulations. HSP-1 samples were diluted to 1 mg/ml and HSP-110 samples to 0.2 mg/ml (as determined by Bradford assay) to be analyzed at a path length of 1 mm (volume: 200 µl). Cuvettes [Quartz Suprasil cuvettes (Hellma Analytics, Germany)] were kept at 20°C under a stream of $N_2$ during measurements. The scanning speed was set to 100 nm/min with a response time of 1 s and a bandwidth of 1 nm. Photomultiplier voltage was monitored during measurements, which were constricted to wavelengths where 800 V were not surpassed.

#### Nematode antibodies

Polyclonal antibodies against HSP-1, C12C8.1, DNJ-12, DNJ-13, DNJ-19, and HSP-110 were raised in rabbits by immunization with the full-length protein (HSP-1, C12C8.1, DNJ-12, DNJ-13, DNJ-19) or a C-terminal fragment for HSP-110 (beginning at amino acid 687), respectively (Charles River, France; and Pineda, Germany). The polyclonal antibody against F44E5.4 was raised in a guinea pig by immunization with the full-length F44E5.4 protein (Pineda, Germany).

#### ATPase assay

The ATPase rate of Hsp70 chaperones was determined by the malachite green assay according to Rauch and Gestwicki (2014) using 0.5 µM of Hsp70s, 0.25 µM J-proteins, and 0.25 µM HSP-110 as well as for the human orthologs (Hsc70, DNAJB1 and Apg2). The reactions were performed in low salt buffer (30 mM Tris–HCl, pH 7.4, 100 mM K-acetate, 5 mM $MgCl_2$, 1 mM β-mercaptoethanol, 10% glycerol) for 2.5 h at 20°C for *C. elegans* chaperones and at 30°C for human chaperones.

#### FRET assay

Purified GST-$HttExon1Q_{48/23}$-CyPet and GST-$HttExon1Q_{48/23}$-YPet were diluted in aggregation buffer (30 mM HEPES-KOH pH 7.4, 150 mM KCl, 5 mM $MgCl_2$, 1 mM DTT) at an equimolar ratio to yield a final concentration of 1.5 µM (0.75 µM each). If not stated otherwise, 5 mM ATP and an ATP regeneration system composed of 3 mM phosphoenolpyruvate (PEP) and pyruvate kinase (Sigma) were added to the reaction. The aggregation was initiated with 14 U PreSP (Roche) per nmol Htt. To monitor prevention of aggregation, the chaperones were added prior to addition of PreSP. The reactions were transferred to a black 384-well plate. For each experiment, triplicates were measured and mean value is shown. Fluorescence signals were measured every 20 min with a Tecan F200 fluorescence plate reader at 20°C for up to 48 h. CyPet donor fluorescence was measured at excitation (Ex): 430 nm/emission (Em): 485 nm; YPet acceptor fluorescence at Ex: 485 nm/Em: 530 nm; the FRET channel (DA) was recorded at Ex: 430 nm/Em: 530 nm. Raw signals were processed by subtracting the fluorescence intensities of unlabeled $HttExon1Q_{48/23}$ in all channels. Signals in the FRET channel were corrected for donor bleed-through (cD) and acceptor cross excitation (cA) using donor and acceptor only samples to obtain the sensitized emission. Finally, sensitized emission was normalized to the acceptor signals (Jiang & Sorkin, 2002). In brief, the FRET efficiency EApp was calculated as follows: E = (DA-cDxDD-cAxAA)/AA with DD = donor channel signal and AA = acceptor channel signal.

Citrate synthase (CS) aggregates were prepared by diluting CS to 10 µM in aggregation buffer (30 mM HEPES pH 7.4, 150 mM KCl, 5 mM $MgCl_2$, 1 mM DTT) and subsequent heating at 50°C for 10 min. Final concentration of aggregates in the FRET assay was 0.15 µM.

#### EM sample preparation

Details for EM sample preparation are provided in the Appendix. At the indicated time points, samples were flash-frozen in liquid nitrogen and then deposited on a carbon-coated formvar copper grid. After 45 s, the sample droplet was blotted with filter paper and negatively stained with 2% uranyl acetate in water. Samples were imaged using a Tecnai F20 (200 keV) transmission electron microscope. For immunogold labeling, fibrils were first formed for 24 h

 

and subsequently incubated with the respective chaperone for 30 min at 20°C and then flash-frozen in liquid nitrogen. The grids were incubated with the samples on drops of washing buffer, primary and secondary antibodies prior to negative staining.

#### Suppression of fibrilization and disaggregation by filter retardation analysis

Please see Appendix.

#### Disaggregation via sedimentation analysis

GST-HttExon1$Q_{48}$-CyPet protein was incubated with 14 U PreSP (Roche) per nmol Htt for 24 h at 20°C to allow cleavage of GST domain and subsequent fibril formation. Afterward, the fibrils were collected by centrifugation at 50,000 *g* for 40 min and resuspended by sonication (2 s 50% duty power level 4) in aggregation buffer (30 mM HEPES-KOH pH 7.4, 150 mM KCl, 5 mM $MgCl_2$, 1 mM DTT) to result in a final concentration of 1.5 μM fibrils. The chaperones were added in the following concentrations: 20 μM HSP-1, 10 μM DNJ-13, and 10 μM HSP-110. For the human chaperones, we used: 30 μM Hsc70, 15 μM DNAJB1, 15 μM Apg2. Disaggregation reaction was initiated by addition of 5 mM ATP as well as a regenerative system (3 mM PEP + pyruvate kinase) and performed at 20°C for nematode and 30°C for human chaperones, respectively. Samples were harvested at the indicated time points and directly centrifuged at 20,000 *g* for 30 min at 4°C. To determine the amount of soluble protein, the fluorescence of the supernatant as well as of the pellet was measured in the Tecan F200 plate reader (excitation: 430 nm; emission 485 nm) in triplicates.

#### Quantification of *in vivo* chaperone concentration by Western blotting

Please see Appendix.

#### Nematode strains, maintenance, and RNAi

Please see Appendix.

#### Fluorescence microscopy

The aggregation propensities of $Q_{35}$-YFP, AT3C$Q_{45}$, AT3C$Q_{63}$, and Htt513$Q_{15}$ were analyzed on day 5 of life. Animals were subjected to RNAi treatment from the first larval stage on and maintained on RNAi plates throughout the experiment. For imaging, nematodes were mounted onto 2% agarose (Sigma) pads on glass slides and immobilized with 2 mM Levamisole (Sigma). Images were taken on a LSM780 confocal microscope at 20× and 63× magnification. The $Q_{35}$-YFP-expressing nematodes were analyzed as whole nematode for quantification of the aggregates, and an image was taken of the head region of the animal; 20 animals were analyzed for each condition. Immunostaining of nematodes was performed as described before (Kirstein-Miles *et al*, 2013).

#### Cell culture and transfection

Please see Appendix.

#### iPSC and NPC generation and validation

CH4 fibroblasts were obtained from the skin biopsy of a HD patient (male, age 25–38, Q length 44Q). CH4 fibroblasts were transfected with episomal plasmids containing seven transcription factors (OCT4, SOX2, KLF4, c-MYC, NANOG, LIN28, and SVLT) using Amaxa Cell Line Nucleofector Kit R (Lonza) to generate induced pluripotent stem cells (iPSCs), as previously described (Lorenz *et al*, 2017). Full characterization of the derived iPSC line demonstrated the successful achievement of pluripotency (Mlody, Bukowiecki, *et al*, in preparation). Human embryonic stem cell (hESC) line H9 (WA09) was purchased from WiCell and employed according to the German law (license to Dr. Prigione). Control NPCs, differentiated from the hESC line H9 using a traditional rosette-based approach, were purchased from Aruna (hNP1, Aruna Biomedicals, Georgia, USA). Neural induction (NI) NPCs were derived from iPSCs following a small molecule-mediated protocol (Lorenz *et al*, 2017). Briefly, iPSCs were split and plated onto feeder-free Matrigel-coated plates in DMEM/F12 medium. The next day, the cells were cultured in NI medium [Neurobasal:DMEM/F12 (1:1), N2 (1×), B27 (1×), hLIF (10 ng/ml), CHIR99021 (4 μM, Cayman Chemical), SB431542 (3 μM, SelleckChem), BSA (0.05%), pen/strep, MycoZap, and L-glutamine]. Compound E (0.1 μM Calbiochem) was added to the NI medium for the first week. Afterward, only NI medium was employed. The obtained line, named as NICH4, was maintained on Matrigel-coated plates and split by scraping with a cell spatula at 80–100% confluence at ratios of 1:2 to 1:5. All cultures were normally kept in a humidified atmosphere of 5% $CO_2$ at 37°C under atmospheric oxygen condition and were regularly monitored against mycoplasma contamination.

#### Immunostaining of NPCs

Cells were fixed with 4% paraformaldehyde (Science Services) for 20 min at RT, washed two times with PBS, and permeabilized using a blocking solution containing 10% FBS and 1% Triton X-100 in PBS and 1% Tween 20 (all Sigma-Aldrich) for 1 h at RT. Primary antibodies were incubated for at least 1 h at RT in the blocking solution and included VIMENTIN (1:300; V6630, Sigma), SOX2 (1:100, sc-17320, Santa Cruz Biotechnology), Ki67 (1:50, DakoCytomation), HES5 (1:50, sc-25395, Santa Cruz Biotechnology), NESTIN (1:200, MAB5326, Millipore), and PAX6 (1:200, 901301, BioLegend). Following washing, the corresponding secondary antibodies were applied (Alexa Fluor, 1:300, Invitrogen, Life Technologies). Counterstaining of cell nuclei was achieved by incubation with 2 μg/ml Hoechst 33342 (Thermofisher, MA, USA) in PBS for 10 min at RT. All images were acquired using the Olympus IX70 microscope (Olympus, Hamburg, Germany) and further processed with Adobe Photoshop CS 6 (Adobe, Munich, Germany).

#### Quantitative real-time PCR of NPCs

Gene expression analysis was performed by quantitative real-time PCR (qPCR) using SYBR Green PCR Master Mix and the ViiA™ 7 Real-Time PCR System (Applied Biosystems). For each target gene, cDNA samples and negative controls were run as technical triplicates using the 384-Well Optical Reaction Plates (Applied Biosystems). Relative transcript level of each gene was calculated

according to the $\Delta\Delta C_T$ method (Livak & Schmittgen, 2001). The data, normalized to the housekeeping gene ACTB and referred to the undifferentiated H9 hESC line, are presented in the figure as $-\Delta\Delta C_T$ values. The sequences of the oligonucleotides can be found in the Appendix.

#### Western blot analysis and filter trap assay of cell culture samples

Please see Appendix.

**Expanded View** for this article is available online.

### Acknowledgements
We acknowledge B. Bukau (ZMBH-DKFZ Alliance Heidelberg) for the overexpression plasmids for the human chaperones Hsc70, Apg2, and DNAJB1, Elise Kikis (University of the South, USA) for providing us with the non-integrated $Htt513Q_{15}$-YFP and $Htt513Q_{128}$-YFP nematode lines, Svea Hohensee, Martina Ringling, and Franziska Wiedemann for technical support, Ellen Malovrh, Marc Bohlmann, and Ashley Zheng are acknowledged for their assistance with some protein assays and Raul Bukowiecki for initial iPSC generation. We acknowledge funding from the DFG (NeuroCure EXC257, SFB740, SPP1623 to JK), DFG (NeuroCure EXC257 PhD fellowship to MLP), Daimler & Benz Stipend (to AS), AXA Research Fund (to KJ), Berlin Institute of Health and Gender Equality Funds (to BM), and the Bundesministerium für Bildung und Forschung (e:Bio young investigator grant AZ.031A318 to AP), the Berlin Institute of Health Collaborative Research Grant (no. 1.1.2.a.3 "Elucidating the proteostasis network to control Alzheimer's disease") funded by the German Federal Ministry for Education and Research (BMBF), the Helmholtz Validation Fund (grant no. HVF-0013 "Enabling Technologies for Drug Discovery against Protein Misfolding Diseases") funded by the Helmholtz Association, Germany (to E.E.W.).

### Author contributions
AS, KA, JK, MI, KJ, MLP, and BM performed experiments. AS, KA, JK, MI, KJ, MLP, BM, and AP analyzed data. JP, AP, and BM contributed reagents and technological know-how. AP, AA, and EEW established the FRET assay for the HttExon1Q48-YPet/CyPet fibrilization. Requests for those reagents should be sent to EEW. JK, AS, and AP designed experiments. JK wrote the manuscript. DM performed EM analysis.

### Conflict of interest
The authors declare that they have no conflict of interest.

## References

Arosio P, Vendruscolo M, Dobson CM, Knowles TP (2014) Chemical kinetics for drug discovery to combat protein aggregation diseases. *Trends Pharmacol Sci* 35: 127 – 135

Balch WE, Morimoto RI, Dillin A, Kelly JW (2008) Adapting proteostasis for disease intervention. *Science* 319: 916 – 919

Balchin D, Hayer-Hartl M, Hartl FU (2016) *In vivo* aspects of protein folding and quality control. *Science* 353: aac4354

Bersuker K, Hipp MS, Calamini B, Morimoto RI, Kopito RR (2013) Heat shock response activation exacerbates inclusion body formation in a cellular model of Huntington disease. *J Biol Chem* 288: 23633 – 23638

Bhattacharyya AM, Thakur AK, Wetzel R (2005) polyglutamine aggregation nucleation: thermodynamics of a highly unfavorable protein folding reaction. *Proc Natl Acad Sci USA* 102: 15400 – 15405

Brehme M, Voisine C, Rolland T, Wachi S, Soper JH, Zhu Y, Orton K, Villella A, Garza D, Vidal M, Ge H, Morimoto RI (2014) A chaperome subnetwork safeguards proteostasis in aging and neurodegenerative disease. *Cell Rep* 9: 1135 – 1150

Buchner J, Grallert H, Jakob U (1998) Analysis of chaperone function using citrate synthase as nonnative substrate protein. *Methods Enzymol* 290: 323 – 338

Chan HY, Warrick JM, Gray-Board GL, Paulson HL, Bonini NM (2000) Mechanisms of chaperone suppression of polyglutamine disease: selectivity, synergy and modulation of protein solubility in *Drosophila*. *Hum Mol Genet* 9: 2811 – 2820

Christie NT, Lee AL, Fay HG, Gray AA, Kikis EA (2014) Novel polyglutamine model uncouples proteotoxicity from aging. *PLoS One* 9: e96835

Cicchetti F, Soulet D, Freeman TB (2011) Neuronal degeneration in striatal transplants and Huntington's disease: potential mechanisms and clinical implications. *Brain* 134: 641 – 652

Consortium HDi (2012) Induced pluripotent stem cells from patients with Huntington's disease show CAG-repeat-expansion-associated phenotypes. *Cell Stem Cell* 11: 264 – 278

David DC (2012) Aging and the aggregating proteome. *Front Genet* 3: 247

Gao B, Greene L, Eisenberg E (1994) Characterization of nucleotide-free uncoating ATPase and its binding to ATP, ADP, and ATP analogues. *Biochemistry* 33: 2048 – 2054

Gao X, Carroni M, Nussbaum-Krammer C, Mogk A, Nillegoda NB, Szlachcic A, Guilbride DL, Saibil HR, Mayer MP, Bukau B (2015) Human Hsp70 disaggregase reverses Parkinson's-linked alpha-synuclein amyloid fibrils. *Mol Cell* 59: 781 – 793

Gusella JF, MacDonald ME (2000) Molecular genetics: unmasking polyglutamine triggers in neurodegenerative disease. *Nat Rev Neurosci* 1: 109 – 115

Havel LS, Li S, Li XJ (2009) Nuclear accumulation of polyglutamine disease proteins and neuropathology. *Mol Brain* 2: 21

Hipp MS, Patel CN, Bersuker K, Riley BE, Kaiser SE, Shaler TA, Brandeis M, Kopito RR (2012) Indirect inhibition of 26S proteasome activity in a cellular model of Huntington's disease. *J Cell Biol* 196: 573 – 587

Hoffner G, Soues S, Djian P (2007) Aggregation of expanded huntingtin in the brains of patients with Huntington disease. *Prion* 1: 26 – 31

Jiang X, Sorkin A (2002) Coordinated traffic of Grb2 and Ras during epidermal growth factor receptor endocytosis visualized in living cells. *Mol Biol Cell* 13: 1522 – 1535

Kakkar V, Mansson C, de Mattos EP, Bergink S, van der Zwaag M, van Waarde MA, Kloosterhuis NJ, Melki R, van Cruchten RT, Al-Karadaghi S, Arosio P, Dobson CM, Knowles TP, Bates GP, van Deursen JM, Linse S, van de Sluis B, Emanuelsson C, Kampinga HH (2016) The S/T-rich motif in the DNAJB6 chaperone delays polyglutamine aggregation and the onset of disease in a mouse model. *Mol Cell* 62: 272 – 283

Kim YE, Hosp F, Frottin F, Ge H, Mann M, Hayer-Hartl M, Hartl FU (2016) Soluble oligomers of PolyQ-expanded Huntingtin target a multiplicity of key cellular factors. *Mol Cell* 63: 951 – 964

Kirstein J, Morito D, Kakihana T, Sugihara M, Minnen A, Hipp MS, Nussbaum-Krammer C, Kasturi P, Hartl FU, Nagata K, Morimoto RI (2015) Proteotoxic stress and ageing triggers the loss of redox homeostasis across cellular compartments. *EMBO J* 34: 2334 – 2349

Kirstein J, Arnsburg K, Scior A, Szlachcic A, Guilbride DL, Morimoto RI, Bukau B, Nillegoda NB (2017) *In vivo* properties of the disaggregase function of J-proteins and Hsc70 in *Caenorhabditis elegans* stress and aging. *Aging Cell* 16: 1414 – 1424

 

Kirstein-Miles J, Scior A, Deuerling E, Morimoto RI (2013) The nascent polypeptide-associated complex is a key regulator of proteostasis. *EMBO J* 32: 1451 – 1468

Kuo Y, Ren S, Lao U, Edgar BA, Wang T (2013) Suppression of polyglutamine protein toxicity by co-expression of a heat-shock protein 40 and a heat-shock protein 110. *Cell Death Dis* 4: e833

Liang V, Ullrich M, Lam H, Chew YL, Banister S, Song X, Zaw T, Kassiou M, Gotz J, Nicholas HR (2014) Altered proteostasis in aging and heat shock response in *C. elegans* revealed by analysis of the global and *de novo* synthesized proteome. *Cell Mol Life Sci* 71: 3339 – 3361

Lipe H, Bird T (2009) Late onset Huntington Disease: clinical and genetic characteristics of 34 cases. *J Neurol Sci* 276: 159 – 162

Livak KJ, Schmittgen TD (2001) Analysis of relative gene expression data using real-time quantitative PCR and the 2(-Delta Delta C(T)) Method. *Methods* 25: 402 – 408

Lorenz C, Lesimple P, Bukowiecki R, Zink A, Inak G, Mlody B, Singh M, Semtner M, Mah N, Aure K, Leong M, Zabiegalov O, Lyras EM, Pfiffer V, Fauler B, Eichhorst J, Wiesner B, Huebner N, Priller J, Mielke T *et al* (2017) Human iPSC-derived neural progenitors are an effective drug discovery model for neurological mtDNA disorders. *Cell Stem Cell* 20: 659 – 674 e659

Macdonald D, Tessari MA, Boogaard I, Smith M, Pulli K, Szynol A, Albertus F, Lamers MB, Dijkstra S, Kordt D, Reindl W, Herrmann F, McAllister G, Fischer DF, Munoz-Sanjuan I (2014) Quantification assays for total and polyglutamine-expanded huntingtin proteins. *PLoS One* 9: e96854

Mattoo RU, Sharma SK, Priya S, Finka A, Goloubinoff P (2013) Hsp110 is a bona fide chaperone using ATP to unfold stable misfolded polypeptides and reciprocally collaborate with Hsp70 to solubilize protein aggregates. *J Biol Chem* 288: 21399 – 21411

Miyoshi N, Oubrahim H, Chock PB, Stadtman ER (2006) Age-dependent cell death and the role of ATP in hydrogen peroxide-induced apoptosis and necrosis. *Proc Natl Acad Sci USA* 103: 1727 – 1731

Monsellier E, Redeker V, Ruiz-Arlandis G, Bousset L, Melki R (2015) Molecular interaction between the chaperone Hsc70 and the N-terminal flank of huntingtin exon 1 modulates aggregation. *J Biol Chem* 290: 2560 – 2576

Morley JF, Brignull HR, Weyers JJ, Morimoto RI (2002) The threshold for polyglutamine-expansion protein aggregation and cellular toxicity is dynamic and influenced by aging in *Caenorhabditis elegans*. *Proc Natl Acad Sci USA* 99: 10417 – 10422

Muchowski PJ, Schaffar G, Sittler A, Wanker EE, Hayer-Hartl MK, Hartl FU (2000) Hsp70 and hsp40 chaperones can inhibit self-assembly of polyglutamine proteins into amyloid-like fibrils. *Proc Natl Acad Sci USA* 97: 7841 – 7846

Navarro A, Sanchez Del Pino MJ, Gomez C, Peralta JL, Boveris A (2002) Behavioral dysfunction, brain oxidative stress, and impaired mitochondrial electron transfer in aging mice. *Am J Physiol Regul Integr Comp Physiol* 282: R985 – R992

Nguyen AW, Daugherty PS (2005) Evolutionary optimization of fluorescent proteins for intracellular FRET. *Nat Biotechnol* 23: 355 – 360

Nikolaidis N, Nei M (2004) Concerted and nonconcerted evolution of the Hsp70 gene superfamily in two sibling species of nematodes. *Mol Biol Evol* 21: 498 – 505

Nillegoda NB, Kirstein J, Szlachcic A, Berynskyy M, Stank A, Stengel F, Arnsburg K, Gao X, Scior A, Aebersold R, Guilbride DL, Wade RC, Morimoto RI, Mayer MP, Bukau B (2015) Crucial HSP70 co-chaperone complex unlocks metazoan protein disaggregation. *Nature* 524: 247 – 251

O'Brien MC, Flaherty KM, McKay DB (1996) Lysine 71 of the chaperone protein Hsc70 is essential for ATP hydrolysis. *J Biol Chem* 271: 15874 – 15878

Olzscha H, Schermann SM, Woerner AC, Pinkert S, Hecht MH, Tartaglia GG, Vendruscolo M, Hayer-Hartl M, Hartl FU, Vabulas RM (2011) Amyloid-like aggregates sequester numerous metastable proteins with essential cellular functions. *Cell* 144: 67 – 78

Rampelt H, Kirstein-Miles J, Nillegoda NB, Chi K, Scholz SR, Morimoto RI, Bukau B (2012) Metazoan Hsp70 machines use Hsp110 to power protein disaggregation. *EMBO J* 31: 4221 – 4235

Rauch JN, Gestwicki JE (2014) Binding of human nucleotide exchange factors to heat shock protein 70 (Hsp70) generates functionally distinct complexes *in vitro*. *J Biol Chem* 289: 1402 – 1414

Scherzinger E, Sittler A, Schweiger K, Heiser V, Lurz R, Hasenbank R, Bates GP, Lehrach H, Wanker EE (1999) Self-assembly of polyglutamine-containing huntingtin fragments into amyloid-like fibrils: implications for Huntington's disease pathology. *Proc Natl Acad Sci USA* 96: 4604 – 4609

Scior A, Juenemann K, Kirstein J (2016) Cellular strategies to cope with protein aggregation. *Essays Biochem* 60: 153 – 161

Simsek-Duran F, Li F, Ford W, Swanson RJ, Jones HW Jr, Castora FJ (2013) Age-associated metabolic and morphologic changes in mitochondria of individual mouse and hamster oocytes. *PLoS One* 8: e64955

Tam S, Geller R, Spiess C, Frydman J (2006) The chaperonin TRiC controls polyglutamine aggregation and toxicity through subunit-specific interactions. *Nat Cell Biol* 8: 1155 – 1162

Wetzel R (2012) Physical chemistry of polyglutamine: intriguing tales of a monotonous sequence. *J Mol Biol* 421: 466 – 490

Wilbanks SM, DeLuca-Flaherty C, McKay DB (1994) Structural basis of the 70-kilodalton heat shock cognate protein ATP hydrolytic activity. I. Kinetic analyses of active site mutants. *J Biol Chem* 269: 12893 – 12898

# Expanded View Figures

**Figure EV1. Controls for Htt fibrilization and the kinetics, point mutations in HSP-1 and HSP-110, and analysis of ATPase rates of HSP-70s and HSP-110.**

A TEM image of untagged HttExon1$Q_{48}$ 24 h post-PreSP treatment. Scale bar: 200 nm.

B Sedimentation analysis of the kinetics of HttExon1$Q_{48}$-CyPet fibrilization. Depicted are the ratios of the supernatant (soluble HttExon1$Q_{48}$-CyPet) and the pellet (insoluble, aggregated HttExon1$Q_{48}$-CyPet) at the indicated time points. The graph shows the average of two independent analyses.

C Analysis of the GST-cleavage reaction of GST-HttExon1$Q_{48}$ via SDS–PAGE in the presence (bottom) and absence (top) of HSP-1, DNJ-13, and HSP-110. The time points are indicated on top, and the migration of the full-length and cleaved GST-HttExon1$Q_{48}$ protein is indicated on the right.

D SDS–PAGE and Coomassie staining of all purified proteins used in this study.

E CD analysis of HSP-1 (red) and the point mutants HSP-1_D10S (blue) and HSP-1_K71E (green) and the blank control (black).

F CD analysis of HSP-110 (red) and the point mutants HSP-110_D7S (blue) and HSP-110_N578Y/E581A (green) and the blank control (black).

G Basal ATPase rates of HSP-1 and HSP-110 and its point mutants. The ATPase rate is indicated on the *y*-axis in pmol ATP/μM Hsp/min ($N = 2$).

H ATPase rates of the Hsp70s: HSP-1 (white), F44E5.4 (light gray), C12C8.1 (dark gray), and F11F1.1 (black) alone and in the presence of the DNJ proteins, DNJ-12, DNJ-13, DNJ-19, and DNJ-24 ($N = 2$).

I Sedimentation analysis of disaggregation of HttExon1$Q_{48}$ fibrils by HSP-1, HSP-110, and DNJ-13 in the presence or absence of ATP after 12 h. Depicted are the ratios of the supernatant (soluble HttExon1$Q_{48}$) and the pellet (insoluble, aggregated HttExon1$Q_{48}$). The error bars represent the standard deviation of three independent experiments ($N = 3$).

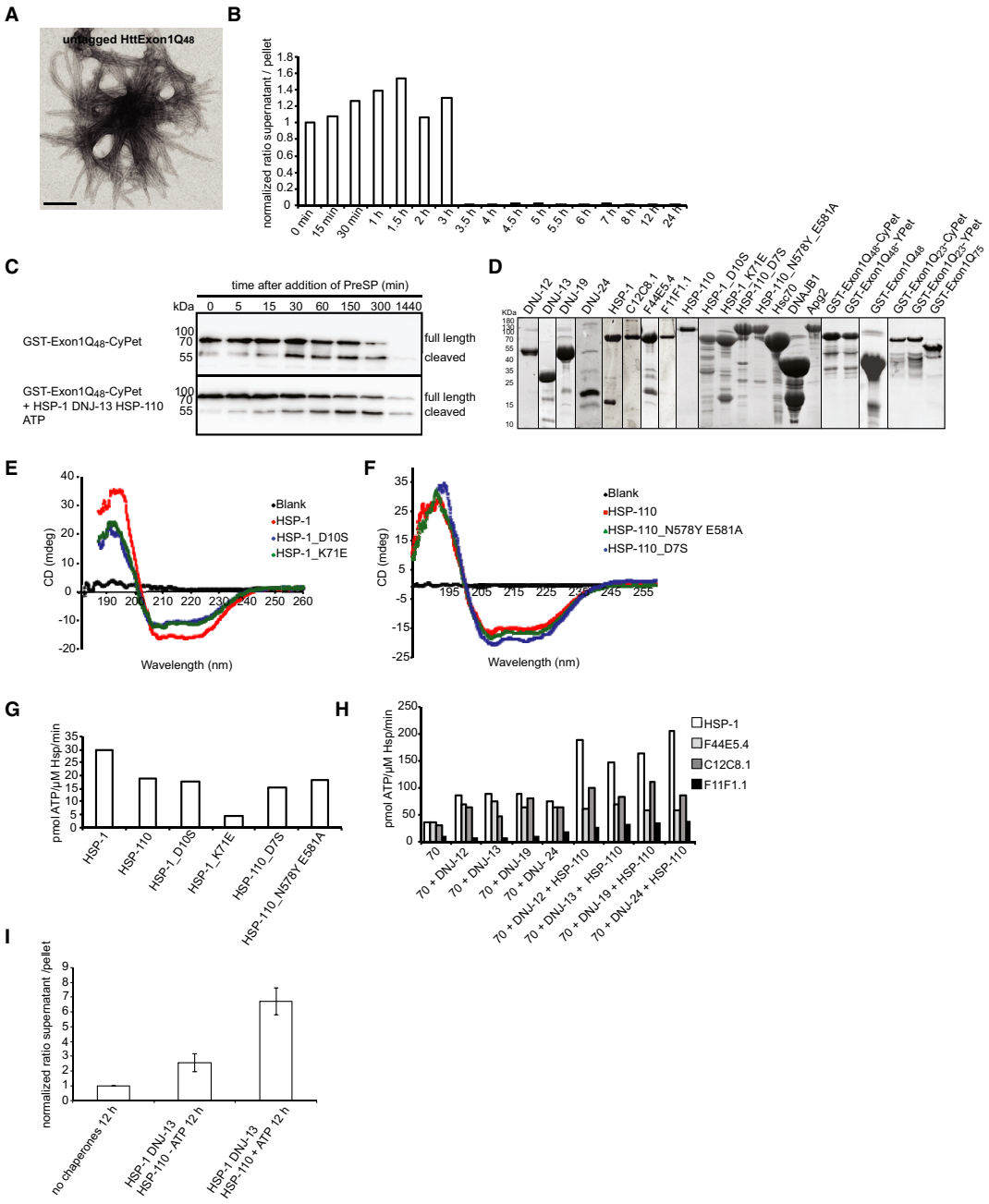


**Figure EV1.**

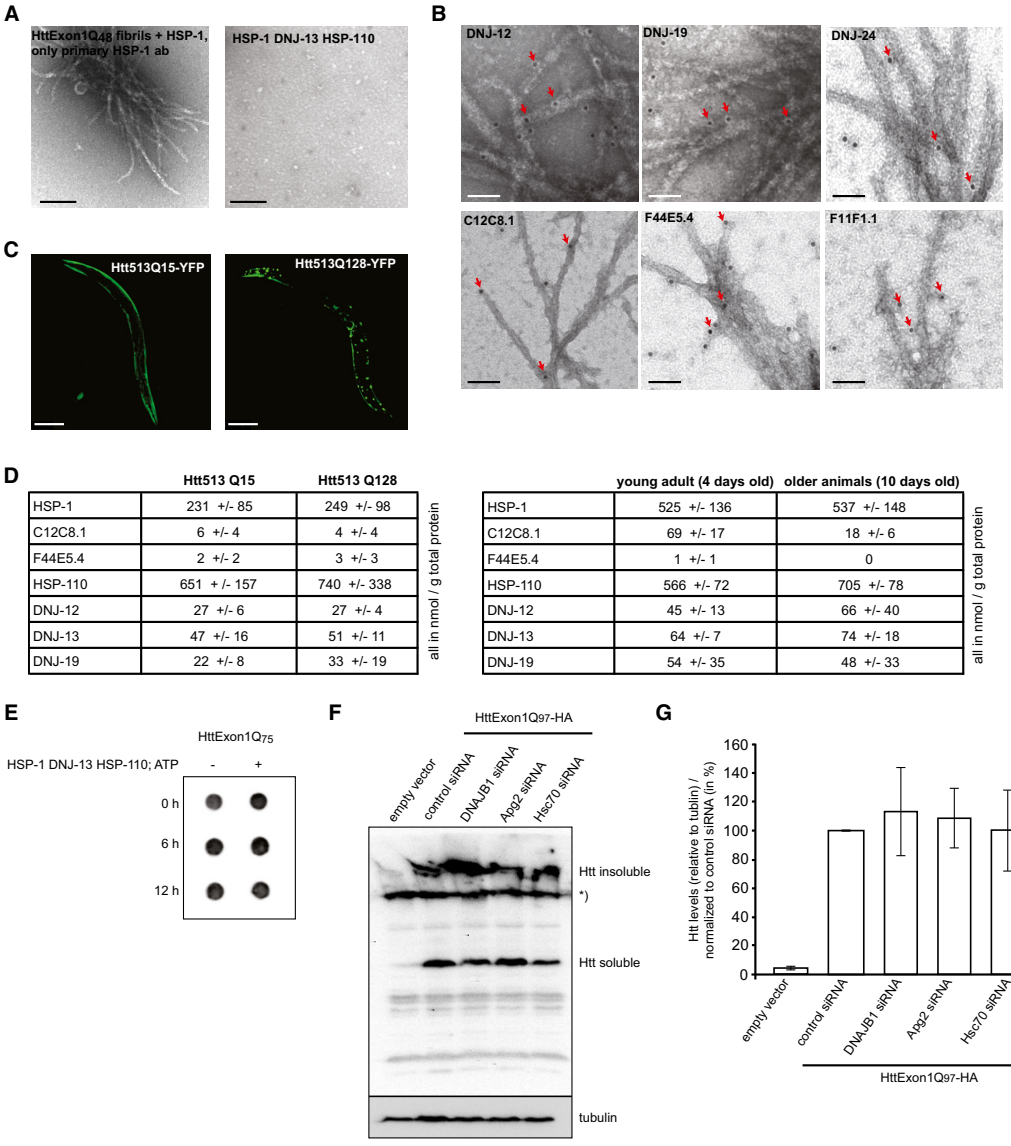


| | Htt513 Q15 | Htt513 Q128 |
|---|---|---|
| HSP-1 | 231 +/- 85 | 249 +/- 98 |
| C12C8.1 | 6 +/- 4 | 4 +/- 4 |
| F44E5.4 | 2 +/- 2 | 3 +/- 3 |
| HSP-110 | 651 + /- 157 | 740 +/- 338 |
| DNJ-12 | 27 +/- 6 | 27 +/- 4 |
| DNJ-13 | 47 +/- 16 | 51 +/- 11 |
| DNJ-19 | 22 +/- 8 | 33 +/- 19 |

all in nmol / g total protein

| | young adult (4 days old) | older animals (10 days old) |
|---|---|---|
| HSP-1 | 525 +/- 136 | 537 +/- 148 |
| C12C8.1 | 69 +/- 17 | 18 +/- 6 |
| F44E5.4 | 1 +/- 1 | 0 |
| HSP-110 | 566 +/- 72 | 705 +/- 78 |
| DNJ-12 | 45 +/- 13 | 66 +/- 40 |
| DNJ-13 | 64 +/- 7 | 74 +/- 18 |
| DNJ-19 | 54 +/- 35 | 48 +/- 33 |

all in nmol / g total protein

**Figure EV2.**

◀ **Figure EV2. Controls for *in vitro* and *in vivo* immunostaining *Caenorhabditis elegans* models of Htt513$Q_{15}$/$Q_{128}$-YFP and quantification of chaperones.**

A On the left: TEM analysis of a control of HttExon1$Q_{48}$ fibrils incubated with HSP-1 and only the primary antibody against HSP-1. On the right: TEM analysis of only the chaperones HSP-1, DNJ-13, and HSP-110. Scale bars: 200 nm.

B Immunostaining of chaperones with HttExon1$Q_{48}$ fibrils for DNJ-12, DNJ-19, DNJ-24, C12C8.1, F44E5.4, and F11F1.1. Scale bars: 50 nm. The red arrows mark the positive immunogold labeling.

C Fluorescence images of nematode lines that were used in this study for the analysis of chaperone expression (Fig 5B and C): Htt513$Q_{15}$-YFP (Htt$Q_{15}$) and Htt513$Q_{128}$-YFP (Htt$Q_{128}$). Scale bars: 200 μm.

D Tables depict the quantification of the chaperone concentrations in Htt513$Q_{15}$-YFP vs. Htt513$Q_{128}$-YFP (top) and wild-type nematodes of 4-day-old (young adults) vs. 10-day-old animals (bottom). Protein levels are depicted as nmol/g total protein. Data show an average of three independent analyses. Error ranges represent the standard deviation.

E Filter retardation analysis of the disaggregation analysis of HttExon1$Q_{75}$ aggregates by HSP-1, DNJ-13, and HSP-110 using an Htt antibody. The time course of the experiment is depicted on the left. No difference in the aggregated state of HttExon1$Q_{75}$ can be observed in the chaperone-containing sample (right lane vs. left lane).

F Western blot analysis of the soluble and insoluble moiety of HttExon1$Q_{97}$ of HEK293T cells upon siRNA-mediated depletion of DNAJB1, Apg2, and Hsc70. The migration of the insoluble and soluble HttExon1$Q_{97}$ protein is indicated on the right. An asterisk indicates a non-specific signal that also appears in the non-transfected HEK393T cells (left lane).

G Quantification of the overall HttExon1$Q_{97}$ levels (soluble + insoluble) of (F). The intensities were normalized to tubulin and represent an average of 3 independent experiments. Error bars represent the standard deviation.

 

# 8. *Curriculum Vitae*

My *curriculum vitae* does not appear in the electronic version of my paper for reasons of data protection.

# 9. Complete List of Publications

**Pigazzini ML**, Marginescu A, Lawrenz M, Kaminski Schierle G, Kirstein J. An expanded polyproline domain maintains mutant HTT soluble in vivo and during aging *(manuscript in preparation)*

Ayala Mariscal SM, **Pigazzini ML**, Protze J, Richter J, Ozel M, Weikum K, Liu F, Kirstein J. Identification of an interaction motif in huntingtin for DNAJB1 *(manuscript in preparation)*

Haenig C, Atias N, Taylor AK, Mazza A, Schaefer MH, Russ J, Riechers S-P, Jain S, Coughlin M, Fontaine J-F, Freibaum BD, Brusendorf L, Zenkner M, Porras P, Stroedicke M, Schnoegl S, Arnsburg K, Boeddrich A, **Pigazzini L**, Heutink P, Taylor JP, Kirstein J, Andrade-Navarro MA, Sharan R, Wanker EE. Interactome Mapping Provides a Network of Neurodegenerative Disease Proteins and Uncovers Widespread Protein Aggregation in Affected Brains. Cell Rep (2020);32:108050.
*Impact Factor 2018: 7.815*

**Pigazzini ML**, Kirstein J. In vivo quantification of protein turnover in aging *C. Elegans* using photoconvertible Dendra2. J Vis Exp (2020);2020:1–18.
*Impact Factor 2018: 1.108*

**Pigazzini ML**, Gallrein C, Iburg M, Kaminski Schierle G, Kirstein J. Characterization of Amyloid Structures in Aging *C. Elegans* Using Fluorescence Lifetime Imaging. J Vis Exp (2020):1–11.
*Impact Factor 2018: 1.108*

Nethisinghe S, **Pigazzini ML**, Pemble S, Sweeney MG, Labrum R, Manso K, Moore D, Warner J, Davis MB, Giunti P. PolyQ tract toxicity in SCA1 is length dependent in the absence of CAG repeat interruption. Front Cell Neurosci (2018);12.
*Impact Factor 2015: 4.609*

Scior A, Buntru A, Arnsburg K, Ast A, Iburg M, Juenemann K, **Pigazzini ML**, Mlody B, Puchkov D, Priller J, Wanker EE, Prigione A, Kirstein J. Complete suppression of Htt fibrilization and disaggregation of Htt fibrils by a trimeric chaperone complex. EMBO J (2018);37:282–99.
*Impact Factor 2015: 9.643*

Pirillo MC, **Pigazzini ML**, Cohen ME, Sousa-Nunes DR. PP55. Oncogenic microrna reveal novel neural tumor model. Neuro Oncol (2017);19:i15–i15.

## 10. Acknowledgements

Firstly, I would like to thank my co-supervisor Janine Kirstein, for her unwavering supervision, even from afar. Thanks also to Ralf Schülein for his support and help, especially in navigating the university system.

To all the Kirstein Berlin Lab members, past and present, a big thank you: for the camaraderie, the advice, the support and the friendship. A special mention to Sara Ayala, my 'master-student cum post-doc', with whom the last year and a half has been a rollercoaster of work, life, lab moving, baking, minions and much more.

I would like to acknowledge also the many FMP people that have helped with the technical/practical aspects of my PhD project throughout the years. Among these the members of the *Cell Imaging* and *Mass Spec* facilities, the PhD representatives and the larger PhD community of both the MDC and FMP. And above all, thank you to my office mate, Claudia Rutz, to whom I owe much laughter, interesting conversations and plenty of my molecular biology, and German, knowledge.

A particular recognition goes to the Wanker lab members, for all the constructive scientific discussions, the many extra-hour events and the shared frustration on working with huntingtin. And of course for their many generous material/technical contributions. I am also grateful for the very fruitful collaboration with Gabi Kaminski Schierle and her team in Cambridge, where I was able to spend some time learning the wonders of microscopy.

Finally, a quick mention to my family, whose quiet unnoticeable support was present throughout this PhD journey. And lastly, I want to thank the people who have made my time in Berlin simply unforgettable. My relationship with this city and the life here has been tumultuous, not least due to the pandemic. A few people have been by my side throughout, in the best of times and the worst of times, encouraging, thoughtful, helpful and endlessly present. Milda, Simon and Simona, to you goes my eternal gratitude - I could not have done it without you.

*Vielen Dank!*